Search for supplementary Higgs Bosons at the LHC

Matiás Rodríguez Vázquez

NNT : 2017SACLS317

THÈSE DE DOCTORAT
DE L'UNIVERSITÉ PARIS-SACLAY
PRÉPARÉE À L'UNIVERSITÉ PARIS-SUD

Ecole doctorale n°564
École Doctorale Physique en Île-de-France (EDPIF)
Spécialité de doctorat : Physique

Search for supplementary Higgs Bosons at the LHC

par

M. Matías RODRÍGUEZ VÁZQUEZ

Thèse présentée et soutenue à Orsay, le 28 Septembre 2017.

Composition du Jury :

Mme	ASMAA ABADA	Prof. *LPT Orsay*	(Président du jury)
M	STEFANO MORETTI	Prof. *University of Southampton*	(Rapporteur)
Mme	GENEVIÈVE BÉLANGER	Prof. *LAPTh Annecy*	(Rapporteur)
M	FABIO MALTONI	Prof. *CP3 Louvain*	(Examinateur)
M.	ULRICH ELLWANGER	Prof. *LPT Orsay*	(Directeur de thèse)

Search for supplementary Higgs bosons at the LHC

Abstract

Despite its incontestable experimental success, the Standard Model of particle physics leaves unanswered many fundamental questions like the hierarchy problem and the origin of dark matter, motivating the study of physics beyond its scope. The NMSSM is a well-motivated extension of the SM addressing these two issues. It features a rich phenomenology accessible, in principle, at the LHC. In particular, the Higgs sector of the NMSSM is extended with respect to the SM giving rise to six scalars. It is the aim of this thesis to study the discovery potential of these extra Higgs bosons at the LHC.
After introducing the NMSSM and its motivation, we first study the discovery prospects for a scalar lighter than the 125 GeV resonance found at CERN, reviewing its possible production and detection at the upcoming runs of the LHC and its possible impact on couplings of the Standard Model Higgs boson.
Next, prospects for searches via Higgs cascades involving extra light and heavy Higgs bosons are presented. Detailed studies by means of Monte Carlo methods are performed, and new dedicated analysis are proposed. These last results are not confined to the NMSSM and can be interpreted in a wide class of models.

Résumé

Malgré un succès expérimental incontestable, le Modèle standard (MS) de la physique des particules laisse de nombreuses questions fondamentales sans réponse, comme le problème de hiérarchie et l'origine de la matière noire, motivant l'étude de la " nouvelle physique". Le Next-to-Minimal Supersymmetric Standard Model (NMSSM) est une extension très intéressante du MS répondant à ces deux problèmes. Il comprend une riche phénoménologie, en principe accessible au Grand Collisionneur de Hadrons (LHC). En particulier, son secteur de Higgs est étendu par rapport au MS, générant six scalaires. Le but de cette thèse est d'étudier le potentiel de découverte de ces bosons de Higgs supplémentaires au LHC.
Après une introduction du NMSSM et de ses motivations, nous étudions d'abord les perspectives de découverte d'un scalaire, plus léger que la résonance à 125 GeV mise en évidence au CERN, en passant en revue ses possibles modes de production et de détection dans les phases à venir du LHC, et ses possibles impacts sur les couplages du boson de Higgs du MS.
Ensuite, les perspectives de recherche via les cascades de Higgs, impliquant des bosons de Higgs supplémentaires légers et lourds, est présentée. Des études détaillées au moyen de méthodes Monte-Carlo ont été réalisées, et de nouvelles analyses dédiées sont présentées. Ces derniers résultats ne sont pas restreints au NMSSM, et peuvent être interprétés dans une large classe de modèles.

La recherche de bosons de Higgs supplémentaires au LHC

De nos jours, la meilleure compréhension des particules élémentaires et de leurs interactions s'exprime dans le cadre de la Théorie Quantique des Champs (TQC). Au cours du dernier siècle, d'immenses progrès ont eu lieu dans le développement de la TQC et des théories de jauge, aboutissant en fin de compte au Modèle Standard (MS) de la physique des particules. Le MS est une théorie cohérente qui unifie les interactions électromagnétiques, forte et faible – trois des quatre forces fondamentales de la nature – au sein du groupe de symétrie de jauge $SU(3)_c \times SU(2)_L \times U(1)_Y$. Le MS a été testé de manière exhaustive au cours des dernières décennies par de nombreuses expériences, qui ont confirmé de manière continue le modèle. Avec la découverte en 2012 par les collaborations ATLAS [1] et CMS [2] d'une particule jusqu'ici compatible avec le boson de Higgs du MS, on dit souvent que le MS est "complet", au sens où toutes les particules prédites ont été observées et jugées compatibles avec le MS vis-à-vis de la sensibilité expérimentale actuelle. Cependant, il existe de nombreuses raisons empiriques de croire que le MS n'est pas la théorie ultime de la nature.

Pour commencer, il ne prend pas en compte la gravité. Les tentatives pour fondre le MS dans un cadre relativiste ont conduit à de la non-renormalisabilité et à des divergences non-physiques. Deuxièmement, un ensemble de robustes observations astrophysiques, en particulier les courbes de rotation des galaxies et l'Amas de la Balle, suggèrent fortement l'existence d'une matière électriquement neutre : la matière sombre [3, 4] (bien que d'autres explications sans particules aient été proposées, voir [5]). Si c'est bien le cas, un (ou des) champ(s) particulaires associé(s) à la matière noire est (ou sont) attendus. Aucun des champs du MS n'est un candidat convenable pour la matière noire.

Un autre problème, largement considéré comme la plus robuste preuve de physique au-delà du modèle standard, est lié à la masse des neutrinos. Dans le cadre du MS, les neutrinos sont des champs sans masse qui interagissent avec le reste de la matière uniquement via l'interaction faible. Cependant, dans les années 60 déjà, des expérimentateurs ont rapporté avoir mesuré des oscillations de saveur des neutrinos [6], impliquant des masses non-nulles [7]. Il y a plusieurs manières de donner une masse aux neutrinos, et dans tous les cas on doit faire appel à la Nouvelle Physique (NP).

D'autres problèmes fondamentaux existent, par exemple l'inexpliquée asymétrie matière-antimatière de l'Univers, ou d'autres problèmes plus conceptuels, comme le fort arbitraire de la théorie (19 paramètres libres qui doivent être déterminés expérimentalement), la non-unification des forces de jauge et le *problème de hiérarchie*.

Arrêtons-nous un moment sur le problème de hiérarchie, que l'on peut résumer comme suit : dans le MS, la masse du boson de Higgs reçoit des corrections quantiques quadratiquement divergentes avec une échelle de coupure Λ:

$$\overbrace{m_h^2}^{\mathcal{O}(M_Z)} \approx (m_h^2)_{\text{bare}} - |\lambda_t|^2 \times \overbrace{\Lambda^2}^{\mathcal{O}(M_{GUT}?)} + \text{log. divergences...} \quad (1)$$

alors que la partie gauche de l'équation correspond à la masse observée à 125 GeV le terme $(m_h^2)_{\text{bare}}$ est un paramètre libre du lagrangien (nu). Donc, on peut conclure que si la nouvelle physique au delà du modèle standard se présente à l'échelle d'énergie Λ (par exemple $\Lambda \sim \Lambda_{\text{Planck}}$ ou $\sim \Lambda_{\text{GUT}}$), c'est à dire que si le MS est une théorie effective à basse énergie d'une théorie plus complète, on devrait s'attendre à une compensation miraculeuse de l'ordre de 32 décimales pour obtenir une valeur de la masse du bosons de Higgs à l'échelle electrofaible. Ce fait étrange, qui est considéré est connu comme le *problème d'ajustement fin* ou le *problème de hierarchie*. Après tout, la nécessité d'ajuster finement les paramètres de la partie droite de l'équation (1.1) est due à l'énorme différence entre l'échelle

d'énergie electrofaible (la masse du Higgs) et l'échelle de la nouvelle physique, probablement la masse de Planck. Cette différence reste inexpliquée.

Que se passe-t-il aux masses des autres particules? Est ce que la masse des fermions ont le même problème? La réponse est non. En effet, les divergences quadratiques ne sont pas présentes dans le cas des masses des fermions : la symétrie chirale agit comme une protection contre les nouvelles larges échelles d'énergie et la brisure de cette symétrie donne naissance à seulement des divergences logarithmiques. En conséquent, le problème de hierarchie peut etre vu comme un manque de symétrie dans le modèle standard pour protéger la masse m_h contre les grandes échelles d'énergie.

La supersymétrie (SUSY) a été pendant une très longue période comme l'un des théories les plus populaires pour résoudre le problème de hierarchie. Accidentellements, les modèles supersymétriques incluent également un candidat potentiel de matière noire et si la SUSY est promue localement, la gravité est incorporée dans le cadre de la supergravité. Dans le contexte de la SUSY, les fermions (bosons) sont incorporés dans des superchamps incluant leur partenaires scalaires (fermioniques). A la fois les composantes bosoniques *et* fermioniques contribuent aux corrections quantiques de la masse du boson de Higgs de telle façon qu'elles s'annulent exactement. La brisure de la SUSY (à travers les termes brisant la SUSY légèrement) donne naissance à des corrections à la masse du Higgs avec une dépendance logarithmique :

$$\delta m_h^2 \approx m_{soft}^2 \times \ln(\Lambda_{GUT}/m_{soft}) + \dots \tag{2}$$

offrant une solution au problème de hierarchie. La SUSY protège donc la masse du boson de Higgs de corrections radiatives. Rappelons nous, toutefois, que l'écart de masses entre les particules du modèle standard et leurs partenaires supersymétriques, donné par les termes brisant la SUSY légèrement $\sim m_{soft}$, ne peuvent pas être trop larges ou bien de larges corrections radiatives seraient réintroduites et par

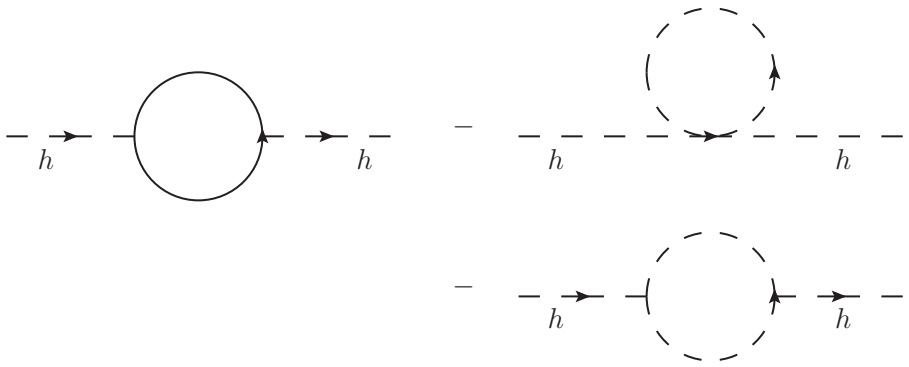

Figure 0.1: Des diagrammes qui contribuent aux corrections quantiques de la masse du boson de Higgs. À gauche : loop qui est dû aux fermions du modèle standart. À droite : loops avec des contributions des bosons supersymétriques. Les diagrammes fermioniques et bosoniques sont annulés entre eux de manière exacte en supersymétrie exacte.

conséquent un problème d'ajustement fin. Pour cela, si la SUSY est responsable de la solution du problème de hierarchie, rendant la théorie naturelle, les nouvelles particules sont attendues avec des masses proches de l'échelle du TeV.

Pour cela, les modèles supersymétriques ont été très largement étudiés et beaucoup de recherches ont été menées auprès des collaborations expérimentales au LHC et ses prédécesseurs.

Dans cette thèse, on étudie les aspects phénoménologiques du secteur du Higgs neutre du NMSSM (Next-to-Minimal Supersymmetric Standard Model). On étudiera en détail la possibilité de découverte offerte par le LHC, explorant les régions les plus prometeuses de l'espace des paramètres de la théorie et en étudiant les stratégies d'études du Higgs prédit par le modèle.

Le plan est le suivant : dans le chapitre 2 nous introduisons le Modèle Standard Minimal Supersymétrique (MSSM) en développant particulièrement le sécteur du Higgs. On passera en revue les limitations du modèle MSSM motivé par son extension immédiate, le NMSSM qui sera présenté au chapitre 3.

Le chapitre 4 est consacré à la perspective de découverte d'une particule légère h_s de type singlet avec une masse $m_{h_s} \lesssim 125$ GeV et son impact potentiel sur les propriétés de l'état de type MS h

(identifié à la particule de 125 GeV découverte). Finalement, au chapitre 5 nous avons présenté une étude Monte Carlo spécifique à la sensibilité de découverte – ou à l'exclusion – au LHC pour une cascade de désintégration du Higgs qui pourrait etre interprétée dans d'autres modèles avec des secteurs de Higgs suffisamments large.

Thèse effectueé au

Laboratoire de Physique Théorique d'Orsay
Bâtiment 210
Université Paris Sud 11
91405 Orsay CEDEX

Contents

Chapter 1

Introduction

As for today, our best understanding of the elementary particles and their interactions is expressed in the context of Quantum Field Theory (QFT). During the last century a tremendous progress has taken place in the development of QFT and gauge theories, ultimately leading to the Standard Model (SM) of particle physics. The SM is a consistent gauge theory unifying the electromagnetic, strong and weak interactions - three of the four known fundamental forces in nature - under the gauge symmetry group $SU(3)_c \times SU(2)_L \times U(1)_Y$. The SM has been exhaustively tested in the last decades at a large number of experiments, being continuously confirmed in all its predictions. With the discovery in 2012 by the ATLAS [1] and CMS [2] collaborations of a particle so far compatible with the SM Higgs boson, it is often said that the SM is "complete", in the sense that all particles predicted by the SM have been measured and confirmed to be compatible with it at the present experimental sensitivity. However, there exist numerous empirical reasons to believe that the SM is not the ultimate theory of nature.

To start with, it does not incorporate gravity. Attempts to embed the SM general in a relativistic framework leaded to non-renormalizability and unphysical divergences. Second, a set of solid astrophysical observations, namely the galaxies rotation velocities and the Bullet Cluster strongly suggest the existence of some electrically neutral kind of matter: dark matter [3, 4] (although other non-particle explanations exist, see [5] for instance). If that is indeed the case, a particle field(s) associated to the dark matter is(are) expected. None of the SM fields are suitable candidates for dark matter.

Another issue, widely considered as the most solid evidence of BSM physics, is related to the mass of the neutrinos. Within the SM, neutrinos are massless fields which interact with the rest of matter only through the weak force. However, already in the 60s experimentalist reported the measurement of neutrino flavour oscillations [6], implying a non-vanishing value for their masses [7]. There is not a unique way to give a mass term to the neutrinos, and in all cases new physics

(NP) must be invoked.

Other fundamental problems exist, e.g. the unexplained matter-antimatter asymmetry of the universe, or other more conceptual issues, like the large arbitrariness of the theory (19 free parameters which must be determined from experiments), the (non)unification of gauge forces and the *hierarchy problem*.

Let us stop for a moment on the hierarchy problem, which we can outline as follows: In the SM, the Higgs boson mass receive quantum corrections which are quadratically divergent with the cut-off regulator Λ:

$$\overbrace{m_h^2}^{\mathcal{O}(M_Z)} \approx (m_h^2)_{\text{bare}} - |\lambda_t|^2 \times \overbrace{\Lambda^2}^{\mathcal{O}(M_{GUT}?)} + \text{log. divergences...} \tag{1.1}$$

while the left-hand side of this expression corresponds to the observed mass ~ 125 GeV, the term $(m_h^2)_{\text{bare}}$ is a free term of the (bare) lagrangian. Hence, one can conclude that if there are new physics beyond the SM showing up at a higher energy scale Λ (for instance $\Lambda \sim \Lambda_{Planck}$ or $\sim \Lambda_{GUT}$), i.e. if the SM is a low energy effective field theory of some more general underlying theory, one would need miraculous cancellations of the order of 32 decimals to have the desired value for the Higgs mass at the electroweak scale. This awkward fact, which is regarded as *unnatural*, is known as the *fine-tuning problem* or the *hierarchy problem*. After all, the necessity to *fine-tune* the parameters in the right-hand side of (1.1) is due to the enormous difference between the electroweak scale (the Higgs mass) and the scale of new physics, probably gravity. This hierarchy in the scales remains unexplained in the SM.

What happens to the other particles masses? Do fermion masses have the same problem? The answer is no. Indeed, power divergences are not present in the case of fermion masses: chiral symmetry acts as a 'protection' against large new scales, and the breaking of chiral symmetry give rise only to logarithmic divergences. For the case of gauge bosons, gauge symmetry protects their masses. Thus, the hierarchy problem can be regarded as a lack of a symmetry in the SM to protect m_h against very high scales.

Supersymmetry (SUSY) has been for long time the most popular theoretical framework to solve the hierarchy problem. Incidentally, supersymmetric models also naturally embed dark matter candidates and, if promoted to be a local symmetry, gravity is incorporated in the so-called super-gravity. In the context of SUSY, fermions (bosons) are embedded into superfields including their scalars (fermions) superpartners. Both the fermionic *and* bosonic components of the superfields contribute to the Higgs mass quantum corrections in such a way that they cancel exactly. The breaking of SUSY (through soft SUSY breaking terms in the lagrangian) gives rise only to logarithmic divergences,

$$\delta m_h^2 \approx m_{soft}^2 \times \ln(\Lambda_{GUT}/m_{soft}) + \dots \tag{1.2}$$

solving the hierarchy problem. SUSY is thus protecting the Higgs mass from large radiative corrections. Recall, however, that the mass gap between the SM particles and their supersymmetric partners, given by the soft SUSY breaking terms $\sim m_{soft}$, could not be too large, or large radiative corrections would be reintroduced and hence a fine-tuning problem. Therefore, if SUSY is responsible for the solution of the hierarchy problem rendering the theory natural (in the sense of not being fine-tuned), the new particles are expected to live at the TeV scale.

For these and other reasons, supersymmetric models have been extensively studied in the literature, and many dedicated searches for supersymmetric particles have been done by the experimental collaborations at the LHC and previous experiments.

In this thesis, we study the phenomenological aspects of the neutral Higgs sector of the Next-to-Minimal Supersymmetric Standard Model (NMSSM). We focus on the discovery power offered by the current LHC experiments, exploring the most promising regions in the parameter space of the theory and devising search strategies for the Higgs particles predicted by the model.

The outline is as follows: in chapter 2 we introduce the Minimal Supersymmetric Standard Model (MSSM), with particular emphasis on its Higgs sector. We review the limitations of the MSSM motivating its immediate extension, the NMSSM, which is presented in chapter 3.

Chapter 4 is devoted to the discovery prospects of a light mostly singlet-like state h_s below $m_{h_s} \lesssim 125$ GeV, and its possible impact on the properties of the mostly SM state h (identified with the 125 GeV discovered particle). Finally, in chapter 5 we present a dedicated Monte Carlo study of the discovery – or exclusion – sensitivities of the LHC for Higgs cascade decays, which could be interpreted in other models with large enough Higgs sectors.

Chapter 2

The Minimal Supersymmetric Standard Model (MSSM)

We have already pointed out in chapter 1 the limitations of the SM and sketched the main ideas behind supersymmetry. We introduce here the minimal supersymmetric extension of the SM, the MSSM. The MSSM consists in a softly broken supersymmetric model that reproduces the SM with the minimum amount of new fields with respect to it.

In this chapter we will introduce the MSSM matter content, its lagrangian and the main properties of the model, with particular attention to the Higgs sector.

2.1 Field content

The matter content of the MSSM is by construction reproducing entirely the SM fermionic fields. Each SM matter field (quarks and leptons) is embedded in a *chiral superfield* including its superpartner. For instance, the left-handed electron field e_L is part of the left-handed electron superfield $\hat{L}_e$, which also includes its scalar superpartner, the (left-handed) selectron $\tilde{e_L}$, with the same quantum numbers. Thus, for each quark (lepton) there is associated a 'squark' ('slepton) with the same gauge charges. Since the gauge group of the model is the same as the one of the SM, i.e. $SU(3)_c \times SU(2)_L \times U(1)_Y$ the chiral superfields have the same quantum number as their correspondent SM fields. There are no extra quarks or leptons in the model beyond the chiral superfields associated to the ones of the SM.

Regarding the Higgs sector, the supersymmetrization is slightly less straight forward. In principle, we could just proceed as we did above: we promote the Higgs boson of the SM to a chiral superfield including its fermionic superpartner (the so-called 'higgsino'), and this should be it. However, such supersymmetric

extension of the SM with only one Higgs chiral superfield leads to an inconsistent model, and a second one should be introduced for various reasons:

1. **Gauge anomalies cancellation**. Gauge anomalies are quantum mechanical effects (loops) that break the gauge symmetry of the classical theory. In a quantum field theory with gauge symmetries, gauge anomalies *have to* be avoided since they lead to unphysical negative-norm degrees of freedom, making the theory inconsistent. In the SM, the diagrams giving rise to a potential gauge anomaly consist in the chiral (left-handed) fermion loops with three gauge bosons attached to it. The condition for the cancellation of these diagrams is

$$\mathrm{Tr}[(T_3)^2 Y] = 0 \tag{2.1}$$

   where T_3 and Y are the third component of the weak isospin and the hypercharge respectively, and the trace runs over the SM left-handed fermions. Expression (2.1) is satisfied in the SM when we include all the three families of quarks and leptons. Now, when we promote the fermionic fields to chiral superfields we introduce new scalar degrees of freedom, which do not contribute to the gauge anomaly cancellation condition (2.1). However, if we embed the the SM Higgs doublet into a chiral superfield, a new chiral fermionic degree of freedom (the higgsino) with hypercharge $Y = 1$[1] is introduced. One higgsino alone contributes to the trace (2.1) spoiling the gauge anomaly cancellation, rendering the theory inconsistent. The easiest way of circumventing this issue is introducing a second Higgs (super)doublet with opposite hypercharge $Y = -1$ in such a way that both new contributions to (2.1) cancel out, preserving the theory anomaly free.

2. **Up and down fermion masses.** Fermions in the SM acquire their mass through the Higgs mechanism. Although up and down type fermions have opposite hypercharges, Yukawa terms for both type of fermions could be written in a gauge symmetric way using only one Higgs doublet. This is thanks to the fact that the **2** representation of $SU(2)$ is equivalent to its conjugate $\bar{\mathbf{2}}$. Indeed, the Yukawa terms

$$y_u(H \cdot q_L)u_R^c + y_d(\tilde{H} \cdot q_L)d_R^c + y_\ell(H \cdot l_L)e_R^c \tag{2.2}$$

   give rise to the masses after symmetry breaking, where $\tilde{H}$ is the complex conjugate of the Higgs field H. However, in the framework of supersymmetry

[1] Here we use the convention for the hypercharge $Y = Q - T_3$, where Q is the electric charge and T_3 is the third generator of $SU(2)_L$. Recall that in the literature is not uncommon to find the alternative definition $Y = 2(Q - T_3)$.

Chiral superfield		Scalar	Fermion	$SU(3)_c$	$SU(2)_L$	$U(1)_Y$
(s)quarks	$\hat{Q}_L^f$	$\tilde{Q}_L^f$	q_L^f	**3**	**2**	1/3
	$\hat{U}_R^{c,f}$	$\tilde{U}_R^{c,f}$	$u_R^{c,f}$	**3**	**1**	-4/3
	$\hat{D}_R^{c,f}$	$\tilde{D}_R^{c,f}$	$u_R^{c,f}$	**3**	**1**	2/3
(s)leptons	$\hat{L}_L^f$	$\tilde{L}_L^f$	l_L^f	**1**	**2**	-1
	$\hat{E}_R^{c,f}$	$\tilde{E}_R^{c,f}$	$e_R^{c,f}$	**1**	**1**	2
Higgs/higgsino	$\hat{H}_u$	$\tilde{H}_u$	H_u	**1**	**2**	1/2
	$\hat{H}_d$	$\tilde{H}_d$	H_d	**1**	**2**	-1 /2

Table 2.1: Chiral superfields of the MSSM, with its corresponding quantum numbers. The index $f = 1 \ldots 3$ denotes the fermion family.

Gauge group	Vector superfield	Vector	Fermion
$U(1)_Y$	$\hat{B}$	B_μ	$\tilde{b}$
$SU(2)_L$	$\hat{W}^i$	W_μ^i	$\tilde{w}^i$
$SU(3)_c$	$\hat{\mathcal{A}}^a$	$\mathcal{A}_\mu^a$	$\tilde{g}^a$

Table 2.2: Vector superfields of the MSSM, containing the gauge bosons and the gauginos.

we cannot write a field *and* its complex conjugate together in the superpotential. Supersymmetry requires that the superpotential itself should be a chiral superfield, and as such it should be a function of the chiral superfields $\mathbf{\Phi}$ alone, and not $\bar{\mathbf{\Phi}}$ [2]. Thus, one doublet is required to give mass to the up-type fermions, H_u, and a second one for the down-type fermions and leptons, H_d.

Finally, each gauge boson of the SM is part of a *vector superfield*, which includes a fermionic supersymmetric partner, the 'gauginos' (gluinos for $SU(3)$, winos for $SU(2)$ and binos associated to $U(1)$). As the gauge bosons, the gauginos transform in the adjoint representation of their associated gauge group.

[2] functions of chiral and antichiral superfields (i.e. complex conjugate chiral superfields) are *vector* superfields.

2.2 Lagrangian

In the framework of softly broken supersymmetry, once one has specified the gauge symmetries and the chiral superfields of a model, the Lagrangian is specified by the superpotential and the soft supersymmetry breaking terms. In the following we consider the R-parity and CP-conserving MSSM. The corresponding superpotential is given by:

$$W_{\rm MSSM} = \mu \hat{H}_u \cdot \hat{H}_d + y_u \hat{Q} \cdot \hat{H}_u \hat{U}^c_R + y_d \hat{H}_d \cdot \hat{Q} \hat{D}^c_R + y_e \hat{H}_d \cdot \hat{L} \hat{E}^c_R \tag{2.3}$$

where the "$\cdot$" denotes the $SU(2)$ product, and the yukawa couplings y_u, y_d and y_e and the superfields $\hat{Q}, \hat{U^c_R}, \hat{D^c_R}, \hat{E^c_R}$ and $\hat{L}$ should be interpreted as matrices and vectors in family space. The first term in (2.3) is the infamous μ term, about which we will discuss later, and is responsible for the higgsinos masses. The other three terms give rise to the usual Yukawa terms that generate the fermion masses, but also include interactions between fermions and sfermions and contributions to the scalar potential (sfermion-sfermion interactions). Recall that, unlike the dimensionless Yukawa terms y_u, y_d and y_e, μ has dimensions of mass and is the only dimensionful parameter of the purely supersymmetric part of the MSSM lagrangian.

The soft supersymmetry breaking terms are included in the lagrangian of the model to explicitly break the unobserved mass degeneracy between particles and their superpartners. In this sense, soft-SUSY broken models such as the MSSM should be regarded as a low-energy limit of an underlying model where SUSY is an exact symmetry, but it is broken spontaneously at a given scale M_{SUSY}. Thus, the soft SUSY breaking part of the lagrangian is just a parametrization of the leftovers of an underlying theory after spontaneous symmetry breaking, just as the fermion mass terms in the SM after electroweak symmetry breaking. The corresponding MSSM soft SUSY breaking couplings and masses are:

$$\begin{aligned} -\mathcal{L}^{\rm soft}_{\rm MSSM} \;=\; & \frac{1}{2}\left(M_3 \tilde{g}\tilde{g} + M_2 \tilde{w}_a \tilde{w}_a + M_1 \tilde{b}\tilde{b}\right) \\ & + (y_u A_u Q \cdot H_u U^c - y_d A_d Q \cdot H_d D^c_R - y_e A_e L \cdot H_d E^c_R + \text{h.c.}) \\ & + m^2_L |L|^2 + m^2_E |E_R|^2 + m^2_Q |Q|^2 + m^2_U |U_R|^2 + m^2_D |D_R|^2 \\ & + m^2_{H_u} |H_u|^2 + m^2_{H_d} |H_d|^2 + B\mu (H_u \cdot H_d + \text{h.c.}). \end{aligned} \tag{2.4}$$

M_3, M_2 and M_1 are the gluino, wino and bino mass terms. The trilinear couplings A_u, A_d and A_e are 3×3 matrices in family space with dimensions of mass, and are in one-to-one correspondence with the yukawa couplings of the superpotential (2.3). The mass terms $m^2_U, m^2_D, m^2_Q, m^2_E, m^2_L$ are also 3×3 matrices in family space, and should be hermitian in order to render the lagrangian real. The last term in (2.4) are the soft-SUSY breaking contributions to the Higgs potential. Although

in principle all these parameters are complex, most of them can be rendered real through field redefinitions to absorb their complex phase. Those having still the possibility of being complex are assumed to be real, restricting ourselves to the CP-conserving MSSM.

Before introducing the soft-SUSY breaking lagrangian (2.4), the purely supersymmetric superpotential (2.3) hardly introduces new free parameters with respect to the SM: only the complex parameter μ. On the other hand, the soft SUSY breaking terms are a priori not fixed in the MSSM, leaving us with 105 new free parameters [8] which introduce a huge arbitrariness in the model.

2.3 Higgs sector and electroweak symmetry breaking

With the lagrangian introduced, let us focus now on the Higgs sector and the mechanism of electroweak symmetry breaking.

We start our discussion deriving the expression for the scalar potential V. The Higgs part of the superpotential (2.3) is:

$$W_{Higgs}^{\text{MSSM}} = \mu \hat{H}_u \cdot \hat{H}_d, \tag{2.5}$$

and the corresponding soft SUSY breaking term (we write only the ones involving the Higgs fields):

$$\mathcal{L}_{Soft}^{\text{MSSM}} = -m_{H_u}^2 H_u^* H_u - m_{H_d}^2 H_d^* H_d - B\mu(H_u H_d + \text{h.c.}). \tag{2.6}$$

This leaves us with a Higgs potential for the MSSM given by:

$$V = \overbrace{V_F + V_D}^{V_{SUSY}} + V_{soft} \tag{2.7}$$

where V_F and V_D are the F- and D-terms obtained from the Higgs superpotential (2.5)[3], and V_{soft} is the Higgs scalar potential from the soft SUSY lagrangian. Let us analyze each term of the scalar potential (2.7):

- The F-term is given by the auxiliary fields F_i:

$$V_F = \sum_i |F_i|^2. \tag{2.8}$$

[3]For a comprehensive review on supersymmetry and the mathematical apparatus behind these results, we refer the reader to [9].

We can obtain algebraically the expression for the auxiliary fields F_i from the equations of motion:

$$F^*_{H_{u_i}} = \mu\epsilon_{ij}H^j_d, \quad F^*_{H_{d_i}} = \mu\epsilon_{ij}H^j_u \tag{2.9}$$

Hence the F-term reads

$$V_F = |\mu|^2\Big(|H_u|^2{+}|H_d|^2\Big) \tag{2.10}$$

- The D-term, associated to the auxiliary fields D of the gauge vector superfields:

$$V_D = \frac{1}{2}D_Y^2 + \sum_{a=1}^{3}\frac{1}{2}D_a^2 \tag{2.11}$$

and again, from the equations of motion for the auxiliary gauge fields D:

$$D_Y = -g_1\sum_i(Y_i|A_i|^2) = \frac{g_1}{2}\left(|H_d|^2{-}|H_u|^2\right) \tag{2.12}$$

$$D_a = g_2\sum_i A^\dagger\frac{\tau^a}{2}A_i \tag{2.13}$$

where $A_i = H_u, H_d$ are the scalar Higgs multiplets, τ^a are the Pauli matrices and g_1 and g_2 are the gauge couplings. One has:

$$V_D = \frac{g_1^2+g_2^2}{8}\left(|H_u|^2{-}|H_d|^2\right)^2 + \frac{g_2^2}{2}\left(|H_u|^2|H_d|^2{-}|H_u\epsilon H_d|^2\right) \tag{2.14}$$

where the antisymmetric tensor ϵ rises and lowers $SU(2)$ indices.

- The soft SUSY breaking term is given by:

$$V_{soft} = m^2_{H_u}|H_u|^2{+}m^2_{H_d}|H_d|^2{+}(B\mu(H_u\epsilon H_d) + h.c.) \tag{2.15}$$

Putting all the pieces together we have:

$$V = \frac{g_1^2+g_2^2}{8}\left(|H_u|^2{-}|H_d|^2\right)^2 + \frac{g_2^2}{2}\left(|H_u|^2|H_d|^2{-}|H_u\epsilon H_d|^2\right) + \tag{2.16}$$

$$(m^2_{H_u}+|\mu|^2)|H_u|^2{+}(m^2_{H_d}+|\mu|^2)|H_d|^2{+}(B\mu(H_u\epsilon H_d) + h.c.), \tag{2.17}$$

expanding the SU(2) doublets,

$$H_u = \begin{pmatrix} H_u^+ \\ H_u^0 \end{pmatrix}, \qquad H_d = \begin{pmatrix} H_d^0 \\ H_d^- \end{pmatrix}, \tag{2.18}$$

the final expression for the scalar potential V reads:

$$\begin{aligned} V = \; & \frac{g_1^2+g_2^2}{8}\left(|H_u^0|^2+|H_u^+|^2-|H_d^0|^2-|H_d^-|^2\right)^2 + \frac{g_2^2}{2}\left|H_u^{+*}H_d^0 - H_u^{0*}H_d^-\right|^2 + \\ & (m_{H_u}^2+|\mu|^2)(|H_u^+|^2+|H_u^0|^2) + (m_{H_d}^2+|\mu|^2)(|H_d^0|^2+|H_d^-|^2) \\ & +(B\mu(H_u^+H_d^- - H_u^0H_d^0) + h.c.). \end{aligned} \tag{2.19}$$

We are now interested in finding a minimum of this potential such that it breaks electroweak symmetry down to electromagnetism $SU(2)_L \times U(1)_Y \to U(1)_{EM}$. Note that we can perform a $SU(2)$ gauge transformation to set $\langle H_u^+\rangle = 0$[4], and hence $\langle H_u\rangle = v_u$ is in the direction of the neutral component, and can be taken real and positive. Also, we see that $\langle H_u^+\rangle = 0$ implies that V_D has the minimum at $\langle H_d^-\rangle = 0$. The $B\mu$ term is the only term which depends on the global phases of the fields, so we can absorb any phase of $B\mu$ into a field redefinition, and we have $B\mu$ real and positive. Since $H_u^0H_d^0$ must be real and positive, $\langle H_u^0\rangle$ and $\langle H_d^0\rangle$ must have opposite phases. We can therefore remove these phases by a $U(1)_Y$ gauge transformation since $Y_{H_u} = -Y_{H_d}$, and then we have the VEVs all real and positive. It follows that CP cannot be spontaneously broken by the Higgs scalar potential since the VEVs and $B\mu$ can be simultaneously be chosen to be real. This implies that the Higgs scalar mass eigenstates can be assigned well defined eigenvalues of CP (at least at tree level).

The minimum of the potential occurs at

$$\begin{aligned} V_{min} \; = \; & \frac{g_1^2+g_2^2}{8}\left(v_u^2-v_d^2\right)^2 + \\ & (m_{H_u}^2+|\mu|^2)(v_u^2) + (m_{H_d}^2+|\mu|^2)(v_d^2) - (B\mu v_u v_d) \\ & \frac{1}{2}\begin{pmatrix} v_u & v_d \end{pmatrix} M^2 \begin{pmatrix} v_u \\ v_d \end{pmatrix} + \frac{g_1^2+g_2^2}{8}\left(v_u^2-v_d^2\right)^2 \end{aligned} \tag{2.20}$$

where $v_u = \langle H_u^0\rangle$,$v_d = \langle H_d^0\rangle$ and

$$M^2 = \begin{pmatrix} m_{H_u}^2 & -B\mu \\ -B\mu & m_{H_d}^2 \end{pmatrix}. \tag{2.21}$$

Vacuum stability requires that the potential is bounded from below when $\phi \to \infty$ for all orientations of the vector $\phi = (H_u, H_d)$. A straight forward analysis shows as that this condition holds if

$$m_{H_u}^2 + m_{H_d}^2 > 2B\mu \tag{2.22}$$

[4]From here onwards, we denote by $\langle H\rangle$ the vacuum expectation value (VEV) of a field H, i.e. its expected value at the minimum of the potential.

is satisfied. Electroweak symmetry breaking requires that the origin is not a minimum, i.e. the determinant of M^2 should be strictly negative;

$$\det M^2 < 0 \quad \Rightarrow \quad m_{H_u}^2 m_{H_d}^2 < (B\mu)^2. \tag{2.23}$$

Provided that (2.22) and (2.23) are satisfied, the conditions for v_u and v_d to be at the minimum are given by $\partial V_{min}/\partial v_u = 0$, $\partial V_{min}/\partial v_d = 0$:

$$\frac{g_1^2+g_2^2}{4} v_u(v_u^2 - v_d^2) + 2v_u(m_{H_u}^2 + |\mu|^2) - 2B\mu v_d = 0 \tag{2.24}$$

$$-\frac{g_1^2+g_2^2}{4} v_d(v_u^2 - v_d^2) + 2v_d(m_{H_d}^2 + |\mu|^2) - 2B\mu v_u = 0 \tag{2.25}$$

It is convenient to define:

$$g^2 = \frac{g_1^2+g_2^2}{2} \tag{2.26}$$

and

$$v_d = v\cos\beta \qquad v_u = v\sin\beta, \qquad \tan\beta = \frac{v_u}{v_d} \tag{2.27}$$

where $v^2 \equiv |v_u|^2 + |v_d|^2 = 1/(2\sqrt{2}G_F) \sim 174$ GeV. The minimization equations become:

$$m_{H_d}^2 + |\mu|^2 - B\mu\tan\beta + \frac{M_Z^2}{2}\cos(2\beta) = 0 \tag{2.28}$$

$$m_{H_u}^2 + |\mu|^2 - B\mu\cot\beta - \frac{M_Z^2}{2}\cos(2\beta) = 0 \tag{2.29}$$

where $M_Z^2 = \dfrac{v^2 g^2}{4}$ is the mass of the Z gauge boson. Combining (2.28), (2.29) and using trigonometric identities $\cot(\beta) + \tan(\beta) = 2\csc(2\beta)$ and $\tan\beta = \dfrac{\sin 2\beta}{\cos 2\beta + 1}$, we find:

$$M_Z^2 = \frac{|m_{H_d}^2 - m_{H_u}^2|}{\sqrt{1-\sin^2(2\beta)}} - m_{H_u}^2 - m_{H_d}^2 - 2|\mu|^2 \tag{2.30}$$

$$\sin(2\beta) = \frac{2B\mu}{m_{H_d}^2 + m_{H_u}^2 + 2|\mu|^2}. \tag{2.31}$$

These equations relate the vev v to the soft SUSY breaking parameters. We see that the realisation of electroweak symmetry breaking implies a relation between the supersymmetric term μ and the soft SUSY breaking terms.

2.3.1 Mass spectrum of the Higgs sector

In order to analyse the mass spectra, we expand the fields around the VEVs (unitary gauge) and decompose the neutral fields in its hermitian components;

$$H_u = \begin{pmatrix} H_u^+ \\ v_u + \frac{1}{\sqrt{2}}(H_{u,r}^0 + iH_{u,i}^0) \end{pmatrix}, \qquad H_d = \begin{pmatrix} v_d + \frac{1}{\sqrt{2}}(H_{d,r}^0 + iH_{d,i}^0) \\ H_d^- \end{pmatrix} \tag{2.32}$$

We can also replace $m_{H_d}^2$ and $m_{H_u}^2$ in the scalar potential (2.19) in favour of $\tan\beta$ and v_u and v_d using the minimization conditions. Thus, one can easily read the mass matrices from the potential by taking derivatives:

- **The CP-odd mass matrix** The CP-odd mass matrix is composed by the imaginary components of the neutral complex Higgs fields H_u^0 and H_d^0. This matrix is a 2×2 real matrix. In the $\left(H_{d,i}^0, H_{u,i}^0\right)$ it takes the form:

$$\mathcal{M}_P^2 = \begin{pmatrix} \frac{\partial^2 V}{\partial H_{d,i}^0 \partial H_{d,i}^0} & \frac{\partial^2 V}{\partial H_{d,i}^0 \partial H_{u,i}^0} \\ \frac{\partial^2 V}{\partial H_{u,i}^0 \partial H_{d,i}^0} & \frac{\partial^2 V}{\partial H_{u,i}^0 \partial H_{u,i}^0} \end{pmatrix} \tag{2.33}$$

$$\Rightarrow \mathcal{M}_P^2 = \begin{pmatrix} \mu B \tan\beta & \mu B \\ \mu B & \mu B \cot\beta \end{pmatrix} \tag{2.34}$$

  By computing the determinant of this matrix, we realize that $\det(M_P^2) = 0$. Thus, there is a (real) Goldstone mode living here, which will become the longitudinal component of the Z boson after spontaneous symmetry breaking (SSB). The non vanishing eigenvalue is given by the trace of M_P^2 (since the trace is conserved after rotating the matrix to its diagonal form):

$$M_A^2 = \frac{2\mu B}{\sin 2\beta} \tag{2.35}$$

  and it constitutes the only CP-odd physical scalar field of the Higgs sector of the MSSM.

- **The CP-even mass matrix** The CP-even mass matrix is composed by the real components of the neutral complex Higgs fields H_u^0 and H_d^0. It is a 2×2 real matrix, which in the $\left(H_{d,r}^0, H_{u,r}^0\right)$ takes the form:

$$\mathcal{M}_S^2 = \begin{pmatrix} \frac{\partial^2 V}{\partial H_{d,r}^0 \partial H_{d,r}^0} & \frac{\partial^2 V}{\partial H_{d,r}^0 \partial H_{u,r}^0} \\ \frac{\partial^2 V}{\partial H_{u,r}^0 \partial H_{d,r}^0} & \frac{\partial^2 V}{\partial H_{u,r}^0 \partial H_{u,r}^0} \end{pmatrix} \tag{2.36}$$

$$\Rightarrow \mathcal{M}_S^2 = \begin{pmatrix} g^2 v_d^2 + \mu B \tan\beta & -g^2 v_u v_d - \mu B \\ -g^2 v_u v_d - \mu B & g^2 v_u^2 + \mu B \cot\beta \end{pmatrix} \tag{2.37}$$

This matrix has two different non vanishing eigenvalues corresponding to the two neutral CP-even Higgs particles of the theory. They are:

$$M_{H,h}^2 = \frac{1}{2}\left(M_A^2 + M_Z^2 \pm \sqrt{\left(M_A^2 + M_Z^2\right)^2 - 4M_A^2 M_Z^2 \cos^2 2\beta}\right) \tag{2.38}$$

- **The charged mass matrix** The mass matrix containing the two complex scalar Higgs fields H_u^+ and H_d^- is given by the 2×2 complex matrix (in the basis $(H_d^-,\, H_u^+)$):

$$\mathcal{M}_{H^\pm}^2 = \begin{pmatrix} \dfrac{\partial^2 V}{\partial H_d^- \partial H_d^-} & \dfrac{\partial^2 V}{\partial H_d^- \partial H_u^+} \\ \dfrac{\partial^2 V}{\partial H_u^+ \partial H_d^-} & \dfrac{\partial^2 V}{\partial H_u^+ \partial H_u^+} \end{pmatrix} \tag{2.39}$$

$$\Rightarrow \mathcal{M}_{H^\pm}^2 = \begin{pmatrix} \left(\dfrac{g_2^2}{2} v_u v_d + \mu B\right)\tan\beta & \dfrac{g_2^2}{2} v_u v_d + \mu B \\ \dfrac{g_2^2}{2} v_u v_d + \mu B & \left(\dfrac{g_2^2}{2} v_u v_d + \mu B\right)\cot\beta \end{pmatrix} \tag{2.40}$$

This matrix has a zero eigenvalue, i.e. a (complex) charged Goldstone boson, which will be 'eaten' by the W boson after SSB. The remaining Higgs mass is

$$M_{H^\pm} = M_A^2 + M_W^2 \tag{2.41}$$

Rotating the Higgs mass matrices: Higgs basis and the decoupling limit

We are now interested in rotating these matrices by a certain angle so they become diagonal, i.e. we want to find the rotation matrices such that give us the physical Higgs particle content of the theory. First of all, we can rewrite the matrices $\mathcal{M}_P^2$, $\mathcal{M}_S^2$ and $\mathcal{M}_{H^\pm}^2$ in a more convenient way:

$$\mathcal{M}_P^2 = \frac{1}{2} M_A^2 \sin 2\beta \begin{pmatrix} \tan\beta & 1 \\ 1 & \cot\beta \end{pmatrix} \tag{2.42}$$

$$\mathcal{M}_S^2 = \frac{1}{2} M_A^2 \sin 2\beta \begin{pmatrix} \tan\beta & -1 \\ -1 & \cot\beta \end{pmatrix} + \frac{1}{2} M_Z^2 \sin 2\beta \begin{pmatrix} \cot\beta & -1 \\ -1 & \tan\beta \end{pmatrix} \tag{2.43}$$

$$\mathcal{M}_{H^\pm}^2 = \frac{1}{2} M_A^2 \sin 2\beta \begin{pmatrix} \tan\beta & 1 \\ 1 & \cot\beta \end{pmatrix} \tag{2.44}$$

It is easy to check that the CP-odd matrix $\mathcal{M}_P^2$ is diagonalized by rotating it by an angle $-\beta$ given in (2.31). Clearly, $\mathcal{M}_{H^\pm}^2$ has exactly the same form of $\mathcal{M}_P^2$ so it is diagonalized by the same angle. On the other hand, $\mathcal{M}_S^2$ has two different contributions, one proportional to the mass of the CP-odd neutral Higgs A and the other to the mass of the Z boson. The corresponding mixing angle α which diagonalize this matrix is given, in the basis $(H_u, H_d, S) \to (h, H)$ by:

$$\cos^2(\beta - \alpha) = \frac{M_h^2 \left(M_Z^2 - M_h^2\right)}{M_A^2 \left(M_H^2 - M_h^2\right)} \tag{2.45}$$

Thus, the neutral gauge eigenstate fields can be expressed in terms of the mass eigenstates by using these rotation matrices:

$$\begin{pmatrix} H_d^0 \\ H_u^0 \end{pmatrix} = \begin{pmatrix} v_d \\ v_u \end{pmatrix} + \frac{1}{\sqrt{2}} R^{-1}(\alpha) \begin{pmatrix} h \\ H \end{pmatrix} + \frac{i}{\sqrt{2}} R^{-1}(\beta) \begin{pmatrix} G \\ A \end{pmatrix} \tag{2.46}$$

where G is the corresponding neutral Goldstone boson. The explicit form of the orthogonal rotation matrices is:

$$R^{-1}(\alpha) = \begin{pmatrix} \cos\alpha & \sin\alpha \\ -\sin\alpha & \cos\alpha \end{pmatrix} \tag{2.47}$$

Thus, the physical states are expressed in terms of the gauge eigenstates by the following expressions:

- for the CP-even mass states:

$$h = \cos\alpha H_{u,r} + \sin\alpha H_{d,r} \tag{2.48}$$
$$H = -\sin\alpha H_{u,r} + \cos\alpha H_{d,r}. \tag{2.49}$$

- the CP-odd state is simply

$$A = \cos\beta A_{u,i} + \sin\beta A_{d,i} \tag{2.50}$$

- the charged Higgs boson:

$$H^\pm = \cos\beta H_u^\pm + \sin\beta H_d^\pm \tag{2.51}$$

- and finally the neutral and charged goldston bosons:

$$G = -\sin\beta A_{u,i} + \cos\beta A_{d,i} \tag{2.52}$$
$$G^\pm = -\sin\beta H_u^\pm + \cos\beta H_d^\pm \tag{2.53}$$

Although the masses of the Higgs bosons are not known a priori (as they depend on the free parameters of the theory), we see from (2.38) that the two eigenvalues for the CP-even states (where the 125 GeV boson should live) are bounded by M_Z and M_A respectively. From current experimental data, and the fact that M_A is given by the soft SUSY breaking terms, we expect $M_A > M_Z$. Thus, it is interesting to analyse the case where the mass gap between H and h is large;

$$M_A^2 \gg M_Z^2. \tag{2.54}$$

From the expressions for the masses given above we find that this limits implies, at first order in $\frac{M_Z}{M_A}$:

$$M_H^2 \sim M_A^2 \sim M_{H^\pm}^2 \tag{2.55}$$
$$M_h^2 \sim M_Z^2 \cos^2 2\beta \tag{2.56}$$

i.e. the masses of the heavy bosons are degenerate: they form $SU(2)$ isospin doublets of degenerate mass, whereas the light h remains light, bounded at tree-level by M_Z. The mixing CP-even angle α can be obtained from (2.45). Indeed, taking $M_A^2 \ll M_Z^2$, (2.45) vanishes and thus we have $\alpha = \beta$. A further analysis of the lagrangian shows us that the fields h' and H' defined by the rotation $(H_{u,r}, H_{d,r}) \xrightarrow{R(\beta)} (h', H')$ are such that h' has the same couplings of a SM Higgs, whereas H' is decoupled form the vector bosons. This limit is known as the *decoupling limit*, and the basis defined by a rotation β in the CP-even Higgs field space is called the *Higgs basis*, since h' couples to SM matter as the SM Higgs does.

This basis is very useful as current experimental data suggest that the 125 GeV resonance found at the LHC has properties very close to the ones expected from a SM Higgs, and thus $h' \sim h$.

2.4 Limitations and extensions of the MSSM

2.4.1 The SM Higgs mass

Recall that the masses of A, H and $H^\pm$ can be in principle arbitrarily large since they all grow with $\mu B/\sin(2\beta)$. On the other hand, the mass of h is bounded above by (from eq. (2.38))

$$M_h^2 < M_Z^2 \cos^2 2\beta < 91 \text{ GeV} \tag{2.57}$$

at tree level. This bound is phenomenologically worrisome, as Higgs searches at LEP would have discovered such a boson [10]. The LHC finally measured a scalar particle compatible with the SM Higgs boson [1, 2] at $m_h \approx 125$ GeV,

raising tension between data and the MSSM prediction (2.57). However, there exist potentially large radiative corrections ΔM_h^2 for this mass [11], dominated by the top quark loop and its two superpartners, the stops. These are given by:

$$\Delta M_h^2 = \frac{3m_t^4}{4\pi^4 v^2}\left(\ln\left(\frac{m_{\tilde{t}}^2}{m_t^2}\right) + \frac{X_t^2}{m_{\tilde{t}}}\left(1 - \frac{X_t^2}{12m_{\tilde{t}^2}}\right)\right), \tag{2.58}$$

where $m_{\tilde{t}}$ is the soft-SUSY stops mass term and X_t is the stop mixing parameter, defined as $X_t = A_t - \mu\cot\beta$. After taking into account these corrections, the bound (2.57) is pushed up to

$$M_h^2 = M_{h,tree}^2 + \Delta M_h^2(m_t, m_{\tilde{t}}) \lesssim 130 \text{ GeV} \tag{2.59}$$

and therefore compatible with the measured value. Nonetheless, the MSSM stop sector requires certain tuning of the masses and mixing parameters in order to accommodate $m_h \approx 125$ GeV [12], which is very near the actual theoretical bound (2.59). This necessity to adjust the parameters to reproduce the Higgs mass reintroduce a fine-tuning problem, called "*the little fine tuning problem*" [12, 13]. Although it is many orders of magnitude less severe than the original hierarchy puzzle presented in chapter 1, it turns out that the MSSM suffers a problem of the same nature that the one that it was meant to solve.

2.4.2 The μ problem

Recall that the only dimensionful parameter introduced in the pure supersymmetric lagrangian is the μ mass term appearing in the superpotential (2.3). If one would have to bet for a value for μ (without knowing about the present phenomenological constraints), probably a natural value for μ would be at the order of either the Grand Unification (GUT) scale $\sim \Lambda_{GUT}$ or Planck scale $\sim \Lambda_{Planck}$, if again we regard the theory as a low energy EFT of an underlying most fundamental (maybe quantum gravity) theory. On the other hand we have many other dimensionful parameters in the full lagrangian $\mathcal{L} = \mathcal{L}^{\text{SUSY}} + \mathcal{L}^{\text{soft}}$, but they have a completely different origin since they are (soft-) SUSY breaking terms, coming from some unknown SUSY breaking mechanism. Hence, we have two different scales appearing in the lagrangian; μ (in principle defined at an unknown scale which could be anywhere) and M_{SUSY} (which is naturally placed at the TeV scale). This is already disturbing.

Indeed, in the full Higgs potential we find that the mass parameter of the Higgs scalars is

$$V_{\text{Higgs}}^{\text{MSSM}} = (\overbrace{|\mu|^2}^{\mathcal{O}(?)} + \overbrace{m_{H_u}^2}^{\mathcal{O}(M_{\text{SUSY}})})(|H_u^0|^2 + |H_u^+|^2) + \dots \tag{2.60}$$

Ultimately $|\mu|^2+m_{H_u}^2$ provides a value for the Higgs VEV which generate the electroweak scale, and the expression above implies that M_{SUSY} is not the only scale requiring an explanation for why M_Z is far below the M_{Planck}, but also μ. One possible way out is to argue that μ actually vanishes due to some unknown extra symmetry. However, doing such a thing faces several problems:

- Phenomenological constraint: Due to the fruitless searches for charginos at LEP, actually not only μ is needed but it has to satisfy $\mu \gtrapprox 100$ GeV.
- $\mu = 0$ enlarges the symmetry of the system introducing a Peccei-Quinn symmetry in the Higgs sector and hence an unacceptable massless axion [14].

So with $\mu = 0$ excluded, one can realize that $|\mu|$ cannot be too large neither, since the Higgs potential must be unstable at its origin ($H_u = H_d = 0$) in order to generate the electroweak SSB. With μ only having positive contributions in (2.60), it must not dominate, but instead must satisfy $|\mu| \lessapprox M_{\mathrm{SUSY}}$. Hence, with both 'natural' values for μ ruled out (i.e. 0 or M_{GUT}), it seems that μ must accidentally take a precise value at the M_{SUSY} scale, and the need for an explanation for this is the μ-problem.

Chapter 3

The Next to Minimal Supersymmetric Standard Model (NMSSM)

3.1 Why the NMSSM?

We finished our presentation of the MSSM pointing out its theoretical 'weaknesses', particularly emphasising the μ-problem. Although explanations for the μ parameter have been proposed within the context of the MSSM [15] under certain assumptions, the NMSSM offers an elegant solution to this problem, by means of a mechanism analogous to the Higgs mechanism that gives masses to the fermions in the SM. In the framework of the NMSSM, the μ term is generated dynamically by the vev of a SM-singlet field $\hat{S}$, which is naturally generated at the SUSY scale M_{SUSY}.

The NMSSM matter content thus is the same as the MSSM one, with the only inclusion of a singlet superfield $\hat{S}$.

3.2 Lagrangian

Instead of working with the most general lagrangian that could be obtained by including one singlet superfield to the MSSM superpotential, we restrict ourselves in this thesis to the so-called $\mathbb{Z}_3$-invariant NMSSM [16]. In this context, the superpotential must remain invariant under the discrete rotation of the superfields by a phase $\mathbf{\Phi} \to e^{\frac{2i\pi}{3}}\mathbf{\Phi}$. As a consequence the remaining superpotential has no dimensionful parameters (thus avoiding a possible reintroduction of a μ-like problem).

The superpotential reads:

$$\begin{aligned} W_{\rm MSSM} &= \lambda \hat{S}\hat{H}_u \cdot \hat{H}_d + \kappa \frac{\hat{S}^3}{3} \\ &\quad + y_u \hat{Q} \cdot \hat{H}_u \hat{U}^c_R + y_d \hat{H}_d \cdot \hat{Q}\hat{D}^c_R + y_e \hat{H}_d \cdot \hat{L}\hat{E}^c_R. \end{aligned} \tag{3.1}$$

Then, a VEV s of $\hat{S}$ of the order of the weak or SUSY breaking scale generates an effective μ term:

$$\mu_{\rm eff} = \lambda s \tag{3.2}$$

solving the μ problem of the MSSM. As expected, new terms appear in the soft SUSY breaking part of the lagrangian, notably a mass term for the singlet scalar as well as trilinear couplings with the doublets and the singlet itself:

$$\begin{aligned} -\mathcal{L}^{\rm soft}_{\rm NMSSM} &= \frac{1}{2}\left(M_3 \tilde{g}\tilde{g} + M_2 \tilde{w}_a \tilde{w}_a + M_1 \tilde{b}\tilde{b}\right) \\ &\quad + m_L^2 |L|^2 + m_E^2 |E_R|^2 + m_Q^2 |Q|^2 + m_U^2 |U_R|^2 + m_D^2 |D_R|^2 \\ &\quad + m_{H_u}^2 |H_u|^2 + m_{H_d}^2 |H_d|^2 + m_S^2 |S|^2 \\ &\quad + (y_u A_u Q \cdot H_u U^c - y_d A_d Q \cdot H_d D^c_R - y_e A_e L \cdot H_d E^c_R \\ &\quad + \lambda A_\lambda H_u \cdot H_d S + \frac{1}{3}\kappa A_\kappa S^3 + \text{h.c.}) \end{aligned} \tag{3.3}$$

As we will see below, the soft SUSY breaking terms, expected to be at the order of the TeV scale, are the only dimensionful terms appearing in the minimization equations. Thus, the soft SUSY breaking scale $M_{\rm SUSY}$ is the only scale of the theory, and the electroweak symmetry breaking can be regarded as a direct consequence of supersymmetry breaking.

3.3 The Higgs sector and EWSB

The electroweak symmetry breaking mechanism is realised in a very similar fashion as in the MSSM - through the vevs of the Higgs doubles v_u and v_d. The Higgs part of the superpotential in the NMSSM is

$$W_{Higgs} = \lambda \hat{S}\hat{H}_u \cdot \hat{H}_d + \frac{\kappa^3}{3}\hat{S}^3 \tag{3.4}$$

where $\hat{S}$ is the chiral superfield for the singlet, which has SM quantum numbers $(1, 1, 0)$. The soft SUSY breaking lagrangian (involving the Higgs fields alone) reads:

$$\mathcal{L}^{\rm MSSM}_{Soft} = -m_{H_u}^2 |H_u|^2 m_{H_d}^2 |H_d|^2 - m_S^2 |S|^2 - \left(\lambda A_\lambda H_u \cdot H_d S + \frac{1}{3}\kappa A_\kappa S^3 + \text{h.c}\right) \tag{3.5}$$

Then, from the SUSY gauge interactions, the F and D terms, and the soft SUSY breaking terms one obtains the Higgs potential:

$$\begin{aligned} V &= |\lambda\left(H_u^+ H_d^- - H_u^0 H_d^0\right) + \kappa S^2|^2 \\ &+ \left(m_{H_u}^2 + \lambda|S|^2\right)\left(|H_u^0|^2+|H_u^+|^2\right) + \left(m_{H_d}^2 + \lambda|S|^2\right)\left(|H_d^0|^2+|H_d^-|^2\right) \\ &\frac{g_1^2+g_2^2}{8}\left(|H_u^0|^2+|H_u^+|^2-|H_d^0|^2-|H_d^-|^2\right)^2 + \frac{g_2^2}{2}|H_u^+ H_d^{0*} + H_u^0 H_d^{-*}|^2 \\ &+ m_S^2|S|^2 + \left(\lambda A_\lambda (H_u^+ H_d^- - H_u^0 H_d^0) S + \frac{1}{3}\kappa A_\kappa S^3 + \text{h.c.}\right) \end{aligned} \tag{3.6}$$

we proceed exactly in the same way that we did for the MSSM: the neutral Higgs fields are obtained by expanding the full scalar potential around the vevs v_u, v_d and s (which can be taken to be real and positive),

$$H_u = \begin{pmatrix} H_u^+ \\ H_u^0 = v_u + \frac{1}{\sqrt{2}}(H_{u,r}^0 + iH_{u,i}^0) \end{pmatrix}, \qquad H_d = \begin{pmatrix} H_d^0 = v_d + \frac{1}{\sqrt{2}}(H_{d,r}^0 + iH_{d,i}^0) \\ H_d^- \end{pmatrix} \tag{3.7}$$

$$S = s + \frac{1}{\sqrt{2}}(S_r + iS_i) \tag{3.8}$$

so one is left to consider the minima of

$$\begin{aligned} V_{min} &= (-\lambda v_u v_d + \kappa s^2)^2 + \frac{g_1^2+g_2^2}{8}(v_u^2 - v_d^2)^2 \\ &+ (m_{H_u}^2 + \lambda s^2)v_u^2 + (m_{H_d}^2 + \lambda s^2)v_d^2 \\ &+ m_S^2 s^2 - 2\lambda A_\lambda v_u v_d s + \frac{2}{3}\kappa A_\kappa s^3. \end{aligned} \tag{3.9}$$

By field redefinitions, we find that λ, v_u and v_d can be taken to be real and positive, whereas κ and s can have both signs.

In order to follow the analogy with the MSSM, it is convenient to define:

$$B_{\text{eff}} = A_\lambda + \kappa s \tag{3.10}$$

Note that B_{eff} and μ_{eff} play the role of the MSSM-like B and μ parameters respectively.

Therefore we have three minimisation equations instead of two, namely $\frac{\partial V}{\partial v_u} = 0$, $\frac{\partial V}{\partial v_d} = 0$ and $\frac{\partial V}{\partial s} = 0$. They are:

$$v_u\left(m_{H_u}^2 + \mu_{\text{eff}}^2 + \lambda^2 v_d^2 + \frac{g_1^2+g_2^2}{4}(v_u^2 - v_d^2)\right) - v_d B_{\text{eff}}\mu_{\text{eff}} = 0 \quad (3.11)$$

$$v_d\left(m_{H_d}^2 + \mu_{\text{eff}}^2 + \lambda^2 v_u^2 - \frac{g_1^2+g_2^2}{4}(v_u^2 - v_d^2)\right) - v_u B_{\text{eff}}\mu_{\text{eff}} = 0 \quad (3.12)$$

$$s\left(m_S^2 + \kappa A_\kappa s + 2\kappa^2 s^2 + \lambda^2(v_u^2 + v_d^2) - 2\lambda\kappa v_u v_d\right) - \lambda v_u v_d A_\lambda = 0 \quad (3.13)$$

The first two equations are of the same form of the minimisation equations in the MSSM (2.24) and (2.25). We define, as usual,

$$v_d = v\cos\beta, \qquad v_u = v\sin\beta, \qquad \tan\beta = \frac{v_u}{v_d}. \quad (3.14)$$

Combining these first two minimization equations, one arrives to the expressions:

$$M_Z^2 = \frac{m_{H_u}^2 - m_{H_d}^2}{\cos 2\beta} - m_{H_u}^2 - m_{H_d}^2 - 2\mu_{\text{eff}}^2, \quad (3.15)$$

and

$$\sin 2\beta = \frac{2\mu B_{\text{eff}}}{m_{H_d}^2 + m_{H_u}^2 + 2\mu_{\text{eff}}^2 + \lambda^2 v^2} \quad (3.16)$$

From the expression above, the parameter μ_{eff} is situated at the electroweak scale, and it is required to be above $\sim$ 100 GeV due to the constraints on chargino searches at LEP [17], and not much larger than M_Z to avoid large cancellations in 3.15.

The third minimisation equation can be solved algebraically for s.

3.3.1 Mass spectrum of the Higgs sector

In order to analyse the mass spectra, we expand the fields around the VEVs in the unitary gauge (3.7). Recall that once the soft Higgs mases are expressed in terms of M_Z, $\tan\beta$ and s, the Higgs sector of the NMSSM at tree level is described by a total of six parameters,

$$\lambda, \quad \kappa, \quad \tan\beta, \quad \mu_{\text{eff}} = \lambda s, \quad A_\lambda \quad \text{and} \quad A_\kappa. \quad (3.17)$$

- **The CP-odd mass matrix** in the $(H_{d,i}, H_{u,i}, S_i)$ basis reads:

$$\mathcal{M}_P'^2 = \begin{pmatrix} \mu_{\text{eff}}B_{\text{eff}}\tan\beta & \mu_{\text{eff}}B_{\text{eff}} & \lambda v_u\left(A_\lambda - 2\kappa s\right) \\ \mu_{\text{eff}}B_{\text{eff}} & \mu_{\text{eff}}B_{\text{eff}}\cot\beta & \lambda v_d\left(A_\lambda - 2\kappa s\right) \\ \lambda v_u\left(A_\lambda - 2\kappa s\right) & \lambda v_d\left(A_\lambda - 2\kappa s\right) & \lambda\left(B_{\text{eff}} + 3\kappa s\right)\frac{v_u v_d}{s} - 3\kappa A_\kappa s \end{pmatrix} \quad (3.18)$$

This matrix always contains a massless Goldstone boson G, who shows up explicitly performing a rotation $(H_{d,i}, H_{u,i}, S_i) \xrightarrow{R(-\beta)} (A', G, S_i)$ in the $(H_{d,i}, H_{u,i})$ sector. After dropping the Goldstone mode, one is left with a 2×2 matrix $\mathcal{M}_P'^2$ in the basis (A', S_i)

$$\Rightarrow \mathcal{M}_P^2 = \begin{pmatrix} 2B_{\text{eff}}\mu_{\text{eff}}/\sin 2\beta & \lambda(A_\lambda - 2\kappa s)v \\ \lambda(A_\lambda - 2\kappa s)v & \lambda(B_{\text{eff}} + 3\kappa s)\dfrac{v_u v_d}{s} - 3\kappa A_\kappa s \end{pmatrix} \tag{3.19}$$

Note that the first diagonal term corresponds to the mass M_A^2 of the MSSM-like CP-odd Higgs A. Thus, we define

$$M_A^2 = \frac{2\mu_{\text{eff}}B_{\text{eff}}}{\sin 2\beta}. \tag{3.20}$$

The physical states, denoted by A (mostly MSSM-like) and a_s (mostly singlet-like) are obtained through a final 2×2 rotation from (A', S_i) towards the mass eigenbasis (A, a_s) by an angle γ :

$$A = A' \cos\gamma - S_i \sin\gamma \tag{3.21}$$
$$a_s = A' \sin\gamma + S_i \cos\gamma \tag{3.22}$$

- **The charged mass matrix** The 2×2 complex valued charged mass matrix in the basis $\left(H_u^+, H_d^{-*} = H_d^+\right)$ is given by

$$\mathcal{M}_\pm'^2 = \left(\mu_{\text{eff}}B_{\text{eff}} + v_u v_d \left(\frac{g_2^2}{2} - \lambda\right)\right) \begin{pmatrix} \cot\beta & 1 \\ 1 & \tan\beta \end{pmatrix} \tag{3.23}$$

Again we see that the form of the matrix is the same as (2.44), so it can be diagonalized by rotating it with $R(-\beta)$. We find one (complex) massless Goldstone mode $G_\pm$ with $M_{G_\pm}^2 = 0$ (which will be 'eaten' by the W charged bosons) and one eigenstate associated to the physical charged Higgs

$$M_{H_\pm}^2 = \frac{2\mu_{\text{eff}}B_{\text{eff}}}{\sin 2\beta} + v^2\left(\frac{g_2^2}{2} - \lambda^2\right) \tag{3.24}$$

We can compare the value of this mass with the one obtained in the MSSM (2.41),

$$M_{H_\pm}^2 = \overbrace{M_A^2 + M_W^2}^{M_{H_\pm^{\text{MSSM}}}^2} - v^2\lambda^2. \tag{3.25}$$

Therefore, the mass of the charged higgses in the NMSSM can be smaller than in the MSSM due to the contribution $-v^2\lambda^2$. Moreover, in contrast with the MSSM where this mass remains positive, in the NMSSM the charged Higgses could acquire VEVs breaking the electromagnetic group $U(1)_{EM}$. λ is then bounded from above by the absence of charged Higgs VEVs.

- **The CP-even mass matrix** Defining $v^2 = 2M_Z^2/(g_1^2+g_2^2) \sim (174\text{ GeV})^2$, the 3×3 CP-even mass matrix in the basis $(H_{d,r}, H_{u,r}, S_r)$ reads[1]:

$$\begin{aligned}
\mathcal{M}^2_{S,11} &= M_Z^2\cos^2\beta + \mu(A_\lambda+\kappa s)\tan\beta\ ,\\
\mathcal{M}^2_{S,12} &= (\lambda v^2 - \frac{M_Z^2}{2})\sin 2\beta - \mu(A_\lambda+\kappa s)\ ,\\
\mathcal{M}^2_{S,13} &= \lambda v\left(2\mu\cos\beta - (A_\lambda+2\kappa s)\sin\beta\right)\ ,\\
\mathcal{M}^2_{S,22} &= M_Z^2\sin^2\beta + \mu(A_\lambda+\kappa s)\cot\beta + \Delta_{\text{rad}}\ ,\\
\mathcal{M}^2_{S,23} &= \lambda v\left(2\mu\sin\beta - (A_\lambda+2\kappa s)\cos\beta\right)\ ,\\
\mathcal{M}^2_{S,33} &= \lambda A_\lambda\frac{v^2}{2s}\sin 2\beta + \kappa s(A_\kappa+4\kappa s)\ .
\end{aligned} \tag{3.26}$$

Here Δ_{rad} denotes the dominant radiative corrections due to top/stop loops,

$$\Delta_{\text{rad}} = \frac{3m_t^4}{4\pi^2 v^2}\left(\ln\left(\frac{m_T^2}{m_t^2}\right) + \frac{X_t^2}{m_T^2}\left(1-\frac{X_t^2}{12m_T^2}\right)\right) \tag{3.27}$$

where m_T is the geometrical average of the soft SUSY breaking stop masses, and $X_t = A_t - \mu/\tan\beta$ with A_t the soft SUSY breaking stop trilinear coupling. It is convenient to rotate the CP-even mass matrix $\mathcal{M}_S^2$ by an angle β in the doublet sector into $\mathcal{M}_S'^2$ in the basis h', H', h'_s (with $h'_s \equiv S_r$):

$$\mathcal{M}_S'^2 = R(\beta)\mathcal{M}_S^2 R^T(\beta) \tag{3.28}$$

The mass matrix $\mathcal{M}_S'^2$ in the basis (h', H', h'_s) has the elements

$$\begin{aligned}
\mathcal{M}'^2_{S,11} &= M_Z^2\cos^2 2\beta + \lambda^2 v^2\sin^2 2\beta + \sin^2\beta\Delta_{\text{rad}}\ ,\\
\mathcal{M}'^2_{S,12} &= \sin 2\beta\left(\cos 2\beta\left(M_Z^2 - \frac{1}{2}\lambda^2 v^2\right) - \frac{1}{2}\Delta_{\text{rad}}\right)\ ,\\
\mathcal{M}'^2_{S,13} &= 2\lambda v\mu\left(1-\sin 2\beta\left(\frac{A_\lambda}{2\mu}+\frac{\kappa}{\lambda}\right)\right)\ ,\\
\mathcal{M}'^2_{S,22} &= M_A^2 + \left(M_Z^2 - \frac{1}{2}\lambda^2 v^2\right)\sin^2 2\beta + \cos^2\beta\Delta_{\text{rad}}\ ,\\
\mathcal{M}'^2_{S,23} &= \lambda v(A_\lambda+2\nu)\cos 2\beta\ ,\\
\mathcal{M}'^2_{S,33} &= \lambda A_\lambda\frac{v^2}{2s}\sin 2\beta + \nu\left(A_\kappa+4\nu\right)\ ,
\end{aligned} \tag{3.29}$$

[1] In the following, we will denote by μ the effective μ term from (3.2).

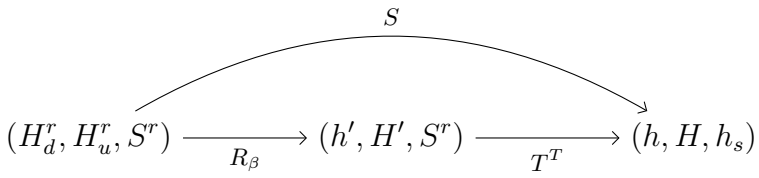

Figure 3.1: Scheme of the rotations from the gauge eigenstates to the mass states through the Higgs basis

This basis (also known as *Higgs basis*) has the advantage that only the component h' of the Higgs doublets acquires a vev v and that, for realistic sets of parameters, it is close to being diagonal: h' has SM-like couplings to fermions and electroweak gauge bosons, the heavy doublet field H' is the CP-even partner of the MSSM-like CP-odd state A, while h'_s remains a pure singlet. Explicitly, the gauge eigenstates in the Higgs basis are given by:

$$H_d = \cos\beta h' - \sin\beta H' \tag{3.30}$$
$$H_u = \sin\beta h' + \cos\beta H' \tag{3.31}$$
$$S = h'_s. \tag{3.32}$$

After an additional final rotation by a 3×3 matrix T we obtain the physical states,

$$\begin{pmatrix} T_{h',h} & T_{h',H} & T_{h',h_s} \\ T_{H',h} & T_{H',H} & T_{H',h_s} \\ T_{h'_s,h} & T_{h'_s,H} & T_{h'_s,h_s} \end{pmatrix} \begin{pmatrix} h \\ H \\ h_s \end{pmatrix} = \begin{pmatrix} h' \\ H' \\ h'_s \end{pmatrix}. \tag{3.33}$$

The mass eigenstates of $\mathcal{M}'^2$ will be denoted by:

- h , dominantly SM-like
- h_s , dominantly singlet-like and
- H , dominantly the MSSM-like heavy scalar.

3.3.2 Couplings of the neutral Higgs bosons

CP-even states

Let us analyze the couplings to vector bosons and fermions in the Higgs basis. Substituting in the lagrangian the corresponding terms using (3.32), we find for

the couplings to fermions:

$$\mathcal{L}_{uuH_u} = \frac{m_u}{v\sin\beta}\bar{u}uH_{u,r} \xrightarrow{R_(\beta)} \frac{m_u}{v}\bar{u}u\left(h' + \cot\beta H'\right) \tag{3.34}$$

$$\mathcal{L}_{ddH_u} = \frac{m_d}{v\cos\beta}\bar{d}dH_{d,r} \xrightarrow{R_(\beta)} \frac{m_d}{v}\bar{d}d\left(h' - \tan\beta H'\right) \tag{3.35}$$

$$\mathcal{L}_{eeH_d} = \frac{m_e}{v\cos\beta}\bar{e}eH_{d,r} \xrightarrow{R_(\beta)} \frac{m_e}{v}\bar{e}e\left(h' - \tan\beta H'\right), \tag{3.36}$$

and for the vector bosons

$$\mathcal{L}_{H_i\to VV} = \left(2\frac{M_W^2}{v}W^{\mu+}W_\mu^- + \frac{M_Z^2}{v}Z_\mu Z^\mu\right)\left(H_{d,r}^0\cos\beta + H_{u,r}^0\sin\beta\right) \tag{3.37}$$

$$\xrightarrow{R_(\beta)} \left(2\frac{M_W^2}{v}W^{\mu+}W_\mu^- + \frac{M_Z^2}{v}Z_\mu Z^\mu\right)h' \tag{3.38}$$

We observe that the couplings of the field h' are the same of those of the SM higgs field, H' remains decoupled from the gauge bosons and h_s', as a pure singlet, has no couplings to the SM particles.

Lastly, we perform a last transformation in CP-even Higgs space via the diagonalization matrix T, defined in (3.33). Then the reduced couplings of the physical Higgs bosons (h, H, h_s) are

$$\kappa_{d,i} = T_{h',i} + \tan\beta T_{H',i} \tag{3.39}$$

$$\kappa_{u,i} = T_{h',i} - \cot\beta T_{H',i} \tag{3.40}$$

$$\kappa_{V,i} = T_{h',i} \tag{3.41}$$

with $i = h, H, h_s$. Recall that the couplings to the vector bosons of the physical states are proportional to their component $\sim h'$, whereas the couplings to fermions can be modified by mixing with the MSSM-like H'.

Apart of the tree level couplings presented above, loop diagrams generate couplings of the CP-even states to photons $\kappa_{\gamma\gamma}$ and gluons κ_{gg}. Both couplings are of crucial importance for studying the Higgs boson phenomenology at the LHC. On the one hand, the effective coupling to gluons is responsible for the main Higgs production channel at the LHC: gluon fusion. This coupling is mediated mainly by heavy quark and squark loops. On the other hand, the effective coupling to photons produces the decay to a pair of photons. The diphoton final state is considered, depending on the mass of the Higgs boson, one of the golden channels for Higgs searches at the LHC. The effective coupling to photons is generated by loop diagrams with all charged particles running in the loop. However, the most sizeable contributions are due to top and vector bosons loops, which incidentally interfere destructively.

Sum rules

Once we have introduced the notation and the different basis that we are working with, we can now make some linear algebra and obtain useful relations. The full rotation matrix from the gauge eigenstates to the mass eigenstates reads, in components,

$$S_{ij} = (T^T)_{ik}(R_{-\beta})_{kj} \tag{3.42}$$

where

$$T^T = \begin{pmatrix} T_{h,h'} & T_{h,H'} & T_{h,h'_s} \\ T_{H,h'} & T_{H,H'} & T_{H,h'_s} \\ T_{h_s,h'} & T_{h_s,H'} & T_{h_s,h'_s} \end{pmatrix}, \qquad R_\beta = \begin{pmatrix} \cos(\beta) & \sin(\beta) & 0 \\ -\sin(\beta) & \cos(\beta) & 0 \\ 0 & 0 & 1 \end{pmatrix} \tag{3.43}$$

The matrix elements of S are:

$$\begin{aligned} (T^T)_{ik}(R_\beta)_{kS} &= T_{ih'_s} && (3.44)\\ (T^T)_{ik}(R_\beta)_{kH_u} &= T_{ih'}\sin\beta + T_{iH'}\cos\beta && (3.45)\\ (T^T)_{ik}(R_\beta)_{kH_d} &= T_{ih'}\cos\beta + T_{iH'}\sin\beta && (3.46) \end{aligned}$$

Using the expressions for the couplings (3.39) and (3.40), one finds,

$$S = \begin{pmatrix} \kappa_D^h\cos\beta & \kappa_U^h\sin\beta & T_{h,h'_s} \\ \kappa_D^H\cos\beta & \kappa_U^H\sin\beta & T_{H,h'_s} \\ \kappa_D^{h_s}\cos\beta & \kappa_U^{h_s}\sin\beta & T_{h_s,h'_s} \end{pmatrix} \tag{3.47}$$

Interestingly, we have written the rotation matrix in terms of β and the couplings of the higgses (and also the singlet mixing, but in could be substituted by the other parameter due to orthogonality relations, as we will see). By orthonormality of the rotations, we obtain the following *sum rules*:

$$\begin{aligned} (\kappa_D^h)^2 + (\kappa_D^H)^2 + (\kappa_D^{h_s})^2 &= \frac{1}{\cos^2\beta} && (3.48)\\ (\kappa_U^h)^2 + (\kappa_U^H)^2 + (\kappa_U^{h_s})^2 &= \frac{1}{\sin^2\beta} && (3.49)\\ T^2_{h,h'_s} + T^2_{H,h'_s} + T^2_{h_s,h'_s} &= 1 && (3.50)\\ (\kappa_D^i\cos\beta)^2 + (\kappa_U^i\sin\beta)^2 + T^2_{i,h'_s} &= 1, \quad i = \{h, H, h_s\} && (3.51) \end{aligned}$$

where $i = h, H, h_s$. Recall that from the orthonormality of T we also find

$$\begin{aligned} T^2_{h,h'} + T^2_{H,h'} + T^2_{h_s,h'} &= 1 && (3.52)\\ \Rightarrow (\kappa_V^h)^2 + (\kappa_V^H)^2 + (\kappa_V^{h_s})^2 &= 1 && (3.53) \end{aligned}$$

which implies that any deviation of the SM-like Higgs boson h in the coupling to vector bosons must be actually a suppression. These relations are of particular importance for the NMSSM Higgs phenomenology: they allow us to set bounds on the coupling of the non-SM states by measuring the properties of h.

Couplings of the CP odd states

As CP odd states, they do not couple to gauge bosons, but only to up- and down-type fermions. Proceeding analogously as we did above, one finds for the couplings

$$\kappa_D^A = \tan\beta\cos\gamma \quad , \quad \kappa_D^{a_s} = \tan\beta\sin\gamma \tag{3.54}$$
$$\kappa_U^A = \cot\beta\cos\gamma \quad , \quad \kappa_U^{a_s} = \cot\beta\sin\gamma \tag{3.55}$$

where the mixing angle γ is the responsible for the coupling of the mostly singlet-like pseudoscalar to matter. With this expressions one can write the total rotation matrix P in terms of the couplings and mixing:

$$P_{i,j} = (R_\gamma)_{i,k}\left(R_{\beta+\frac{\pi}{2}}\right)_{k,j}; \tag{3.56}$$

$$P = \begin{pmatrix} \kappa_D^A\cos\beta & \kappa_U^A\sin\beta & -\sin\gamma \\ -\cos\beta & \sin\beta & 0 \\ \kappa_D^{a_s}\cos\beta & \kappa_U^{a_s}\sin\beta & \cos\gamma \end{pmatrix} \tag{3.57}$$

Using the orthonormality of this matrix we obtain the following sum rules:

$$(\kappa_D^A)^2 + (\kappa_D^{a_s})^2 = \tan^2\beta \tag{3.58}$$
$$(\kappa_U^A)^2 + (\kappa_U^{a_s})^2 = \cot^2\beta \tag{3.59}$$
$$(\kappa_D^A\cos\beta)^2 + (\kappa_U^A\sin\beta)^2 = \cos^2\gamma \tag{3.60}$$
$$(\kappa_D^{a_s}\cos\beta)^2 + (\kappa_U^{a_s}\sin\beta)^2 = \sin^2\gamma \tag{3.61}$$

As the CP-even bosons, the pseudoscalars A and a_s have loop-induced couplings to photons and gluons. However, these are in general different to their CP-even counterparts. Pseudoscalars do not couple to vector bosons and thus W and Z loops do not contribute to the effective coupling $\kappa_{\gamma\gamma}$. Consequently, the destructive interference between quark loops and gauge bosons loops do not take place and $\kappa_{\gamma\gamma}$ can be enhanced with respect to the corresponding couplings of the CP-even states.

Trilinear couplings

There exist in the NMSSM a large number of possible trilinear couplings between the CP-even and CP-odd Higgs bosons. However, the expressions for the trilinear couplings of the mass eigenstates (h, H, h_s) are very complicated involving most of the parameters (3.17). For the complete set of coupling including all terms we refer the reader to [16]. Nonetheless, we can obtain relatively simple expressions for the scalar couplings in the Higgs basis (h', H', h'_s) [18], which could be regarded as a good approximation as $h' \sim h$ according to recent LHC data. Recall, however, that $H' \sim H$ and $h'_s \sim h_s$ do not necessarily hold at the same time. We present here only the trilinear couplings involving the SM state h':

$$
\begin{aligned}
h'h'h' &= \frac{1}{4v}\left(\lambda^2 v^2 \sin^2 2\beta + M_Z^2 \cos^2 2\beta\right) && (3.62)\\
H'h'h' &= \frac{-3}{2v}\sin 2\beta \cos 2\beta (M_Z^2 - \frac{1}{2}\lambda^2 v^2) && (3.63)\\
H'H'h' &= \frac{1}{4v}\left(\lambda^2 v^2 + (\lambda^2 v^2 - M_Z^2)\right)(1 - 2\sin 2\beta^2) && (3.64)\\
h'h'h_s &= \frac{\lambda\mu}{\sqrt{2}}\left(1 - \sin 2\beta\left(\frac{A_\lambda}{2\mu} + \frac{\kappa}{\lambda}\right)\right) && (3.65)\\
h'H'h'_s &= \frac{\lambda A_\lambda}{\sqrt{2}}\cos 2\beta && (3.66)\\
h'h'_s h'_s &= \frac{1}{2} v\lambda(\lambda - \kappa \sin 2\beta) && (3.67)\\
h'a'_s A' &= \frac{\lambda A_\lambda}{\sqrt{2}} - \sqrt{2}\kappa\mu && (3.68)\\
h'a'_s a'_s &= \frac{1}{2} v\lambda(\lambda + \kappa \sin 2\beta). && (3.69)
\end{aligned}
$$

Although these couplings do not correspond exactly to the actual physical Higgses, we can infer some interesting properties: In the limit $h = h'$, the first diagonal element in (3.29) should be an eigenstate, i.e. $\mathcal{M}'^2_{S,12} = \mathcal{M}'^2_{S,13} = 0$. Recall that from the above expressions we have $h'h'H' \propto \mathcal{M}'^2_{S,12}$ and $h'h'h'_s \propto \mathcal{M}'^2_{S,13}$, and hence in the limit $h = h'$ these couplings vanish, implying that double SM Higgs production from decays of H/h_S are suppressed (if kinematically allowed). On the other hand, couplings of the SM Higgs h with pairs of singlets as or hs could be potentially non zero, giving to sizeable branching ratios when the masses of the bosons permit the decay. The couplings $h'H'h_s$ and $h'a'_s A'$ depend mainly on the soft SUSY breaking trilinear coupling A_λ, and could be potentially large in natural regions of the NMSSM parameter space, as we will see in the next chapter.

3.4 The SM Higgs Mass and the little fine-tuning problem

We showed in sec 2.4 how within the MSSM the mass of ~ 125 GeV of the SM-like Higgs state h is not easy to explain. At tree level, this is bounded from above by M_Z, and accordingly large radiative corrections requiring large scalar top (stop) masses and/or mass splittings well above 1 TeV are needed in order to uplift the mass of the SM-like Higgs state from M_Z to ~ 125 GeV [19–26].

But heavy stop masses/mass splittings lead to large radiative corrections to a soft SUSY breaking Higgs mass term, which has to be tuned against the μ parameter if it is much larger than M_Z (see [27] and refs. therein). Accordingly the Higgs mass of about 125 GeV aggravates a little finetuning problem within the MSSM, pointed out already in the context of LEP bounds on the Higgs mass in [28–31].

The situation changes considerably when adding a gauge singlet superfield $\hat{S}$. After rotation to the Higgs basis, the first diagonal term of the CP-even mass matrix (3.29),

$$\mathcal{M}'^2_{S,11} = M_Z^2 \cos^2 2\beta + \lambda^2 v^2 \sin^2 2\beta + \sin^2\beta \Delta_{\rm rad}, \tag{3.70}$$

is associated to the mass of the mostly SM Higgs. We identify the first term in the right-hand side as the tree level upper bound for the Higgs mass in the MSSM, whereas the second term is proportional to the singlet coupling λ. Also, as a new state h'_s with unknown and unbounded mass is introduced in the CP-even sector, mixing effects on the Higgs mass should be revisited. Thus in the NMSSM two distinct mechanisms can lead to additional tree level contributions to the mass of the SM-like state h with respect to the MSSM case:

a) If λ is large enough ($\lambda^2 > (g_1^2 + g_2^2)/2$, where g_1 and g_2 are the electroweak gauge couplings) and $\tan\beta$ is small enough ($\tan\beta \lesssim 6$), the additional quartic coupling $\sim \lambda^2 h^4$ in the scalar potential lifts its mass above M_Z. However, $\lambda \gtrsim 1$ (so-called λ-SUSYy [32,33]) would be required in order to push the tree level mass from M_Z to 125 GeV in which case λ runs into a Landau singularity well below the GUT scale. In order to avoid this we confine ourselves subsequently to $\lambda \lesssim 0.75$.

b) If the mostly singlet-like state H_S has a mass below 125 GeV, mixing between h_s and h (more precisely, among the weak eigenstates) leads to an increase of the mass of the latter. The impact of such mixings on the Higgs spectrum of the NMSSM has been known for a while [34–39], but became particularly interesting once the mass of $\sim$ 125 GeV of the mostly SM-like state had been measured [19, 40–62]. The mass shift of up to ~ 8 GeV occurs now mostly for large $\tan\beta$ and smaller $\lambda \approx 0.04 - 0.1$, the latter in order to avoid constraints from LEP on a Higgs-like state with a mass below ~ 114 GeV [10]. (The increase of the mass

of the SM-like state h through mixing implies a decrease of the lighter singlet-like state h_s.) Hence the corresponding region in parameter space is clearly distinct from the one where the quartic SM-Higgs self coupling is enhanced.

Therefore, the NMSSM can alleviate the little fine tuning problem of the MSSM in these two regions of parameter space, rendering the theory more natural and still sharing the benefits of supersymmetric extensions of the SM with the MSSM. A more detailed study of the uplift of the Higgs mass beyond the MSSM bound is presented in chapter 4.

Chapter 4

Phenomenology of a light singlet in the NMSSM

4.1 Introduction

We saw in 3.4 that the NMSSM features natural regions in its parameter space, in the sense that it can easily accommodate a ~ 125 GeV Higgs boson without relying on large radiative corrections from stops loops. Two different (not necessarily exclusive) NMSSM-specific mechanisms were presented for uplifting the tree level mass of the mostly SM state, namely a large λ term and/or mixing effects.

In the present chapter we consider both mechanisms, but confine ourselves to the case where the mass of the mostly singlet-like state h_s is below 125 GeV: This situation is preferred also in the large λ–small $\tan\beta$ regime, since singlet-doublet mixing would always imply a decrease of the mass of the SM-like state if the singlet-like state is heavier, and mixing is hard to avoid if λ is large (unless h_s is very heavy and/or the corresponding off-diagonal element in the mass matrix happens to be small). On the other hand a mass of the mostly singlet-like state h_s below ~ 60 GeV would lead to dominant decays of h into pairs of h_s unless λ (and hence the mixing angle) is very small; also the LEP constraints are quite strong for this mass range [10]. We found that a sizeable positive mass shift for the SM-like state is unlikely here.

It is known that singlet-doublet mixing has two distinct phenomenological consequences:

a) The mostly singlet-like state inherits couplings to SM gauge bosons and fermions from the SM-like state proportional to the (sinus of the) mixing angle. This leads to non-vanishing production cross sections for h_s, and its potential discovery at the LHC.

b) Simultaneously, the couplings of h to gauge bosons and fermions get reduced.

The uncertainties of the measured couplings of h at the run I [63] and run II [64–66] of the LHC are expected to decrease further after collecting more data at the upcoming runs [67, 68].

Throughout this chapter we will study in how far the combination of both sources of future information can constrain the presence – or lead to a discovery – of a light singlet-like Higgs boson in the NMSSM, as function of the NMSSM specific mass shift of the SM-like state. We also indicate the possible production of h_s in decays of heavier MSSM-like H/A states.

In the next section we recall the phenomenological constraints on the Higgs sector relevant for the present study. In sec. 4.3 we define a NMSSM specific mass shift $\Delta_{\rm NMSSM}$ of the SM-like Higgs state. Then, in sec.4.4 we discuss the search channels for the light resonance h_s. Finally, in section 4.5 we describe the scans over the parameter space, and in section 4.6 we present the results of the scans as function of $\Delta_{\rm NMSSM}$: H_S diphoton signal rates at 8 and 13 TeV c.m. energy, modifications of the couplings of H_{SM}, and correlations among them. We discuss and compare prospects for tests of the scenarios under study, including the possible production of H_S in decays of heavy MSSM-like H/A states. Finally we conclude in section 4.7.

4.2 Phenomenological constraints

To start with, we have to collect the available constraints on the light-singlet scenario from LEP and measurements at the LHC. First, bounds on couplings to the Z boson times the branching fraction of an additional light Higgs boson into $b\bar{b}$ and gluons originate from LEP [10], as we see in fig. 4.1.

Second, limits originate from direct searches for extra (lighter) Higgs states in the diphoton channel by ATLAS [69] and CMS [70]: despite the relatively small diphoton branching fraction this final state is the most promising one to search for, in particular in view of the possibility that the diphoton branching fraction of h_s can be considerably larger than the one of a SM-like Higgs boson of corresponding mass [47, 49, 58, 61, 62, 71–76].

Third, limits originate from the potential reduction of couplings of h to SM gauge bosons and fermions through mixing with a gauge singlet. The corresponding measurements of production and decay mode dependent signal strengths of ATLAS and CMS at run I have been combined by the collaborations in [63]. Global fits to the couplings (or the coupling modifiers) require, in principle, likelihood grids including information on deviations from Gaussianity and correlations among uncertainties in particular for identical final states from different production modes. Moreover such global fits depend crucially on the assumptions on the underlying model like custodial symmetry (identical modifications of couplings to

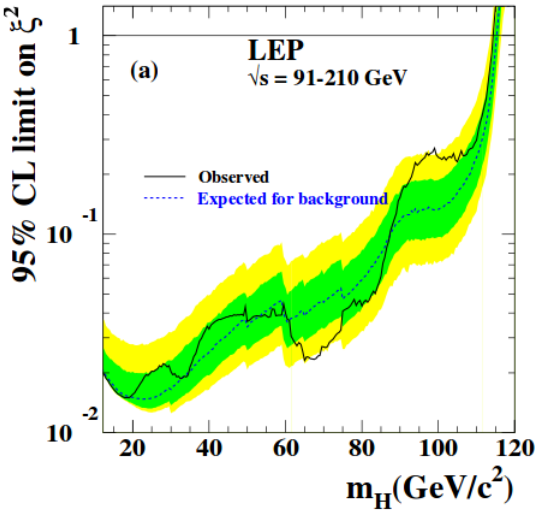

Figure 4.1: Upper bound on the coupling to vector bosons $\xi^2 = \kappa_V^2$ from LEP, where SM branching ratios to b quarks and τ leptons have been assumed. The full line indicates the observed limit, whereas the dashed line corresponds to the observed limit at 95% CL. The green and yellow bands correspond to the usual 68% and 95% confidence levels around the expected value.

W and Z bosons), correlated modifications of couplings to b quarks and τ leptons like in specific Higgs doublet models, and possible additional contributions to loop induced couplings to gluons and photons.

The latest global fits including assumptions corresponding to the NMSSM (custodial symmetry, correlated modifications of couplings to b quarks and τ leptons, possible additional contributions notably to the loop induced coupling to photons) have been performed in [77]. We have checked that their combined signal strengths are very close to the ones in [63] and use, for the scan of the NMSSM parameter space (see below), their 95% CL on signal strengths of h (verifying only subsequently the bounds from [63]). Electroweak precision data (the W boson mass) do not constrain the parameter space of the NMSSM with a light h_s [78]. Overall, in the NMSSM the experimental constraints on the $h - h_s$ mixing angle (for m_{h_s} below 125 GeV) are similar to the ones obtained from studies within simple singlet-extensions of the non-supersymmetric SM [60, 79–82].

All these constraints restrict the available parameter space of the NMSSM, and will be included in our numerical analysis detailed in sec. 4.5.

4.3 Uplifting the Higgs mass

We showed in sec. 2.4 how the MSSM tree level bound rises a tension between the theoretical MSSM prediction for m_h and its measured value. Indeed, after the measurement at the LHC of a SM-like Higgs with mass $\sim$125 GeV, the MSSM requires large radiative corrections $\Delta_{\rm rad}$ to reach the adequate mass, hence the "little fine tuning problem" [27–31] (although the problem was already present before the LHC due to the non-discovery of the Higgs at LEP, setting a bound $m_h > 114$ GeV) . In sec. 3.4 we presented two NMSSM-specific mechanisms to uplift the mass of h at tree level: First, a term proportional to λ, which is numerically relevant for $\tan\beta \lesssim 6$ and large λ. Avoiding a Landau singularity below the GUT scale requires $\lambda \lesssim 0.75$, limiting the possible uplift of the mass of the SM-like Higgs state to $\lesssim 17$ GeV.

A second possibility to uplift the tree-level mass of the SM-like Higgs state has recently been studied in some detail in [49,56]: If the diagonal term $\mathcal{M}'^2_{S,33}$ in (3.29) associated with the mass of the singlet-like Higgs state h'_s is smaller than $\mathcal{M}'^2_{S,11}$, $h' - h'_s$ mixing induced by the term $\mathcal{M}'^2_{S,13}$ in (3.29) shifts upwards the mass of the SM-like Higgs state h. The dominant contribution to $\mathcal{M}'^2_{S,13}$ originates from the first term $2\lambda v\mu$, which gets reduced by the second term $-\lambda v(A_\lambda + 2\nu)\sin 2\beta$. This reduction becomes small for moderate to large values of $\tan\beta$ [49,56]. On the other hand, $h' - h'_s$ mixing induces couplings of the lighter eigenstate h_s to electroweak gauge bosons, $b\bar{b}$ and gluons (through top quark loops). Such couplings of a state with a mass below 114 GeV are constrained by LEP [10]. This limits the region of λ for a sizeable uplift the mass of the SM-like Higgs state to $\lambda \sim 0.04...0.1$, and the possible uplift the mass of the SM-like Higgs state to $\lesssim 8$ GeV [49, 56].

Subsequently we intend to quantify the NMSSM-specific uplifts of the the mass of the SM-like Higgs state. To this end we define a mass shift $\Delta_{\rm NMSSM}$ of the mostly SM-like Higgs state due to the NMSSM specific effects, from the second term in (3.70) and/or from $h' - h'_s$ mixing. Contributions from $h' - h'_s$ mixing are easy to identify; it suffices to compare the second eigenvalue of $\mathcal{M}^2_S$ (corresponding to M^2_h) to the case where $\lambda,\ \kappa \to 0$ (keeping μ fixed, which requires to keep the ratio κ/λ fixed). Such a definition of $\Delta_{\rm NMSSM}$ has already been employed in [49, 56]. In addition we want to keep track of the NMSSM contribution from the second term in (3.70) relative to the MSSM, which is relevant for small $\tan\beta$ only. But keeping small $\tan\beta$ would reduce the MSSM-like tree level value $m_Z^2\cos^2 2\beta$, and it would not be "fair" to compare the NMSSM to the MSSM for low values of $\tan\beta$. Hence we evaluate the contribution to $\Delta_{\rm NMSSM}$ in the large λ-low $\tan\beta$ regime of the NMSSM by comparing to the MSSM ($\lambda,\ \kappa \to 0$ as before) with a large value of $\tan\beta = 40$. (The SM-like Higgs mass in the MSSM is practically independent of

$\tan\beta$ for $\tan\beta > 40$.) Therefore, for a given set of parameters we define:

$$\Delta_{\rm NMSSM} = m_h - \max_{\tan\beta} m_h\Big|_{\lambda,\kappa\to 0} \simeq m_h - m_h\Big|_{\lambda,\kappa\to 0,\ \tan\beta=40} . \tag{4.1}$$

Clearly, larger values of $\Delta_{\rm NMSSM}$ require smaller radiative corrections $\Delta_{\rm rad}$ to $\mathcal{M}'^2_{S,11}$ and alleviate correspondingly the little hierarchy problem. Accordingly $\Delta_{\rm NMSSM}$ can be interpreted as an approximate measure of naturalness.

4.4 Search channels

After identifying NMSSM natural regions for uplifting the Higgs mass, and quantifying them through $\Delta_{\rm NMSSM}$, we are interested in studying in how far such natural regions in the parameter space of the NMSSM can be tested in the future, as function of $\Delta_{\rm NMSSM}$ and the mechanism for an NMSSM-specific uplift of the mass of the SM-like Higgs state. Since $h' - h'_s$ mixing has a negative effect on $\Delta_{\rm NMSSM}$ for $m_{h_s} > 125$ GeV (also if $\Delta_{\rm NMSSM}$ originates mainly from the second term in (3.70)) we will concentrate on $m_{h_s} < 125$ GeV.

From the sum rules obtained in the previous chapter, we know that the reduced couplings to vector bosons of the CP-even states should satisfy:

$$\kappa_V^2(h) + \kappa_V^2(h_s) + \kappa_V^2(H) = 1 . \tag{4.2}$$

$h' - h'_s$ mixing will necessarily generate $\kappa_V^2(h_s) \neq 0$ and hence reduce $\kappa_V^2(h)$, which is already constrained by Run I data [63] and more recently from Run II data [64]. Similarly, the state h_s picks up couplings to fermions by both $h' - h'_s$ and $H' - h'_s$ mixing, leading to non-vanishing values for $\kappa_U(h_s)$ (the reduced coupling of h_s to up-type quarks) and $\kappa_D(h_s)$ (the reduced coupling of h_s to down-type quarks). Then loop diagrams generate non-vanishing values for $\kappa_{gg}(h_s)$ (the reduced coupling of h_s to gluons) and $\kappa_{\gamma\gamma}(h_s)$ (the reduced coupling of h_s to diphotons). It is important to note that the coupling of h_s to down-type quarks can suffer from cancellations among the contributions from $h' - h'_s$ and $H' - h'_s$ mixing, respectively [72]. This can result in a reduced branching fraction $BR(h_s \to b\bar{b})$. Since this decay constitutes the dominant contribution to the total width of h_s, its reduction implies enhanced branching fractions into other final states like $\gamma\gamma$. It is thus not astonishing that the $BR(h_s \to \gamma\gamma)$ can be larger than the one of a SM-Higgs boson of corresponding mass, leading to $\kappa_{\gamma\gamma}(h_s) > 1$.

Thus, present constraints and future discoveries/constraints can originate from:

- direct searches for h_s in the diphoton final state, which had been carried out by ATLAS for 65 GeV $< m_{h_s}$ [69] and by CMS for 80 GeV $< m_{h_s} <$ 115 GeV [70].

- measurements of the reduced signal rates/couplings (with respect to the SM) of h. In the case of $h' - h'_s$ mixing, these signal rates/couplings diminish proportional to the mixing angle.

- possible production of h_s in decays of the MSSM-like states H/A.

Comparing the corresponding sensitivities allows to verify under which conditions natural NMSSM scenarios with $m_{h_s} < 125$ GeV can be tested at future runs at the LHC, depending on the mechanism for the NMSSM-specific uplift of the mass of the SM-like Higgs state. To this end we have scanned the parameter space of the NMSSM as described in the next section.

4.5 Numerical analysis

We have performed these calculations with the public code `NMSSMTools_4.4.0` [83,84] including up to two-loop radiative corrections to the Higgs mass matrices as obtained in [85]. All phenomenological constraints explained in sec. 4.2, including the absence of Landau singularities below the GUT scale and, notably, constraints from Higgs searches in various channels at LEP are applied as in `NMSSMTools` (except for $(g-2)_\mu$).

The NMSSM specific parameters in Eq. (3.70) are varied in the ranges

$$\begin{aligned} &0.001 \leq \lambda < 0.75, \quad 0.001 \leq \kappa \leq 0.75, \quad 1 \leq \tan\beta \leq 50, \\ &0 \leq A_\lambda \leq 2.5 \text{ TeV}, \quad -1 \text{ TeV} \leq A_\kappa \leq 0, \quad 100 \text{ GeV} \leq \mu \leq 250 \text{ GeV} ; \end{aligned} \tag{4.3}$$

we found that wider ranges of the trilinear couplings A_λ, A_κ and μ (including negative values of κ and/or μ) have practically no impact on our results. The soft SUSY breaking squark masses of the third generation m_{U_3}, m_{D_3}, m_{Q_3} and the stop mixing parameter A_t are confined to ranges below 1 TeV in order to avoid too large fine tuning:

$$700 \text{ GeV} \leq m_{U_3} = m_{D_3} = m_{Q_3} \leq 1 \text{ TeV}, \qquad -1 \text{ TeV} \leq A_t \leq 1 \text{ TeV} . \tag{4.4}$$

(For $|A_t| \leq 1$ TeV, third generation squark masses below ~ 700 GeV do not allow to reach 125.1 ± 3 GeV for m_h even in the NMSSM.) The lightest physical stop mass $m_{\tilde{t}_1}$ satisfies $m_{\tilde{t}_1} \gtrsim 480$ GeV.

The soft SUSY breaking mass terms and trilinear couplings for the sleptons have been set to 500 GeV and 550 GeV respectively, whereas for the squarks of first two generations the masses are set to 2 TeV. The gluino mass is chosen as $m_3 = 1.6$ TeV, and the other soft SUSY breaking gaugino masses such that they satisfy approximately universal relations at the GUT scale, i.e. $m_2 = 2m_1 = m_3/3$. (All these parameters have practically no impact on our results.)

For each point in the parameter space satisfying the phenomenological constraints, including a SM-like Higgs state with a mass of 125.1 ± 3 GeV (allowing for theoretical uncertainties) and couplings of h to gauge bosons and fermions in the 95% CL ranges given in [63, 77], we further require $m_{h_s} < m_h$. Then we compute for each point $\Delta_{\rm NMSSM}$ according to the procedure described above, and various observables like reduced couplings and signal rates for the relevant Higgs states shown in the next section.

4.6 Results

Due to the limited range (4.4) for the soft SUSY breaking squark masses of the third generation and the stop mixing parameter, all viable points need a non-vanishing value of $\Delta_{\rm NMSSM}$ in the range 4 GeV $\lesssim \Delta_{\rm NMSSM} \lesssim$ 17 GeV in order reach a SM-like Higgs mass of 125.1 ± 3 GeV. Hence this range for the soft SUSY breaking squark masses of the third generation and the stop mixing parameter, motivated by alleviating the little hierarchy problem, is not viable in the MSSM.

Turning to the possible mechanisms for an uplift of the mass of the SM-like Higgs state, it follows from the discussion in section 3.3 that these take place in different regions of λ and $\tan\beta$: contributions to $\Delta_{\rm NMSSM}$ up to ~ 17 GeV from the second term in (3.70) (limited by the absence of a Landau singularity of λ below the GUT scale) are possible for large λ and $\tan\beta \lesssim 6$; subsequently this region will be denoted as "large λ" (LLAM) region. The region where contributions to $\Delta_{\rm NMSSM}$ from $h' - h'_s$ mixing are sizeable (up to ~ 8 GeV) is characterised by a small value of λ and large $\tan\beta$. Subsequently we call this region the "large mixing" (LMIX) region.

The viable points are shown in the $\lambda - \tan\beta$ plane in Fig. 4.2, including the possible values of $\Delta_{\rm NMSSM}$ in the form of a color code. One can clearly distinguish the two "islands" of valid points in the plane which can lead to a substantially different phenomenology, but both featuring a lower fin- tuning than in the MSSM, as discussed in sec. 3.4 and the references therein. In the following subsections we show various observables which can help to test these scenarios.

4.6.1 Searches for h_s in the diphoton final state

As already stated above, the ATLAS and CMS collaborations have published results from searches for additional BSM Higgs bosons with masses below 125 GeV in the diphoton final state [69, 70], leading to upper bounds on corresponding signal rates. First we have to verify whether these upper bounds lead to constraints on the parameter space of the NMSSM considered above. To this end we have used the public code `SusHi 1.5` [86] to obtain the NNLO gluon fusion production cross

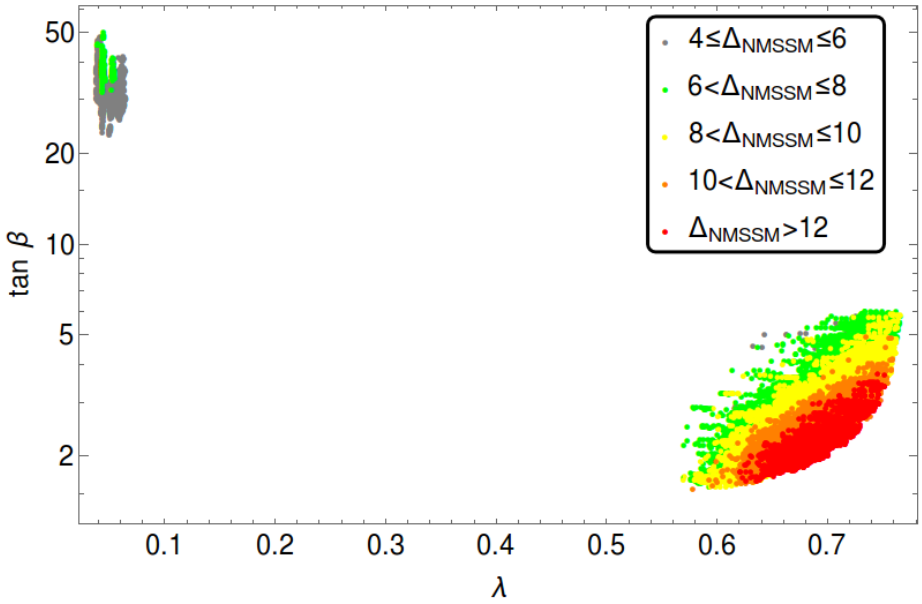

Figure 4.2: $\lambda - \tan\beta$ plane showing the viable points and $\Delta_{\rm NMSSM}$ in the form of a color code. The island in the upper-left corner corresponds to the region where $\Delta_{\rm NMSSM}$ originates from $h' - h'_s$ mixing (LMIX), whereas the island in the large λ regime (LLAM) corresponds to the region with large contributions to $\Delta_{\rm NMSSM}$ from the second term in (3.70).

section for a SM-like Higgs boson, and multiplied it by the reduced coupling of h_s to gluons $\kappa^2_{gg}(h_s)$ given by the output of NMSSMTools. Finally the production cross section is multiplied by the $BR(h_s \to \gamma\gamma)$ as given by NMSSMTools.

On the upper side of Fig. 4.3 we show the resulting signal rates at $\sqrt{s} = 8$ TeV c.m. energy, together with the ATLAS [69] and CMS [70] limits from direct searches as function of m_{h_s}. Here the LMIX region apprears as a grey-green island within the much larger LLAM region. On the lower side of Fig. 4.3 we show the resulting signal rates at $\sqrt{s} = 13$ TeV c.m. energy, once the constraints from ATLAS and CMS searches have been applied.

We see in Figs. 4.3 that in the grey-green LMIX region m_{h_s} is confined to the mass range 88 GeV $\lesssim m_{h_s} \lesssim$ 102 GeV, a consequence of the parameter range (4.4) and the corresponding lower limit on $\Delta_{\rm NMSSM} \gtrsim 4$ GeV. In order to obtain such values of $\Delta_{\rm NMSSM}$ through $h' - h'_s$ mixing, the mixing angle has to be relatively large leading to sizeable couplings of h_s to electroweak gauge bosons. These, in turn, are allowed by LEP only in the corresponding mass range where, actually, a mild excess of events is seen [10].

The recent ATLAS and CMS searches have not yet been sensitive to the possible signal rates $\sigma(gg \to h_s \to \gamma\gamma)$ in the LMIX region of the NMSSM, due to the

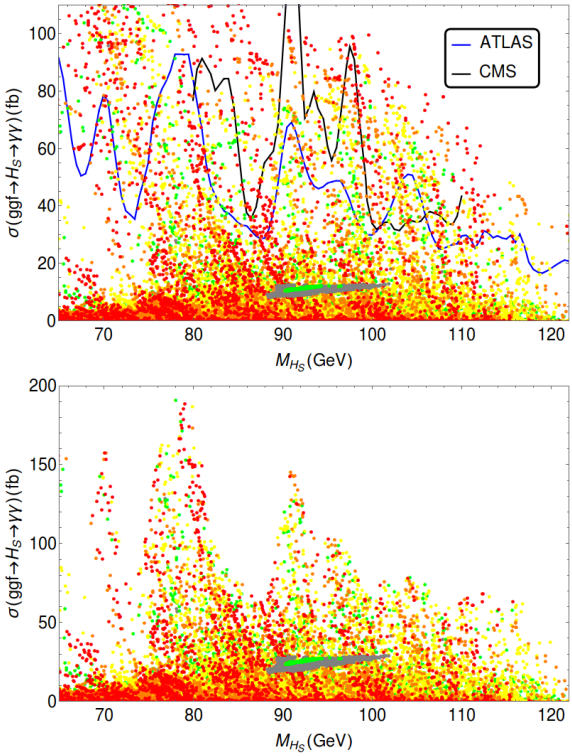

Figure 4.3: Top: Possible signal rates (in femtobarns) $\sigma(gg \to h_s \to \gamma\gamma)$ at a c.m. energy of $\sqrt{s} = 8$ TeV, together with the ATLAS [69] and CMS [70] limits from direct searches. The grey-green island corresponds to the LMIX region, the rest to the LLAM region. Bottom: Signal rates for the same process at $\sqrt{s} = 13$ TeV for the remaining points once the upper bounds from ATLAS and CMS have been applied.

absence of a possible enhancement of the $BR(h_s \to \gamma\gamma)$ (see below). Fig. 4.3 (bottom) indicates, on the other hand, that the LMIX region could be completely tested once searches at $\sqrt{s} = 13$ TeV c.m. energy become sensitive to $\sigma(gg \to h_s \to \gamma\gamma) \sim 20$ fb.

Within the LLAM (large λ) region both m_{h_s} and $\sigma(gg \to h_s \to \gamma\gamma)$ can vary over much larger ranges and, indeed, the ATLAS and CMS searches have started to test parts of the LLAM region where this signal rate is particularly large. On the other hand this signal rate can also be quite small in the LLAM region where $h' - h'_s$ mixing is possible, but not mandatory. This part of the LLAM region will be hard to test via searches for direct h_s production.

It is interesting to decompose $\sigma(gg \to h_s \to \gamma\gamma)$ into production cross sections and branching fractions, which allows to estimate signal rates in other channels and to understand the origin of the varying signal rates in Fig. 4.3. In Fig. 4.4 we show the production cross section of h_s at $\sqrt{s} = 8$ TeV (top) and $\sqrt{s} = 13$

TeV (bottom) with the same color code for $\Delta_{\rm NMSSM}$ as in Fig. 4.2, omitting the points excluded by ATLAS or CMS. We observe that, for the allowed mass range 88 GeV $\lesssim m_{h_s} \lesssim$ 102 GeV, $\sigma(gg \to h_s)$ is indeed larger in the LMIX region than in the LLAM region, since the couplings of h_s to fermions (here: to the top quark) are relatively large. However, the $BR(h_s \to \gamma\gamma)$ shown on the left hand side of Fig. 4.5 clarify that these can be (much!) larger for h_s than for a SM-like Higgs (shown as blue line) only for parts of the LLAM region, never within the LMIX region; only within the LLAM region a suppression of the $BR(h_s \to b\bar{b})$ is possible (as shown on the lower figure of Fig. 4.5) which is required in order to enhance the $BR(h_s \to \gamma\gamma)$.

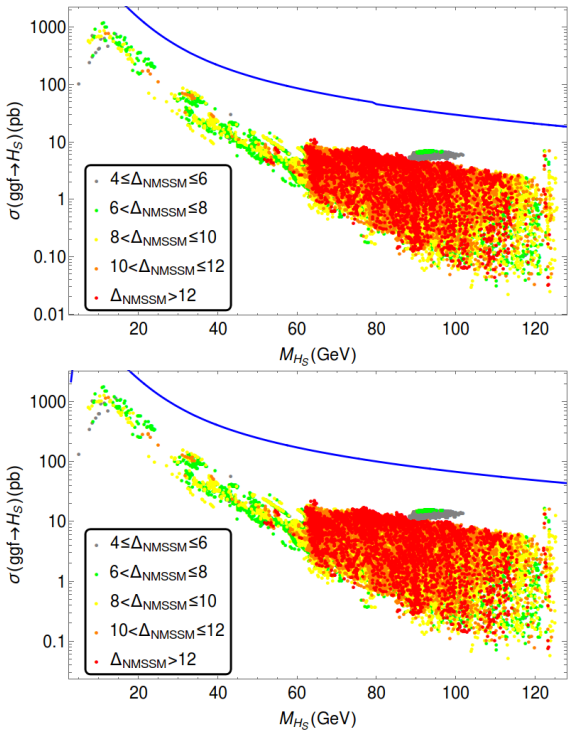

Figure 4.4: Production cross section of h_s at $\sqrt{s} = 8$ TeV (top) and $\sqrt{s} = 13$ TeV (bottom) with the color code for $\Delta_{\rm NMSSM}$. The blue line indicates the corresponding ggF cross section for a SM Higgs boson of the same mass. The grey-green island corresponds to the LMIX region.

Finally both Figs. 4.4 and 4.5 show that very few viable points exist for $m_{h_s} <$ 60 GeV (in the LLAM region only): Such light states can be produced in decays $h \to h_s h_s$ and would reduce the observed h signal rates into SM-like final states to inadmissible levels. The $h - h_s - h_s$ coupling can be small for large λ, however, due to (rare) accidential cancellations among the various contributing terms. (This

mass range has not been shown in Fig. 4.3 since the experiments have not been sensitive to it.)

4.6.2 Reduced Couplings of h

As stated above the LMIX (and LLAM) regions can have an impact on the reduced couplings of h, actually both due to $h' - h'_s$ mixing and $h' - H'$ mixing induced by the final diagonalisation of the mass matrix $\mathcal{M}'^2$ (3.29). The ATLAS and CMS measurements of the reduced couplings of h at the first run of the LHC have been combined in [63], and prospects for future measurements have been published in [67] (ATLAS) and [68] (CMS).

First we show in Fig. 4.6 the reduced couplings $\kappa_V(h)$ and $\kappa_{\gamma\gamma}(h)$ for the viable points. The LMIX and LLAM regions can be distinguished clearly in Fig. 4.6: As before the LMIX region corresponds to the thin grey-green strip, the LLAM region to the remaining part dominated by mostly red points (for which 12 GeV $<$

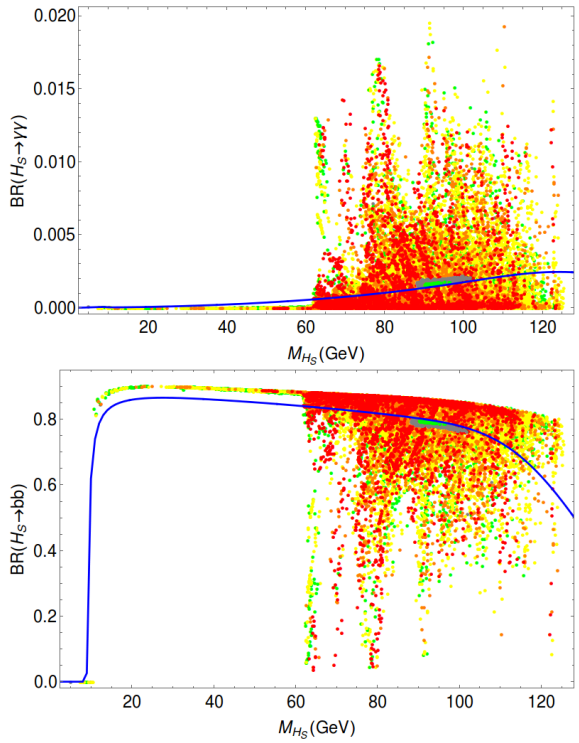

Figure 4.5: Branching ratios of h_s into photons (top) and $b\bar{b}$ (bottom) versus its mass. The blue line indicates the corresponding branching ratios for a SM Higgs boson of the same mass. The grey-green island corresponds to the LMIX region, in which the branching ratios are very SM-like.

$\Delta_{\rm NMSSM} < 17$ GeV).

From the recent ATLAS-CMS combination in [63] one finds for the scenario relevant here (custodial symmetry, i.e. $\kappa_Z(h) = \kappa_W(h) \equiv \kappa_V(h) \leq 1$) that $\kappa_V(h) \gtrsim 0.83$ at the 95% CL level. The prospects for the measurements of $\kappa_V(h)$ at the run II of the LHC in [67] (ATLAS) and [68] (CMS) depend on uncertainty scenarios and, of course, on the integrated luminosity. For 300 fb^{-1} one expects uncertainties of about 5% at the 1σ level, i.e. the possibility to set a lower bound on $\kappa_V(h)$ of ~ 0.9 at the 95% CL level. Such a bound can test the green $\Delta_{\rm NMSSM} > 6$ GeV region of the LMIX scenario, but reduced uncertainties of about 7% at the 95% CL level at 3000 fb^{-1} integrated luminosity could test the LMIX scenario completely. Again, the LLAM scenario can be tested only partially by measurements of $\kappa(h)$. The prospects for constraining (or detecting) the LMIX/LLAM scenarios via measurements of $\kappa_{\gamma\gamma}(h)$ are similar, but somewhat less promising due to the larger foreseen uncertainties at both 300 fb^{-1} and 3000 fb^{-1} integrated luminosity [67, 68].

Apart by future measurements of individual values of reduced couplings of h, informations or constraints on scenarios predicting deviations from the SM can be obtained by considering correlations among reduced couplings. To this end we show in Figs. 4.7 the correlations of $\kappa_V(h)$ with the reduced couplings of h to down-type fermions ($\kappa_D(h)$) and gluons ($\kappa_{gg}(h)$).

Like in Fig. 4.6 these correlations are very pronounced in the LMIX scenario,

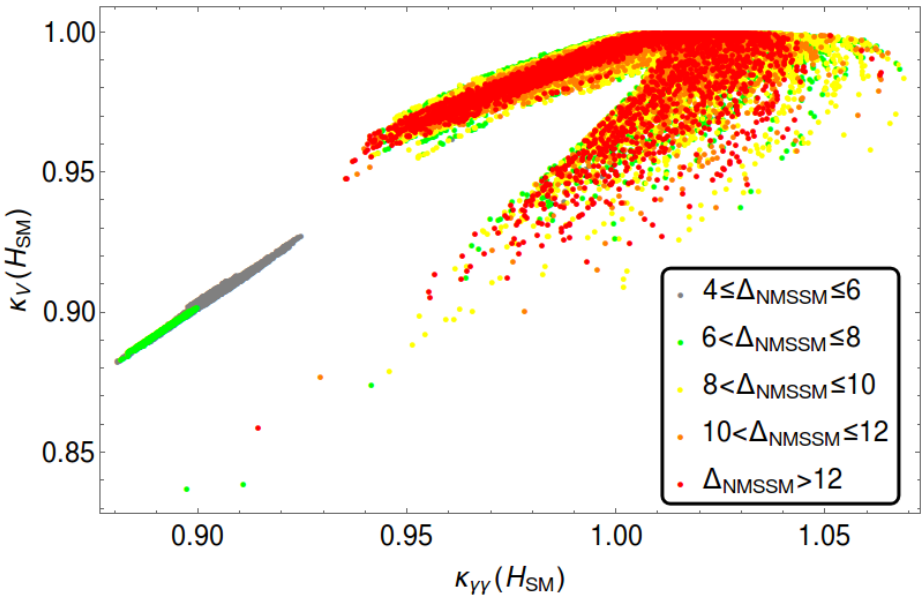

Figure 4.6: Reduced couplings $\kappa_V(h)$ and $\kappa_{\gamma\gamma}(h)$ for the viable points, including a color code for $\Delta_{\rm NMSSM}$.

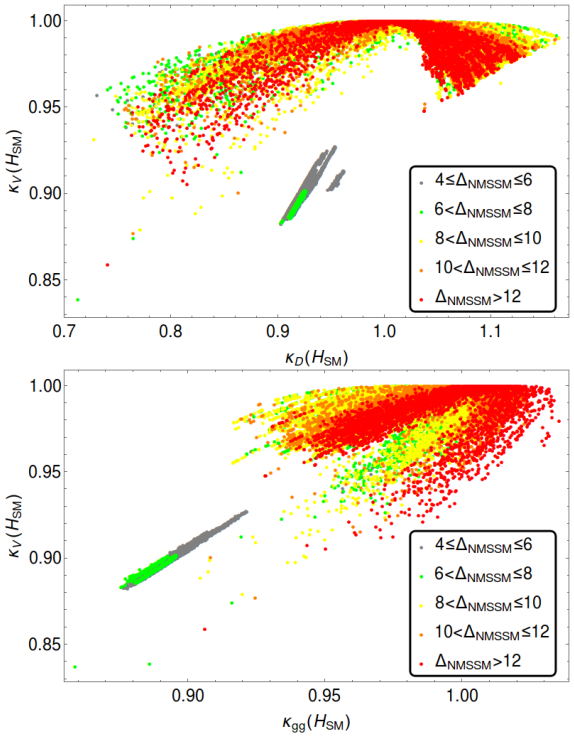

Figure 4.7: Correlations of $\kappa_V(h)$ with the reduced couplings of h to down-type fermions (top) and gluons (bottom). In both plots the two regions LLAM and LMIX are clearly separated.

but in the LLAM scenario a wide range of $\kappa_D(h)$ is possible: a reduction of the coupling of h to down-type fermions originates from negative contributions to this coupling from $h' - H'$ mixing. As for h_s, a corresponding reduction of the $BR(h \to b\bar{b})$ can lead to an enhanced $BR(h \to \gamma\gamma)$ as observed in Fig. 4.6. However, positive contributions to the coupling of h to down-type fermions are possible as well, with opposite consequences. The two regions $\kappa_D(h) > 1$ and $\kappa_D(h) < 1$ explain the origin of the two "branches" of $\kappa_V(h)$ visible in Fig. 4.6 as well on the lower figure of Fig. 4.7. Unfortunately, the couplings of h can also be very SM-like, like in the alignment limit studied recently in [18].

Next we turn to correlations between the reduced couplings of h and the signal rates $\sigma(gg \to h_s \to \gamma\gamma)$ discussed in the previous subsection. In Figs. 4.8 we show $\sigma(gg \to h_s \to \gamma\gamma)$ against $\kappa_V(h)$ (top) and $\sigma(gg \to h_s \to \gamma\gamma)$ against $\kappa_{\gamma\gamma}(h)$ (bottom). These figures allow to verify the possible complementarity of measurements of $\sigma(gg \to h_s \to \gamma\gamma)$ and the reduced couplings of h: In order to test the LMIX region (the grey-green island on the left hand side), the necessary limits on $\sigma(gg \to h_s \to \gamma\gamma)$ and/or $\kappa_V(h)$ can now be deduced together. The LLAM region can become visible either by an enhanced $\sigma(gg \to h_s \to \gamma\gamma)$ or a reduced

$\kappa_V(h)$, but not both. Unfortunately, a low signal rate $\sigma(gg \to h_s \to \gamma\gamma)$ as well as $\kappa_V(h) \sim 1$ are possible simultaneously. From the lower side of Figs. 4.8 we see that enhanced signal rates $\sigma(gg \to h_s \to \gamma\gamma) \gtrsim 50$ fb and enhanced reduced couplings $\kappa_{\gamma\gamma}(h)$ are incompatible in the LLAM region.

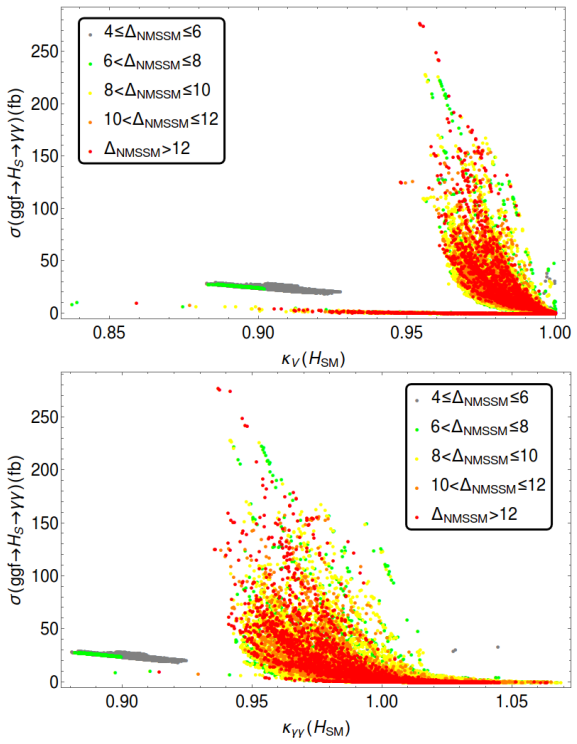

Figure 4.8: Top: Correlations among the diphoton signal rate of h_s and $\kappa_V(h)$. Bottom: Correlations among the diphoton signal rate of h_s and $\kappa_{\gamma\gamma}(h)$.

4.6.3 h_s production via decays of heavy states H/A

Another way to produce a light h_s is through the decays of heavy (MSSM-like) states H/A. First we have to find out which masses of H/A are possible in the LMIX/LLAM regions of the NMSSM considered here. In Fig. 4.9 we show the regions of viable points in the $\tan\beta - m_A$ plane, which helps to clarify that these points are not ruled out by searches for MSSM-like H/A in the $\tau^+\tau^-$ final state (from here onwards, m_A denotes the physical mass of the MSSM-like CP-odd state A): The LMIX region with large $\tan\beta$ features very heavy H/A states, to which searches at the LHC are not sensitive (due to the heavy value of the mass $m_{H/A} > 1TeV$). The LLAM region is characterized by lower $\tan\beta$ such that the associate production of H/A states with b quarks is not very enhanced; instead,

their production via gluon fusion becomes feasable in principle [87]. The part of the LLAM region where $m_A \gtrsim 500$ GeV and $\tan\beta \gtrsim 3$ corresponds, however, to the difficult region where the reduced couplings of h are very SM-like and h_s has a low signal rate in the $\gamma\gamma$ channel; in this region also the search for the MSSM-like states H/A seems difficult [88].

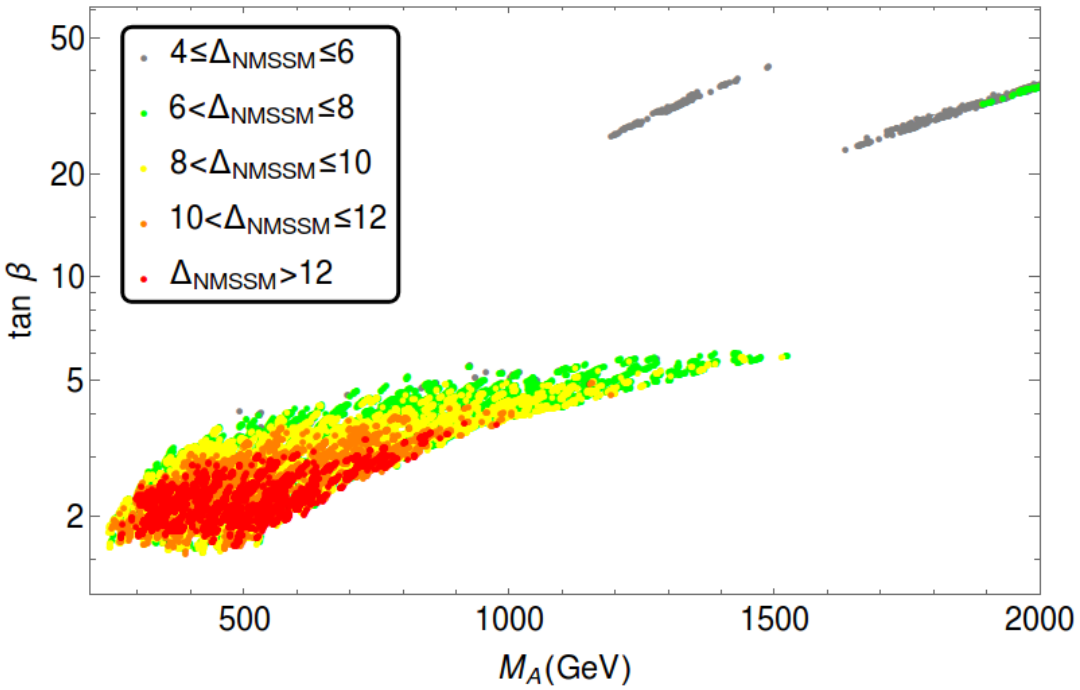

Figure 4.9: Viable points in the $\tan\beta - m_A$ plane.

Promising decays of H/A into h_s are $A \to Z + h_s$ and $H \to h + h_s$. Since the kinematics of $A \to Z + h_s$ is very similar to the one of $H \to Z + a_s$ investigated in [89], the studies of the $Z \to l^+l^-$ ($l \equiv e, \mu$) and $a_s \to b\bar{b}$ final states in [89] can be employed, including their sensitivity curves as function of m_{a_s} (now interpreted as m_{h_s}). First we show what signal cross sections can be expected as function of m_A. The signal cross section $\sigma(ggF \to A \to Z + h_s)$ is shown on the left hand side of Fig. 4.10 as function of m_A; clearly, visible signal rates can only be expected for $m_A \lesssim 400$ GeV within the LLAM region. On the right hand side of Fig. 4.10 the range of signal cross sections $\sigma(ggF \to A \to Z + b + \bar{b})$ is shown as function of m_{h_s}, and compared to the expected sensitivities at the run II of the LHC for integrated luminosities of 300 fb^{-1} (blue) and 3000 fb^{-1} (black) (from [89]). Hence, detectable signal rates in this channel are indeed possible in the LLAM region of the NMSSM without, however, covering it completely.

The process $H \to h + h_s$ can also be searched for in various final states as $4b$, $2b2\tau$ and $2b2\gamma$; one is handicapped, however, by the a priori unknown mass of h_s.

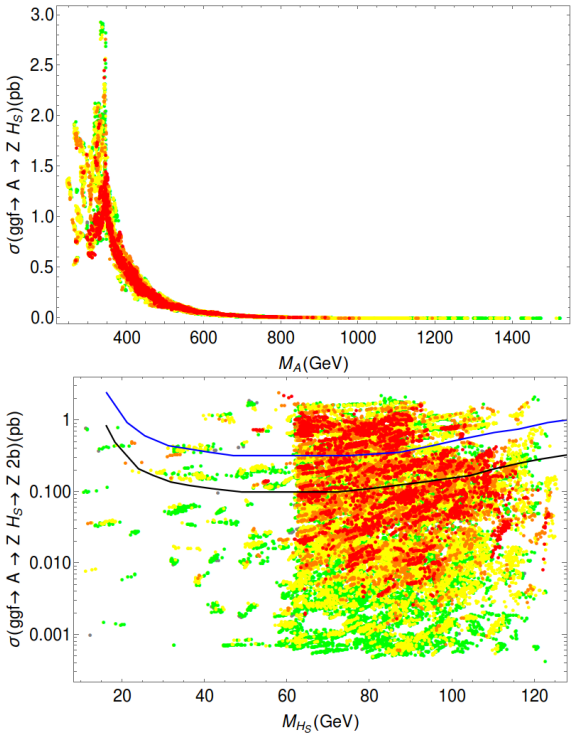

Figure 4.10: Top: Signal cross section $\sigma(ggF \to A \to Z + h_s)$ as function of m_A for a c.m. energy of $\sqrt{s} = 13$ TeV. Bottom: Signal cross section $\sigma(ggF \to A \to Z + b + \bar{b})$ as function of m_{h_s}, compared to the expected sensitivities for a integrated luminosities of 300 fb^{-1} (blue) and 3000 fb^{-1} (black) (from [89]).

In Fig. 4.11 we show the cross section $\sigma(ggF \to H \to h + h_s)$ as function of m_H for a c.m. energy of $\sqrt{s} = 13$ TeV on the left, and the (dominant) signal cross section $\sigma(ggF \to H \to h + h_s \to 4b)$ as function of m_{h_s} on the right. In the region of the NMSSM parameter space considered here a_s is, however, not particularly light; we found that, in the (wider) LLAM region, m_{a_s} varies from ~ 80 to ~ 300 GeV, but from ~ 60 to ~ 180 GeV in the (narrower) LMIX region. Search strategies including background studies for searches for h_s/a_s in Higgs-to-Higgs decays will be studied in various channels in the next chapter of this thesis.

4.7 Conclusions

We have studied a region in the NMSSM parameter space in which the mass of the SM-like Higgs boson is uplifted by $\sim 4-17$ GeV, allowing for both stop masses and $|A_t| \leq 1$ TeV alleviating the little fine tuning problem of the MSSM. This region features a lighter mostly singlet-like Higgs state h_s with a mass in the $60-125$ GeV

range if the uplift is due to singlet-doublet mixing (the LMIX region). Confining ourselves to values of $\lambda \lesssim 0.75$, this mass range of h_s is also natural in the LLAM region where the uplift originates from the additional quartic term $\sim \lambda^2$ in the potential of the SM-like Higgs boson.

The aim of this chapter is the study of possible direct or indirect searches for a light h_s at the run II of the LHC. Three possibilities have been considered:
a) Direct production of h_s in gluon fusion, with h_s decaying into diphotons. Corresponding searches have been conducted recently by ATLAS and CMS (the results of which have been taken into account), and are the most promising also for the run II of the LHC.
b) Modified reduced couplings of the SM-like Higgs state h through singlet-doublet mixing (both in the LMIX and the LLAM regions).
c) Production of h_s in decays of heavier H/A states, where we confined ourselves to the most promising $A \to Z + h_s$ and $H \to h + h_s$ channels.

We found that the LMIX region can be tested if searches for BSM Higgs bosons in the mass range $88 - 102$ GeV become sensitive to signal cross sections $\sigma(gg \to h_s \to \gamma\gamma) \sim 20$ fb. Alternatively, the LMIX region can be tested if mea-

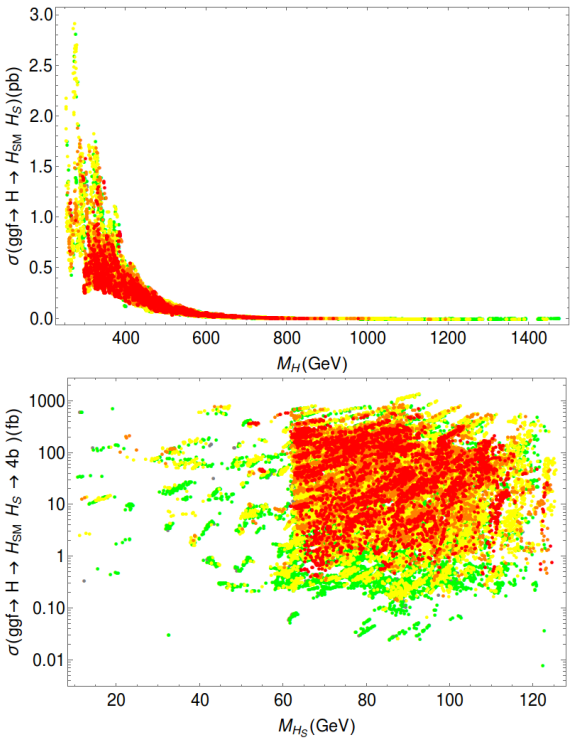

Figure 4.11: Total ggF production cross section for $H \to h + h_s$ at a c.m. energy $\sqrt{s} = 13$ TeV (top), and the signal cross section into $b\bar{b}b\bar{b}$ versus the mass of h_s (bottom).

surements of the reduced coupling $\kappa_V(h)$ of the SM Higgs boson to electroweak gauge boson exclude (or confirm) the region $\kappa_V(h) \lesssim 0.93$. Since the H/A states are always quite heavy in the LMIX region (with masses well above 1 TeV), h_s detection via H/A seems impossible in the near future, and tests of the LMIX region have to rely on one of the two measurements above, which seems feasable if the projected sensitivities can be reached.

On the other hand it is difficult to test the entire LLAM region even if h_s is light (with a mass below 125 GeV), the range considered here: both the signal cross section $\sigma(gg \to h_s \to \gamma\gamma)$ and the deviation of the reduced couplings of h from one can simultaneously be very small. However, in other parts of the LLAM region both the signal cross section $\sigma(gg \to h_s \to \gamma\gamma)$ and the deviation of the reduced couplings of h from one can be much larger than in the LMIX region; these parts of the LLAM region will be the first ones to be tested. In a part of the "difficult" LLAM region, but for which the H/A states are not too heavy (with masses $\lesssim$ 400 GeV), the detection of h_s at least via $ggF \to A \to Z + h_s$ and $ggF \to H \to h + h_s$ is possible. Studies on the possible detection of h_s via other H/A decay channels (including larger masses of h_s) will be presented in the next chapter.

Chapter 5

Searches via Higgs cascades

5.1 Introduction

Extended Higgs sectors are frequent properties of models beyond the Standard Model (BSM). Such extra states can have very small couplings to quarks, leptons and SM gauge fields. For instance, for singlets under the SM gauge symmetries such renormalizable couplings are disallowed by gauge invariance. The direct production cross sections for these states are then strongly suppressed in all channels. On the other hand, couplings of singlets to SU(2) Higgs doublets of the SM- or BSM-type are possible and typically present in BSM models. This allows for the discovery of such states in cascade decays of heavy BSM SU(2) Higgs doublets, provided the production cross sections of the latter are large enough.

The final states after BSM-Higgs to BSM-Higgs + SM-Higgs cascades typically correspond to the ones in searches for resonant SM-Higgs (h) pair production: mainly $b\bar{b}b\bar{b}$, $b\bar{b}\tau\tau$ and $b\bar{b}\gamma\gamma$. Corresponding searches have been performed at the LHC by ATLAS [90–95] and by CMS [96–110]. However, one of the SM-like Higgs bosons would now be replaced by a lighter or heavier BSM-Higgs boson. One can argue that the cross sections for such processes can be more promising than for resonant SM-Higgs pair production:

a) A sizeable ggF production cross section of a heavy scalar or pseudoscalar Φ, i.e. a sizeable coupling of Φ to top quarks, requires Φ to possess a sizeable SU(2)-doublet component. However, since h is also a SU(2)-doublet, trilinear couplings $\Phi - h - h$ (with Φ a pure doublet) violate the SU(2) symmetry and must be proportional to a SU(2) symmetry breaking vev; the latter is limited from above by the Z/W masses which limits the possible partial width for $\Phi \to h + h$. (The concurrent $\Phi \to t\bar{t}$ is always possible if Φ can be produced in ggF and is heavier than $2\,m_t$.)

b) In the case $ggF \to \Phi \to h + H'$ with Φ a pure doublet, the trilinear coupling

$\Phi - h - H'$ can be SU(2) invariant if H' is a singlet. In models with extended Higgs sectors including both an extra doublet and a singlet, such a coupling can thus be much larger than the Z/W masses leading to sizeable $\Phi \to h + H'$ partial widths.

In Two-Higgs-Doublet-Models of type II such as the Minimal Supersymmetric Standard Model (MSSM) the production cross sections for extra CP-even (H) and CP-odd (A) Higgs doublets are not suppressed, and are dominated by gluon-gluon-fusion (ggF) for $\tan\beta$ not too large [11,87,88]. H or A can thus play the rôle of Φ above. The Next-to-Minimal Supersymmetric Standard Model (NMSSM) [16,111] contains additional CP-even (h_s) and CP-odd (a_s) singlet-like states which can be light, with masses below M_H or M_A. One finds that the $BR(H \to h_s + h)$ and $BR(A \to a_s + h)$ can be up to $\sim 50\%$ [18,58,112,113], for the reasons given above and detailed in the next section.

In the NMSSM this offers the possibility to produce otherwise practically invisible mostly singlet-like states h_s/a_s in cascade decays of H/A [18, 58, 112, 113]. It is the aim of the present chapter to study the prospects for discovery or exclusion of, simultaneously, H/A and h_s/a_s states in $ggF \to H \to h_s + h$ or $ggF \to A \to a_s + h$ in the final states $b\bar{b}b\bar{b}$, $b\bar{b}\tau\tau$ and $b\bar{b}\gamma\gamma$. Supersymmetry plays no rôle here, accordingly our results are applicable to any models with similarly extended Higgs sectors.

We will adopt various strategies from the searches for resonant SM Higgs pair production by ATLAS [90–95] and by CMS [96–110]. Moreover, for m_{h_s} near 125 GeV we can compare our backgrounds and expected 95% CL upper limits and $5\,\sigma$ discovery limits on the cross sections times branching fractions to the ones obtained in these publications.

On the other hand, the analyses presented here are complicated by the fact that the masses m_{h_s}/m_{a_s} are not known *a priori*. An important aspect of optimal search strategies are m_{h_s}/m_{a_s} dependent selection criteria (cuts) on events, hence different analyses should be performed, varying the assumptions on m_{h_s}/m_{a_s}. Only at the end of each of these analyses a search for a resonance-like bump in the total invariant mass of the h_s/a_s plus h decay products, which should correspond to M_H/M_A, is proposed.

In the next section we discuss shortly the Higgs sector of the NMSSM and the couplings relevant for the processes considered here. In section 3 we present features of our signal simulations. In section 4 we discuss the optimal search strategy for the $b\bar{b}b\bar{b}$ final state, and compare expected 95% CL upper limits and $5\,\sigma$ discovery limits on the cross sections times branching fractions to the ones possible in the NMSSM. Sections 5 and 6 are devoted to the $b\bar{b}\tau\tau$ and $b\bar{b}\gamma\gamma$ final states. All these search strategies and results are identical for $ggF \to H \to h_s + h$ and $ggF \to A \to a_s + h$, for notational simplicity we will refer to $H \to h_s + h$ only.

Also the cross sections times branching fractions in the NMSSM are very similar and will be shown for $ggF \to H \to h_s + h$ only. In section 7 we conclude with a summary and an outlook.

5.2 Higgs cascades in the NMSSM

Decays of a heavy Higgs state into two lighter Higgs states occur in the presence of trilinear Higgs couplings. Most of the trilinear Higgs couplings in the $\mathbb{Z}_3$-invariant NMSSM originate from quartic terms in the Higgs potential (see expression (3.6)) proportional to two powers of λ, κ or the electroweak gauge couplings, once the (neutral) Higgs fields are expanded around their vevs and decomposed into their real and imaginary parts (see eqs. (3.7)). Hence the trilinear couplings are proportional to the vevs v_u, v_d or s. A notable exception are trilinear Higgs-dependent soft SUSY breaking terms, in particular

$$\lambda A_\lambda H_u \cdot H_d S + h.c. \tag{5.1}$$

where the dimensionful parameter A_λ can be much larger than Higgs vevs.

In order to obtain its impact on trilinear couplings among Higgs mass eigenstates, the mass matrices have to be diagonalized. In the CP-even sector, where one deals with a 3×3 mass matrix, a first step in this direction is a rotation in the SU(2) doublet sector into the Higgs basis, already introduced in sec. 3.3 and reminded here:

$$H^0_{u,r} = \sin\beta h' - \cos\beta H', \qquad H^0_{d,r} = \cos\beta h' + \sin\beta H' \tag{5.2}$$

where the vev of H' is zero, and the vev of h' is equal to the one of the Standard Model Higgs boson. The corresponding rotation of the imaginary components $H^0_{u,i}$ and $H^0_{d,i}$ (with $\beta \to -\beta$) diagonalizes their 2×2 mass matrix exactly and generates the Goldstone boson together with the MSSM-like pseudoscalar A'. The latter still mixes with the singlet-like S_i, but typically both differ little from the mass eigenstates A and a_s.

Performing the rotation (5.2) in (5.1) and using the previous approximations in the CP-even and CP-odd sectors, one obtains the trilinear couplings

$$\frac{\lambda A_\lambda}{\sqrt{2}} \left(\frac{\tan^2\beta - 1}{\tan^2\beta + 1} h \left(H h_s - A a_s \right) + \dots \right) \tag{5.3}$$

where the omitted terms are suppressed by $\tan\beta$. Hence, for not too small $\tan\beta \to 1$, trilinear couplings g_{hHh_s} and g_{hAa_s} are generated which have no analog in the MSSM, and are larger than all other trilinear Higgs couplings if λA_λ is large.

On the other hand the masses $m_{H/A}$ of the nearly degenerate mostly MSSM-like states H/A are approximatively given by

$$m^2_{H/A} \sim \mu \left(A_\lambda + \frac{\kappa}{\lambda}\mu \right) \frac{1+\tan^2\beta}{\tan\beta} \,, \tag{5.4}$$

which limits A_λ from above for fixed $m_{H/A}$, $\tan\beta$, small $|\kappa/\lambda|$ and $\mu \gtrsim 100$ GeV (as required by lower LEP bounds on higgsino-like charginos).

The production cross section for the mostly MSSM-like states H/A is dominated by ggF [11, 87, 88]; at $\sqrt{s} = 13 - 14$ TeV and for $\tan\beta \sim 2 - 3$ (typical in the NMSSM) they are $\gtrsim \mathcal{O}(1\,\text{pb})$ up to $m_{H/A} \sim 600$ GeV. The trilinear couplings g_{hHh_s} and g_{hAa_s} induce the decays $H \to h + h_s$ and $A \to h + a_s$ if kinematically allowed. The branching fractions $BR(H/A \to h + h_s/a_s)$ can be as large as $\sim 50\%$, in contrast to the decay $H \to h + h$, which is largely suppressed in this phenomenologically favoured regime.

The singlet-like states $\Phi_S = h_s/a_s$ have small couplings to quarks, leptons and gauge fields induced by mixings with h', H' and A'. Hence the production cross sections for Φ_S are typically small, and their discovery may have to rely on $H/A \to h + \Phi_S$ decays. Via the couplings induced by mixing, Φ_S can decay into the same channels as h and H/A. For $m_{\Phi_S} > 2m_t$, decays into $t\bar{t}$ are dominant, whereas decays $\Phi_S \to b\bar{b}$ dominate for $m_{\Phi_S} < 2m_t$. For $m_{h_s} > 250$ GeV, decays $h_s \to h + h$ are possible, leading to double-resonant tri-Higgs production (not considered here). Decays $\Phi_S \to \tau^+ + \tau^-$ are practically always possible. For the regions in the NMSSM parameter space with m_H not too large, and all present constraints on the signal rates of h being satisfied, the $BR(\Phi_S \to \gamma + \gamma)$ is in the $0.1 - 0.3\%$ range, making this decay observable as well. Henceforth we will consider resonant $b\bar{b}b\bar{b}$, $b\bar{b}\tau^+\tau^-$ and $b\bar{b}\gamma\gamma$ final states originating from $\Phi_S \to b\bar{b}$, $\Phi_S \to \tau^+\tau^-$ and $\Phi_S \to \gamma\gamma$ decays.

Of interest will be the product of cross sections times branching fractions $\sigma(ggF \to H/A) \times BR(H/A \to H_{125} + \Phi_S \to b\bar{b}b\bar{b},\ b\bar{b}\tau^+\tau^-$ and $b\bar{b}\gamma\gamma)$ for various masses M_H and M_{Φ_S}, for realistic regions in the parameter space of the NMSSM. To this end we have performed scans using the public code `NMSSMTools_5.1.0` [83, 84] including the radiative corrections from [85]. All phenomenological constraints, including the absence of Landau singularities below the GUT scale and, notably, constraints from Higgs searches in various channels at LEP and LHC are applied. These include searches for H in the $H \to \tau\tau$ channel, with H produced in association with b-quarks.

The results of these scans for $\sigma(ggF \to H) \times BR(H \to h + h_s \to b\bar{b}b\bar{b},\ b\bar{b}\tau^+\tau^-$ and $b\bar{b}\gamma\gamma)$ will be compared to the sensitivities in different final states in the next sections. The ggF production cross sections for H have been obtained from the CERN Yellow Report web page [114] at NNLO+NNLL, after an appropriate

rescaling of the H-gluon-gluon coupling provided by `NMSSMTools_5.1.0`. This rescaling includes the possible modification in the production rate by stops running in the loop, which are assumed heavier than ~ 750 GeV to avoid phenomenological constraints from stops searches. Also the $BR(H \to h + h_s)$, $BR(h \to b\bar{b})$ and $BR(h_s \to b\bar{b})$ are taken from `NMSSMTools_5.1.0`. In the Figures showing the 95% CL exclusion limits and $5\,\sigma$ discovery cross sections, viable values for the cross sections times branching fractions in the parameter space of the NMSSM will be indicated as light shaded blue regions.

For simplicity we will use the notation $ggF \to H \to h + h_s$ in the following. The same search strategies apply to $ggF \to A \to h + a_s$.

5.3 Signal simulation

The signal events have been generated using the publicly available code `aMC_SusHi 2.3.3` [115]. `aMC_SusHi` allows the generation of Higgs bosons produced in gluon gluon fusion at NLO QCD. The code employs the `MadGraph_aMC@NLO` framework linked with `SusHi` [86], where the latter provides the amplitudes of the involved diagrams. Thus, full dependence on the quark masses is included, in a MC@NLO-type matching with the `Pythia6.4` parton shower. All events have been generated at a center of mass energy of $\sqrt{s} = 13$ TeV. We remark that no BSM loops have been included in the simulation (e.g. stops loops), however, the impact of such effects in the kinematic distributions only affects the high $p_T(H)$ tail and can safely be neglected.

We apply the NNPDF2.3NLO PDF set [116], with the corresponding value of the strong coupling constant, linked with `LHAPDF6` [117]. Both the renormalization and factorization scales are chosen on an event-wise basis. Such dynamical scale choice sets

$$\mu_R = \mu_F = H_T/2 \equiv \frac{1}{2}\sum_i \left(m_i^2 + p_T^2(i)\right)^{1/2}, \tag{5.5}$$

where i runs over all final state particles and m_i and $p_T(i)$ are their mass and transverse momentum, respectively. This choice is meant to take into account the effects from hard radiation and corresponds to a value of $m_H/2$ in the soft/collinear limit $p_T \to 0$, which is the current recommendation for the total inclusive cross section in the gluon fusion process [118].

As stated above, the events are showered using `Pythia6.4`. The heavy Higgs boson is produced in the gluon fusion channel at the matrix element level by `MadGraph_aMC@NLO`. Its decay into a SM Higgs with a mass $m_h = 125$ GeV and an extra scalar and the decays of both scalars into b-quark pairs are treated with `Pythia`.

m_H (GeV)	m_{h_s} (GeV)
350	[25, 215], steps of 10 GeV
425	[25, 215], steps of 10 GeV; [230, 290], steps of 20 GeV
500	[25, 215], steps of 10 GeV; [230, 370], steps of 20 GeV
625	[25, 215], steps of 10 GeV; [230, 295], steps of 20,25 GeV
750	[25, 200], steps of 10 GeV; [220, 620], steps of 20 GeV
1000	[25, 500], steps of 25 GeV; [500,800] steps of 50 GeV

Table 5.1: Pairs of (m_H, m_{h_s}) generated for the present work. 150k events were generated for each pair.

We generated 150k unweighted events for each pair (m_H, m_{h_s}), which is generally more than the total number of expected events at the HL-LHC (L=3000 fb^{-1}) for the typical $pp \to H \to hh_s \to b\bar{b}b\bar{b}, b\bar{b}\tau\tau, b\bar{b}\gamma\gamma$ cross sections in the NMSSM [18, 112]. Therefore the statistical fluctuations in our signal samples will be smaller than those expected for the LHC, even at its high luminosity regime. In the present work we have considered signals where the mass of the heavy state runs from 350 GeV up to 1 TeV, and the mass of the other non-SM Higgs involved in the decay within [25 GeV, $m_H - 125$ GeV]. Table 5.1 shows the steps that have been used.

Since the widths of the non-SM states h_s and H, Λ_{h_s} and Λ_H vary non-trivially with the model parameters, the samples were generated with a fixed values for the widths set to $\Lambda_H = 1$ GeV and $\Lambda_{h_s} = 10^{-3}$ GeV. For the NMSSM, the total widths of H are below $M_H/50$ in all cases, below $M_H/100$ for $M_H < 500$ GeV, hence the narrow width approximation is well satisfied.

At parton level, jets are required to have a $p_T > 20$ GeV and $\eta < 2.5$. Finally, all samples are passed through `Delphes` for detector simulation, including b-tagging as described in 5.4.1. Jets are clustered with `FastJet v3.0.1` using an anti-k_T algorithm with $\Delta R = 0.4$.

The same event generator, showering and hadronization codes, as well as the generator level cuts, will be used for all the background samples. Also, the same scale setting and PDF set will be used for all the backgrounds, unless explicitly stated. The detector simulation and jet clustering will also be treated in the same way for the signal and for the background. However, different b-tagging capabilities will be implemented in the different channels.

5.4 The $b\bar{b}b\bar{b}$ channel

Searches for resonant SM Higgs pair production in the $b\bar{b}b\bar{b}$ final state have been performed before by ATLAS at 8 TeV [90, 92, 93] and at 13 TeV [94], and by CMS at 8 TeV [97, 99, 101] and at 13 TeV [102, 103].

Searches for $ggF \to H \to h_s + h \to b\bar{b}b\bar{b}$ are complicated by the presence of two unknown masses of H and h_s. A naive approach would be to require one $b\bar{b}$ pair with a mass near 125 GeV, and to look for simultaneous excesses in the plane of invariant masses of the other $b\bar{b}$ pair and the total $4b$ invariant mass. However, this approach does not allow to optimize cuts as function of different masses of H and h_s. An at least $\sim 20\%$ gain in efficiency can be obtained as follows:
a) Choose a tentative value for m_{h_s}, $m_{h_s}^{\text{test}}$ (mass hypothesis), and optimise the cuts and the choice of $b\bar{b}$ pairs as function of this value;
b) Search subsequently for an excess in the total $4b$ invariant mass (suitably corrected, see below).

In the following subsections we discuss the background simulation and validation, and finally the results for the expected 95% CL upper limits and $5\,\sigma$ discovery limits on the cross sections times branching fractions as function of m_H and m_{h_s}. The latter are compared to production cross sections times branching fractions in the NMSSM.

5.4.1 Background simulation

For the $b\bar{b}b\bar{b}$ channel, the dominant background consists in QCD multijet production, whereas other sources such as top-quark pair production have less impact on the final shape and event yield of the $b\bar{b}b\bar{b}$ background.

The simulation of the QCD multijet background is very challenging due to the many possible sources of b jets. Apart from those coming from the Matrix Element (ME) generator, one could obtain b quarks in the splitting of gluons from the Parton Shower (PS). Also, lighter quarks (mainly charm quarks) and gluon jets could be misidentified as b jets by the b-tagger algorithm (explained in the next subsection). Thus, one should in principle generate all relevant final-state partonic multiplicities in the ME generator and merge them (either at LO [119–121] or NLO [122, 123]) in order to account for all possible such sources described above. However, we found sufficient to consider the inclusive processes $b\bar{b}jj$ and $b\bar{b}b\bar{b}$ at the ME level. Indeed, lower multiplicities such as bbj were studied individually and found to have a negligible contribution to the background when requiring 4 b jets in the final state. On the other hand, adding an extra jet would have a minimum impact in the invariant mass distributions of the b jet systems, and its contribution to the total number of events could be accounted for by means

of an NLO K-factor including the real emission diagrams. We have found that with the chosen b-tagging working point and the selection criteria of the proposed search strategies, the misidentification of light quarks apart from charms could be neglected in a good first approximation. Also, b-pairs produced in the PS from hard gluon jets (also from the matrix element $bbjj$) give rise to negligible contributions after selection criteria. Therefore, our simulation of the multijet background will consist only in the process $b\bar{b}b\bar{b}$ and $b\bar{b}c\bar{c}$ at parton level, with no need of merging higher (or lower) multiplicities (see table 5.2 for the details on their simulation). Finally, the LO cross sections obtained using `MadGraph5` have been rescaled by the best available higher order K-factors [124].

In addition to the the QCD multijet processes, we also considered for this work the $t\bar{t}$ contribution to the $b\bar{b}b\bar{b}$ background. This process features a large cross section, and leads to a high multiplicity final state through the hadronic decay of the top quark. The $t\bar{t}$ background consists mainly in events where $t \to \bar{b}W \to \bar{b}jj$, leading to three jets for each top quark. Thus, in practice all events of the $t\bar{t}$ contribution to the $b\bar{b}b\bar{b}$ background a charm quark from the W decay is mistagged as a b jet (light flavours have a much smaller mistag rate, see next section) and paired with the b quark from the top quark decay to form a Higgs candidate. In order to reduce this contribution, we apply a so-called $t\bar{t}$-veto similar to the one applied by the experimental collaborations in similar searches. The idea is basically to discard events where we can reconstruct a W boson and a t quark in the event. In each event, we take the non b-tagged jets (extra jets) and pair each of them with the $b\bar{b}$ dijets if they satisfy $\Delta R(j_{\text{extra}}, jj_i) < 1.5$; these are top quark candidates. Then, W candidate from a top quark candidate is reconstructed by summing the 4-momentum of the extra jet with the b-jet of the dijet which is closer in ΔR to it. Finally, we compute the value of the variable:

$$\chi^2_{tt} = \left(\frac{m_W - \tilde{m}_W}{\sigma_{m_W}}\right)^2 + \left(\frac{m_t - \tilde{m}_t}{\sigma_{m_t}}\right)^2, \tag{5.6}$$

where m_W and m_t are the invariant masses of the W boson and top quark candidates, $\sigma_{m_W} = 0.1 m_W$, $\sigma_{m_t} = 0.1 m_t$, $\tilde{m}_W = 80.4$ GeV and $\tilde{m}_t = 172.5$ GeV. If

Process (ME)	σ_{LO}(pb)	# events	K-factor	equiv. luminosity
$b\bar{b}c\bar{c}$	40298.4 pb	10M	1.3 (NLO)	4.7 fb^{-1}
$b\bar{b}b\bar{b}$	761.6 pb	20M	1.7 (NLO)	13.5 fb^{-1}
$t\bar{t}$	461 pb	15M	1.7 (NNLO+NNLL)	17.4 fb^{-1}

Table 5.2: Processes considered in the study of the contributions to the total $b\bar{b}b\bar{b}$ background

for some possible combination in an event we find $\chi^2_{tt} < 3.2$, the event is considered compatible with the top quark decay hypothesis and hence rejected. After applying the $t\bar{t}$ veto, the $t\bar{t}$ background supposes around $\sim$5% of the dominant multijet background described above for all the analysis that we propose in this work, while the signal is barely affected by the veto algorithm.

For the normalization, we computed the LO cross sections for $t\bar{t}$ using `MadGraph5_aMC@NLO`, and the code `top++2.0` [125] to obtain the NNLO+NNLL K-factor.

We end the description of the background modelling by mentioning that we have not accounted for pile-up nor underlying event effects for simplicity, pointing out that there exist recent studies [126] showing that modern techniques are able to considerably reduce the effects of pile-up contamination in the $b\bar{b}b\bar{b}$ final state.

b-tagging

The b-tagging algorithm is included in the detector simulation which is done using `Delphes 3.3.3`. The default ATLAS card is used to simulate the detector. In this framework, one has to provide `Delphes` with the efficiency for b-tagging and light quark mistagging as a function of p_T and η. The ATLAS collaboration has presented in [127] the current b-tagging performance using Run I data, and also CMS recently presented its b jet identification performance using 2016 data [128]. Although ATLAS has recently released the expected performance at the HL-LHC regime for b-tagging [129], in the present work we reproduce the expected performances for the b-tagging algorithms in RUN-II reported by ATLAS in [130]. In the projection study [130], a multivariate b-taging algorithm named `MV2` is presented, which is based in a boosted decision tree (BDT) algorithm to discriminate b-jets from light (u, d, s-quark or gluon jets) and c-jets. The `MV2` algorithm outputs for each jet a real number within [-1,1], and then different working points are defined by a single cut value on the `MV2` tagging algorithm output distribution. They are chosen to provide a specific b-jet efficiency on a $t\bar{t}$ sample. A looser cut on this output results in a higher efficiency for the b-taging, but at the price of also increasing the rate of light-jets (mainly charm quarks) being misidentified as b-jets.

For studying the $b\bar{b}b\bar{b}$ final state we take the working point named $\epsilon_b = 70\%$, as the experimental collaborations do for the current searches for Higgs pair production in the $b\bar{b}b\bar{b}$ final state [131]. This working point is chosen to maximize the sensitivity, also minimizing the impact of mistagged light jets.

The b-tagging efficiency and the mistagging efficiency as a function of the transverse momentum of the jet, reported by ATLAS [130], were fitted to analytical functions given by:

$$\epsilon_b(p_T) = b * \tan(c * p_T) \left(\frac{a}{1 + d * p_T} \right), \tag{5.7}$$

where we have approximated the efficiency dependence on η and the average pile-up to be flat. The light-flavour mistagging is fitted to a linear function. These functions, which are the default setting in the ATLAS card in `Delphes 3.3.2` , were given to the detector simulation routine to mimic the expected performance of Run 2. However, recall that the b-tagging algorithms are continuously improved by the experimental collaborations, and therefore the one presented here could be regarded as a conservative approach when making predictions for the HL-LHC regime. In table 5.3 we present the explicit values of the fits for the tagging algorithms.

Algorithm	a	b	c	d
b-tagging	30	0.8	0.003	0.086
c-tagging	1	0.02	0.02	0.0034
light-jet-tag.	$\epsilon_{\text{light}}(p_T) = 0.002 + 7.3 \cdot 10^{-6} \cdot p_T$			

Table 5.3: Fit parameters for the tagging algorithms as a function of p_T .

Validation of the background simulation

In this section we make a comparison of our background modelling based on the Monte Carlo techniques described above, with real data collected by the ATLAS collaboration [131]. This analysis reports a search for resonant double SM Higgs production, which could be identified with our search for the case where $m_{h_s} = m_h$=125 GeV. As the analysis reported non-observation of BSM physics and a very good agreement with their background prediction, we use their measurement in the $b\bar{b}b\bar{b}$ final state to directly compare their data with our predictions for the same c.m.e. and luminosity, by reproducing the analysis and applying it to our background sample.

It is important to remark here that the methods for predicting the expected multijet background used by the experimental collaborations are not based on MC simulations, but on data-driven methods instead. We make here a brief exposition of the data-driven modelling technique used in [131] before a direct comparison of the reported results therein with our MC simulation.

It is also convenient to define here the concepts of sidebands and control regions since, as we will see, for certain search strategies we can easily extrapolate in a real experiment the data-driven methods for the double SM Higgs production to the case where the mass m_{h_s} is unknown.

Data-driven modelling

The data-driven method is based on the use of sidebands and control regions to estimate the behaviour of the background in the region of interest for the search, the so-called signal region. For the case of $b\bar{b}b\bar{b}$, the technique consists in using an independent sample of events selected using the same trigger and selection requirements as for the final analysis, with the exception that the condition of having four b-tagged is relaxed to only two b-jets, where the other two jets are not tagged (named 2-tag sample). Clearly, the cross section of the process $pp \to b\bar{b}jj$ is much larger than $pp \to b\bar{b}b\bar{b}$, and therefore the number of expected events increases dramatically. Thus the signal contamination for this sample is absolutely negligible for the typical signal cross section at study: any Higgs-to-Higgs signal will be buried under the overwhelming QCD processes. Recall that in doing this we have assumed that the kinematics of the non b-jets and b-jets are the same, which is indeed the case when we can approximate the b quarks to be massless.

On this 2-tag sample, a sideband is defined as a signal-free region in the plane of the two dijets invariant masses, not too far from the region where we expect the signal (signal region, see expression (5.9)) in order to ensure that the kinematic properties are preserved. The shape of the 4-tag background is modelled here, and then tested in a control region defined as the region in the $m^1_{2j} - m^2_{2j}$ plane between the sideband and the signal region. The definitions of the sideband and control region are chosen such that both are orthogonal to the signal region and to give approximately the same number of events. Finally, the normalization of the multijet background prediction (i.e. the total number of expected events in the actual 4-tag regions) is set by rescaling the total number of events in each region of the 2-tag sample by a factor μ_{multijet}:

$$\mu_{\text{multijet}} = \frac{N^{\text{4-tag}}_{\text{data}} - N^{\text{4-tag}}_{t\bar{t}}}{N^{\text{2-tag}}_{\text{data}} - N^{\text{2-tag}}_{t\bar{t}}}, \tag{5.8}$$

where $N^{\text{2-tag}}_{\text{data}}$ and $N^{\text{4-tag}}_{\text{data}}$ are the number of events measured from data in the sideband region of the 2-tag and 4-tag sample respectively, and the yields $N^{\text{2-tag}}_{t\bar{t}}$ and $N^{\text{4-tag}}_{t\bar{t}}$ are meant to account for the $t\bar{t}$ contaminations of the samples and are computed using MC simulations.

However, there exists a fundamental problem when modelling a 4 b-tagged background out from a 2-tag sample: the b-tagging efficiencies vary as a function of the jets p_T and η, and therefore each jet in the event is associated to different b-tagging efficiency. To circumvent this issue, ATLAS carries out a reweighting procedure to correct these differences introduced by the additional b-tagging requirements. For details on this procedure we refer to [131]. This effect highlights the necessity to adequately reproduce the b-tagging algorithms used by the experimental collaborations when doing a realistic MC-based $b\bar{b}b\bar{b}$ background modelling.

MC vs data

In order to validate the modelling of the background in our Monte Carlo approach, we discuss a direct comparison of our background sample with available data from the ATLAS analysis [131], at $\sqrt{s} = 13$ TeV with an integrated luminosity of $10.1 fb^{-1}$. We recall here that it is reported in the experimental paper that after the full event selection 95% of the background consists of multijet events, whereas only a 5% is due to $t\bar{t}$, in very good agreement with our MC results.

Proceeding as detailed in [131], we reproduce the analysis using the same event selection and cuts. Then, we require at least four b-tagged jets, and use the four p_T leading ones to construct the Higgs boson candidates. The pairing algorithm used by ATLAS, based on the distance in the dijets invariant masses plane to the point (120 GeV, 115 GeV), is reproduced. The final analysis discriminant is the total invariant mass of the system, m_{4b}.

Recall that our MC simulation (of $\sim 2{\cdot}10^7$ events in the $b\bar{b}b\bar{b}$ sample) reproduces a luminosity similar to the one from the ATLAS search, and therefore the statistical errors are expected to be comparable. Thus, we carry out our comparison directly using the MC events instead of fitting it to an analytical function.

The signal region is defined such that the Higgs bosons candidates' masses should lie within $X_{hh} < 1.6$, with:

$$X_{hh} = \sqrt{\left(\frac{m_{2j}^{lead} - 120 \text{ GeV}}{0.1 m_{2j}^{lead}}\right)^2 + \left(\frac{m_{2j}^{subl} - 115 \text{ GeV}}{0.1 m_{2j}^{subl}}\right)^2}, \tag{5.9}$$

where the terms in the denominators represent the widths of the Higgs boson candidates. Such ellipse-like shape is meant to account for the experimental correlation between the dijets invariant masses.

Lastly, we normalize the sample to the corresponding integrated luminosity and the LO cross section times the NLO K-factor, which has been approximated to be flat (i.e. constant in all phase space).

A comparison with the ATLAS data is presented in fig. 5.1. Still (and expectedly) our simulated background falls below the measured data given in Fig. 5.1 in [94]. On the upper hand side of Fig. 5.1 we show the measured m_{4b} distribution from in Fig. 5.1 in [94], and our MC result with statistical errors expected for 10.1 fb^{-1} of integrated luminosity. The lower part shows the ratio MC/data bin by bin. At least for the interesting region $m_{4b} > 350$ GeV an overall reweighting of our multijet background, as performed in [94], seems appropriate. A best fit is obtained with a rescaling of 1.55 ± 0.27. The $t\bar{t}$ background is left untouched, and remains at $\sim 4.6\%$ (after applying a $t\bar{t}$ veto and the above cuts, and after rescaling). The comparison of the m_{4b} distribution of our background after rescaling to the data from [94] is shown on the lower side of Fig. 5.1.

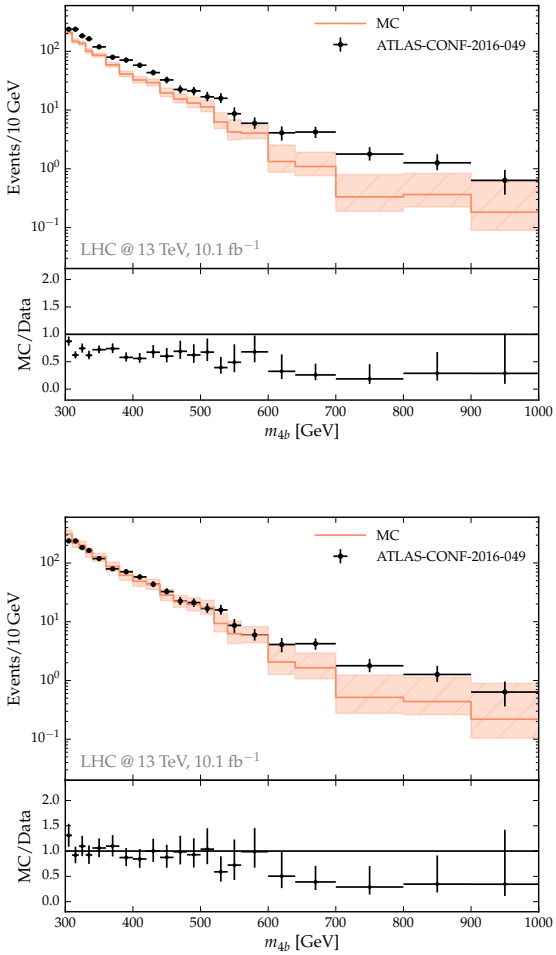

Figure 5.1: Left hand side: measured m_{4b} distribution from in Fig. 5 in [94], and our MC result with statistical errors expected for 10.1 fb^{-1} of integrated luminosity. The lower part shows the ratio MC/data bin by bin. Right hand side: the m_{4b} distribution of our background after rescaling, compared to the data from Fig. 5 in [94].

Finally, we remark that we have validated our background by comparing it with data from a search for resonant double SM Higgs production, i.e. featuring two SM Higgs bosons of $m_h = 125$ GeV. In the present work we extend this search to $H \to hh_s$, where at least one of the produced scalars has a mass of 125 GeV but the other one could be in principle in any kinematically allowed region. Clearly it is somewhat optimistic to assume that the rescaling of the multijet background by 1.55 ± 0.27 remains valid for $m_{h_s} \neq 125$ GeV. In the absence of data from sidebands this is, however, the best we can do. Subsequently ± 0.27 will be used as systematic uncertainty of our background estimation for all m_{h_s}, a number to be considered as indicative. However, if we estimate the expected sensitivity as $Z = \frac{S}{\sqrt{B}}$, we conclude that even an underestimation of the background of around 60% of the actual number of events yielded in a real experiment, translates into a expected sensitivity $\sim 29\%$ more 'optimistic' than the observed one. We consider such precision sufficient for the purposes of this feasibility study.

5.4.2 Event reconstruction and selection

Resolved vs. boosted topologies

b-quarks are not colour-singlet states, and thus they hadronize. They have a long decay giving rise to large cascades of QCD states radiated from them. As a consequence, jets associated to b-quarks are generally wide, and for $\sqrt{s} = 13$ TeV the jet definition (through a anti-k_T algorithm, for instance) with $\Delta R = 0.4$ is usually a good description of the physical jet. However, in topologies where the $b\bar{b}$ pair decays from a heavy or very boosted resonance, the jets associated to two individual b quarks may be very collimated and eventually merge with each other, and the algorithm cannot longer resolve the two separated b-quark jets. This implies a loss of the signal efficiency in such kinematic regions, named boosted-regions, and therefore a loose of discovery power if we insist in requiring four $\Delta R = 0.4$ b-jets. The region where the algorithms can resolve four $\Delta R = 0.4$ b-jets for the signal events in the $b\bar{b}b\bar{b}$ final state is called the "resolved" region. For our case, it is in general sufficient to take $m_H < 1$ TeV and $m_{h_s} > 35$ GeV to remain in the resolved region.

However, in recent years methods for analysing the finer structure of jets have been developed. In these so-called jet substructure methods, events are clustered with larger cone radius (typically $\Delta R = 1.0$), and then in a further step the algorithm goes backwards to disentangle two jets out from the original one, following some criteria that the user has to define. For further details on jet substructure methods we refer to [134] or [135] for a review. For the case of double SM Higgs production in the $b\bar{b}b\bar{b}$ final state, the ATLAS collaborations has released searches

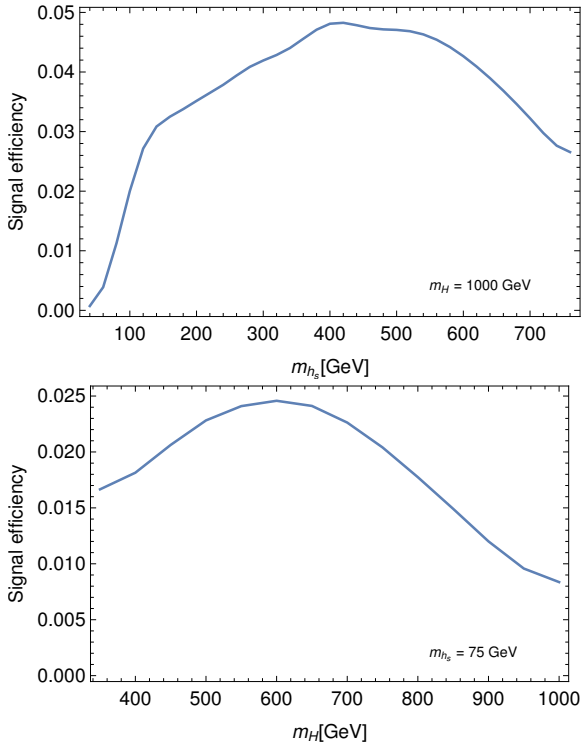

Figure 5.2: Signal efficiencies for the resolved analysis described in sec. xx. On the left (right), the signal efficiency as a function of the mass m_{h_s} (m_H) for a fixed $m_H = 1$ TeV (m_{h_s} =75 GeV). In both cases we can observe the loss of signal efficiency for $m_H \gg m_{h_s}$.

analysing both the resolved and boosted regions separately: the resolved analysis is applied for masses of the heavy resonance up to 1000 GeV, whereas the boosted analysis is used for higher masses. Upper limits on the resonant production have been established ranging between 2 and 1000 fb for masses between 300 and 3000 GeV, at $\sqrt{s} = 13$ TeV and $\mathcal{L} = 11.3\text{fb}^{-1}$, and similar results were found by CMS.

The boosted topology plays an important role only for large values of m_H, approximately above 1 TeV (although light h_s states $m_{h_s} < 70$ GeV may give rise to boosted b-pairs at $m_H < 1$ TeV). However, the typical NMSSM cross sections for large values of m_H becomes way too small for detection even including boosted b-jets. For this reasons, in the present work we restrict ourselves to resolved topologies. For the analysis here presented, jets are clustered with a radius parameter $\Delta R = 0.4$. We require each event to have at least 4 b-tagged jets of which we take only the 4 p_T leading jets to construct the two Higgs candidates, each with $p_T > 40$ GeV and $\eta < 2.5$.

It is important to remark here that even if we consider only regions where we are able to resolve 4 b-jets, there are other effects which may difficult the

reconstruction task. On the one hand, we have the semileptonic decays of the b-hadrons, which give rise to invisible parts which can not be accounted for. On the other hand, jets clustered with a radius parameter $\Delta R = 0.4$ not necessarily include all the tracks from the original b-quark, in particular if the b-pairs are produced at large angles (as it is the case when h and h_s are produced with very low momentum). Not accounting for these missing tracks results in lower invariant masses.

Reconstruction, selection and cuts

For the pairing of the b-jets to reconstruct the Higgs candidates we can use in this strategy the information provided by the test mass $m_{h_s}^{\text{test}}$ in the mass-based algorithm for looking for the adequate pairs. Thus, at each step of the scan, the algorithm computes all the possible pairings with their corresponding dijet invariant masses, and picks the pair that minimizes its distance in the dijet invariant mass plane $\left(m_{b\bar{b}}^{(1)}, m_{b\bar{b}}^{(2)}\right)$ to the point $(115\text{ GeV}, m_{h_s}^{\text{test}} \cdot 0.85)$ (or $(m_{h_s}^{\text{test}} \cdot 0.85, 115\text{ GeV})$). After pairing, the $b\bar{b}$ system with an invariant mass closer to 115 GeV is tagged as the SM Higgs boson.

Following the recipes of [131] for the case of double Higgs production, we define a signal region in the dijet invariant masses plane as:

$$\chi_{hh_s} = \sqrt{\left(\frac{m_{b\bar{b}}(h) - 115\text{ GeV}}{0.11 m_{b\bar{b}}(h)}\right)^2 + \left(\frac{m_{b\bar{b}}(h_s) - 0.85 m_{h_s}^{\text{test}}}{0.11 m_{b\bar{b}}(h_s)}\right)^2} < 2 \tag{5.10}$$

In fig. 5.3 we show the distribution of events in the dijet masses plane before cuts for the case when $m_{h_s}^{\text{test}} = m_{h_s}$, with the signal region contour illustrated by the black curve. We see that for the case when the scan hits the correct mass, the reconstruction of both bosons is generally good and both masses m_{h_s} and m_H can in general be obtained quite well.

The kinematic cuts were obtained in the same way as in the previous sections, and were optimized as a function of the test mass $m_{h_s}^{\text{test}}$ and the total invariant mass of the event, m_{4b}. The cuts on the dijets p_T are:

$$p_T^h > 1.56\text{ GeV} + 0.4 m_{4b} - 0.13 m_{h_s}^{\text{test}} - 160 m_{h_s}^{\text{test}}/m_{4b}\text{ GeV} \tag{5.11}$$

for the Higgs-tagged dijet and

$$p_T^{h_s} > 11.92\text{ GeV} + 0.4 m_{4b} - 0.15 m_{h_s}^{\text{test}} - 166 m_{h_s}^{\text{test}}/m_{4b}\text{ GeV} \tag{5.12}$$

for the second dijet. Since we only use the 4 p_T leading b jets in the event, an event not satisfying these cuts is automatically discarded. In fig. 5.4 we show the

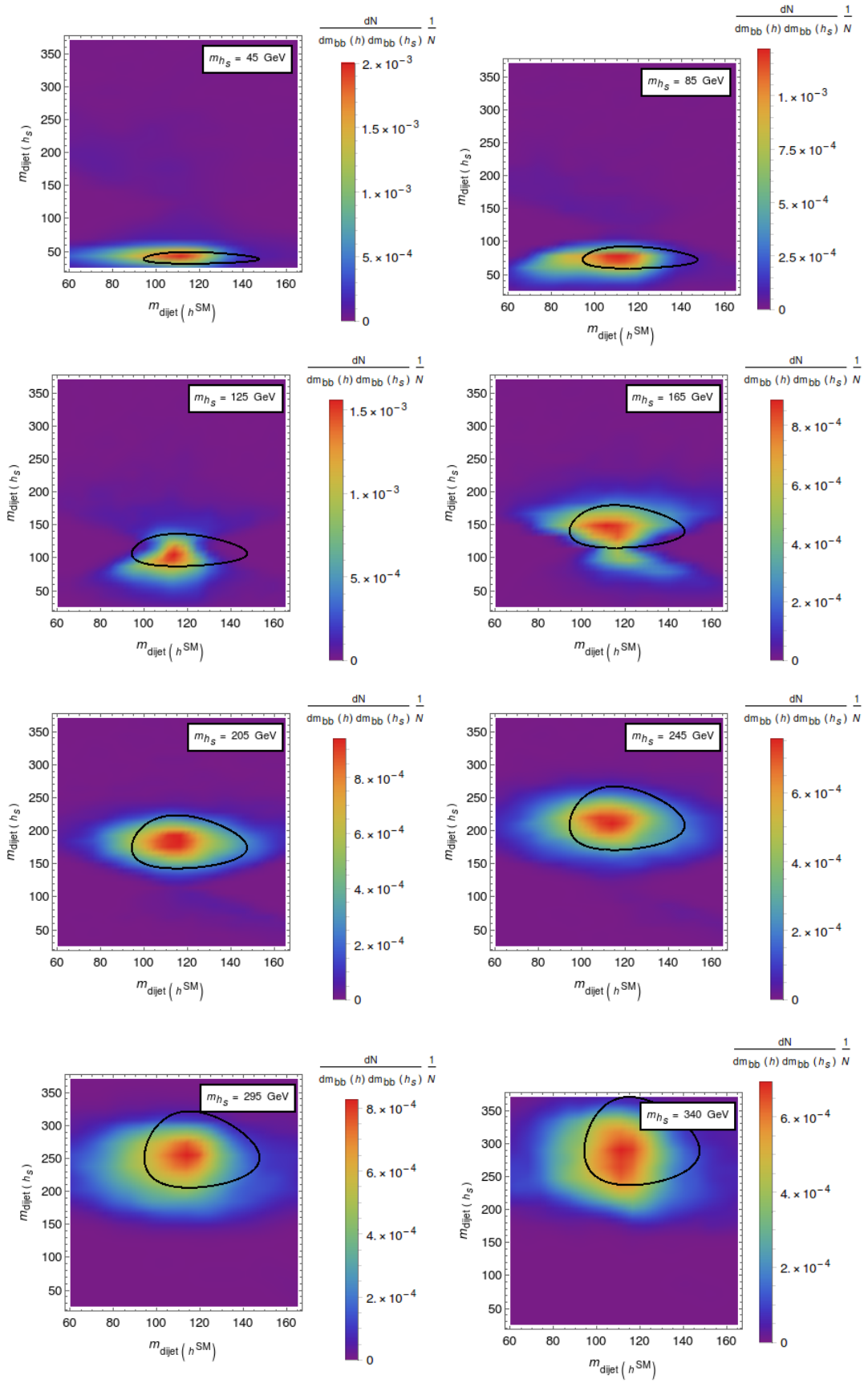

Figure 5.3: Distribution of the dijet invariant masses for m_H=500 GeV and various values for m_{h_s} using the mass algorithm for pairing, in case the test mass of the analysis $m_{h_s}^{\text{test}}$ coincides with the mass m_{h_s}. The black contour represents the signal region defined in eq. 5.10.

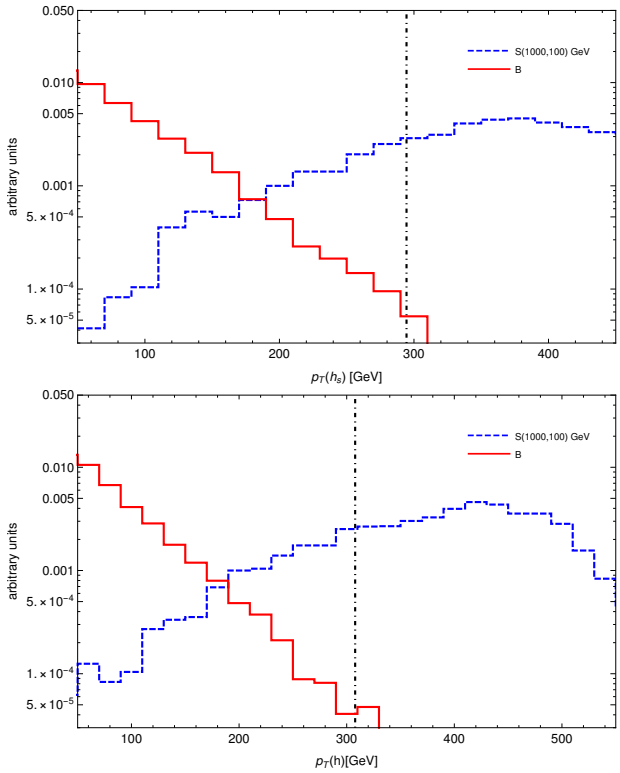

Figure 5.4: Distribution of the p_T cuts of the h_s (top) and the Higgs-tagged (bottom) dijets for the signal and background at $\sqrt{s} = 13$ TeV, for the case $m_H = 1000$ GeV and $m_{h_s} = 100$ GeV. The black vertical line indicates the approximated value of the cut, assuming $m_{4b} \approx m_H$.

p_T distribution of the background and signal for the case $m_H = 1000$ GeV and $m_{h_s} = 100$ GeV.

The acceptance times efficiency at each stage of the selection process is shown in figs. 5.5 and 5.6 for some illustrative signals.

The fact that we assume the mass m_{h_s} allows us to define a corrected total invariant mass m_X given by:

$$m_X = m_{4b} - m^h_{b\bar{b}} + 125 \text{ GeV} - m^{h_s}_{b\bar{b}} + m^{\text{test}}_{h_s} \tag{5.13}$$

This definition accounts for the effects of both $b\bar{b}$ systems and greatly improves the reconstruction of m_H producing a much better 4-body invariant mass resolution, specially at large masses m_{h_s}. As we see in figure 5.7, the signal peak results sharper and centred in the correct H mass, while barely affecting the background.

Regarding the size of the steps in the scan on $m^{\text{test}}_{h_s}$, ideally small steps should be taken to assure that any signal present in the sample can be tested. Here we

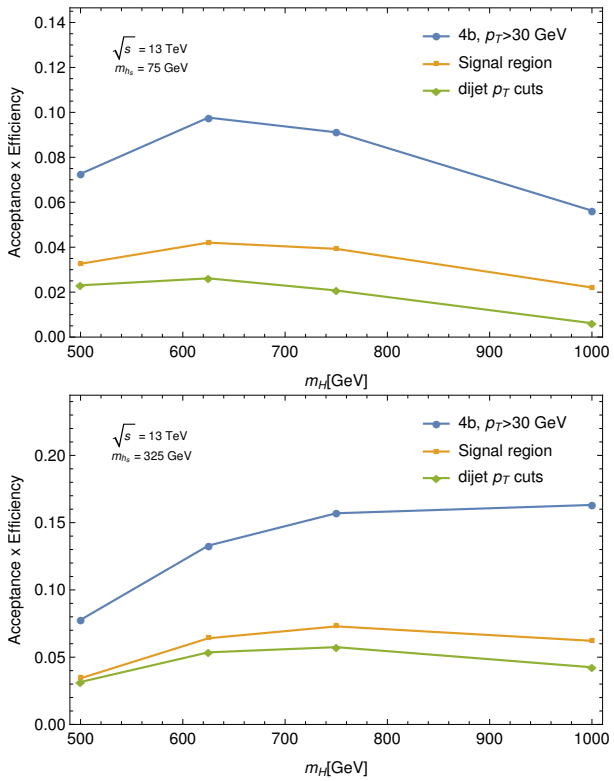

Figure 5.5: The selection efficiency as a function of the heavy resonance mass m_H at each stage of the event selection for a mass for h_s of $m_{h_s} = 75$ GeV (top) and $m_{h_s} = 325$ GeV (bottom)

estimate the minimum step size to be taken such that it guarantees that the scan does not miss any possible excess, given the size of the signal region 5.3. Since the signal could be approximately modelled by a Gaussian, we take as step size two times the standard deviation of the narrower signal in the $b\bar{b}(h_s)$ distribution, which corresponds to the case $m_{h_s} = 25$ GeV (and is approximately constant for all m_H). Thus we have $\Delta m_{h_s}^{\text{test}} = 9$ GeV. However, the width of the $b\bar{b}(h_s)$ distribution for the signal increases with the mass of the resonance h_s and thus larger steps could be taken for larger values of m_{h_s} . For instance, form $m_{h_s}^{\text{test}} \geq 200$ GeV onwards, the steps could be taken as $\Delta m_{h_s}^{\text{test}} = 40$ GeV

Modelling the background

As in the previous case, the background depends on the assumed window on m_{h_s}, and hence it should be modelled at each step in the scan over m_{h_s}. We fit the m_X background by means of a MLE method, as described in appendix A. We found

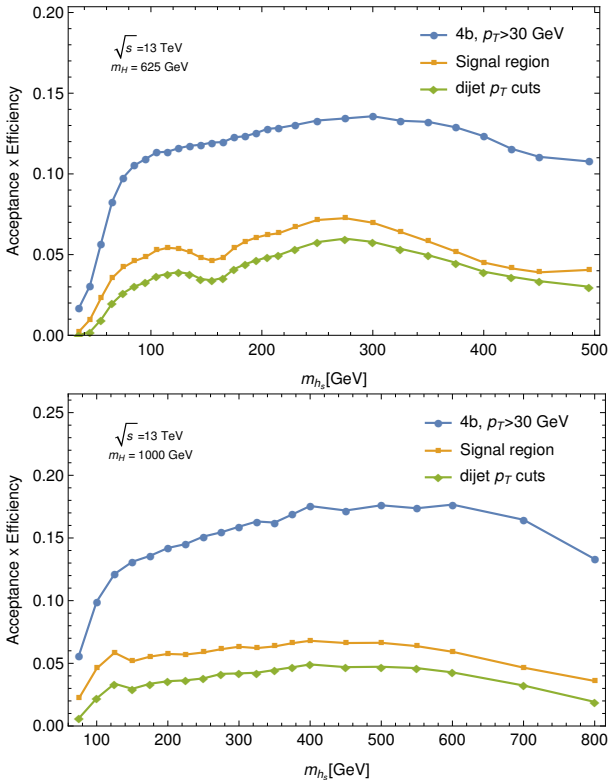

Figure 5.6: The selection efficiency as a function of the mass m_{h_s} at each stage of the event selection for a mass for H of $m_H = 625$ GeV (left) and $m_H = 1000$ GeV (right)

that the 4 parameter Gamma distribution, given by

$$f(x;\alpha,\beta,\gamma,\mu) = \begin{cases} \dfrac{\gamma e^{-\left(\frac{x-\mu}{\beta}\right)^{\gamma}} \left(\frac{x-\mu}{\beta}\right)^{\alpha\gamma-1}}{\beta\Gamma(\alpha)} & x \geq \mu \\ 0 & x < \mu \end{cases} \tag{5.14}$$

provides a very good agreement with data from the Monte Carlo. In fig. 5.8 we show the MC data for the background and the corresponding fit for two values of the test mass $m_{h_s}^{\text{test}}$. In the lower panels the standardized residuals for each bin are shown.

Unlike the case of the dijet background, the m_X background has only one maximum, placed at masses generally below our region of interest. Therefore, the search for a heavy resonance $m_H > 350$ GeV will consist in looking for a bump in a monotonically decreasing background, which simplifies the bump hunting task.

In the framework of a real experiment, this strategy allows for the definition of sidebands and control regions very similar to those used in the resonant double Higgs production searches in the $b\bar{b}b\bar{b}$ channel for modelling the background using

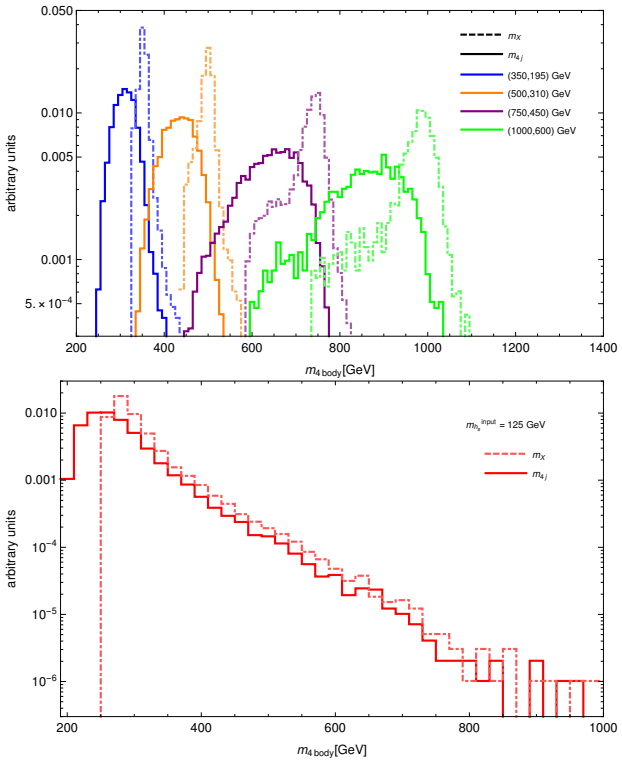

Figure 5.7: Reconstruction of the 4 body final state using m_{4b} (solid) and m_X (dashed), as defined in eq. 5.13, for various signal samples (top) and the background (bottom) under the hypothesis m_{h_s}= 125 GeV, at $\sqrt{s} = 13$ TeV. The distributions are normalized to the total value of the integral.

data. In order to define such regions, it would be sufficient to relax the b-tagging requirements and define orthogonal regions in the neighbourhood of that defined in eq. 5.10.

5.4.3 Discovery cross sections $X^{5\sigma}$ and exclusion limits

Given the m_X distribution of the background for various hypothetical values of m_{h_s} and the m_X distributions of signals as in Fig. 5.7 one can, following the statistical methods from [136] and described in the appendix B, obtain values for 95% CL exclusion limits and $5\,\sigma$ discovery limits for cross sections times branching fractions into the $b\bar{b}b\bar{b}$ final state as function of the integrated luminosity, m_H and m_{h_s}.

In the case of an integrated luminosity of 13.3 fb^{-1} at 13 TeV we can compare the expected 95% CL exclusion limits on cross sections times branching fractions to the ones given by ATLAS in Fig. 11 in [94], for $m_X = 300 \ldots 1000$ GeV and $m_{h_s} \sim 125$ GeV. (This ATLAS search was actually dedicated to spin 2 resonances

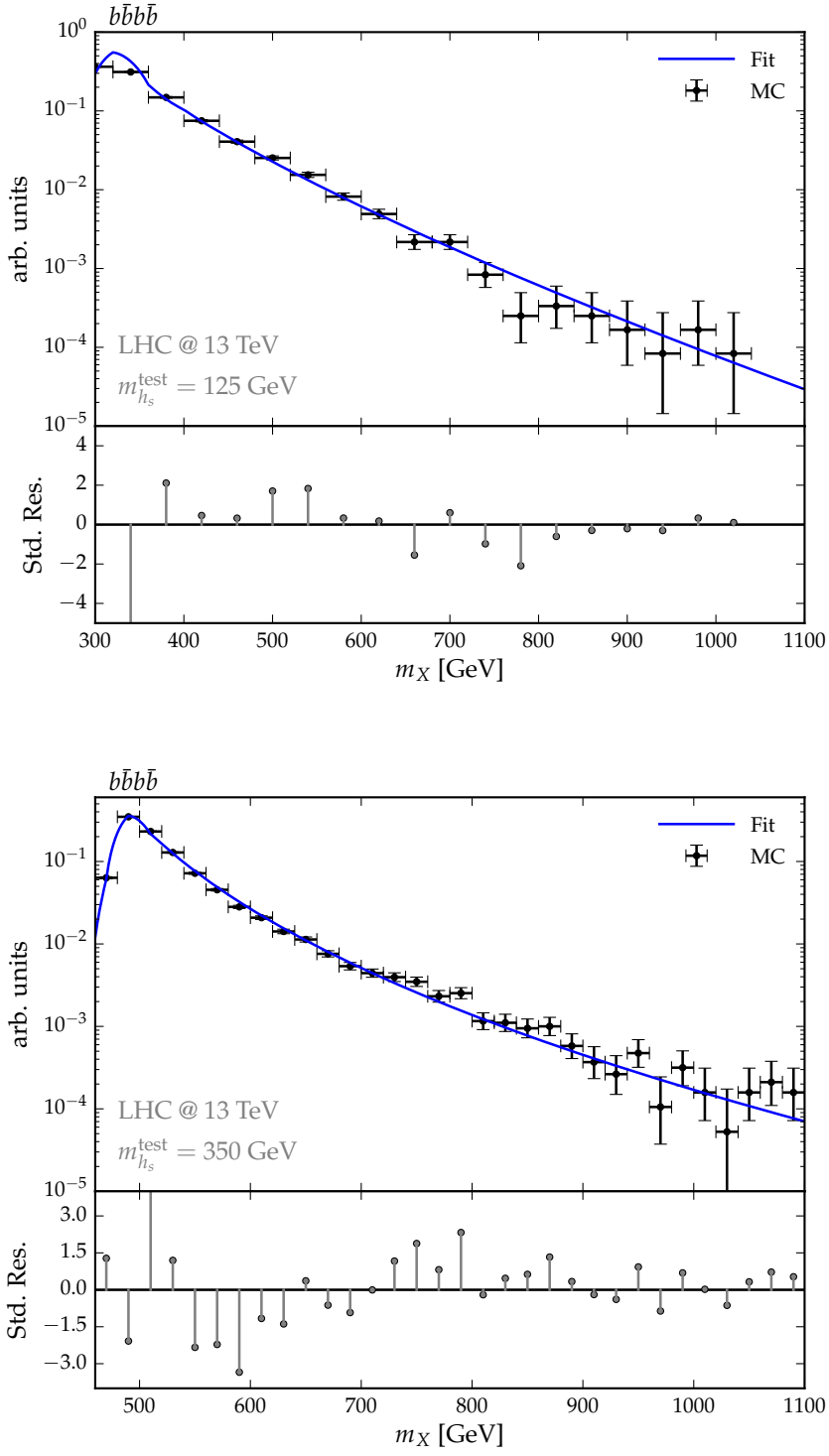

Figure 5.8: Distribution of the 4-body invariant mass m_X for the QCD multijet background obtained with the Monte Carlo (error bars), and the corresponding analytical fit using the Gamma distribution (blue line) , for $m_{h_s}^{\text{test}}$= 125 GeV (up) and $m_{h_s}^{\text{test}}$= 350 GeV (down). The standardized residuals for each bin are shown below the distributions. The events yield has been normalized to L = 300 fb^{-1} for illustration purposes.

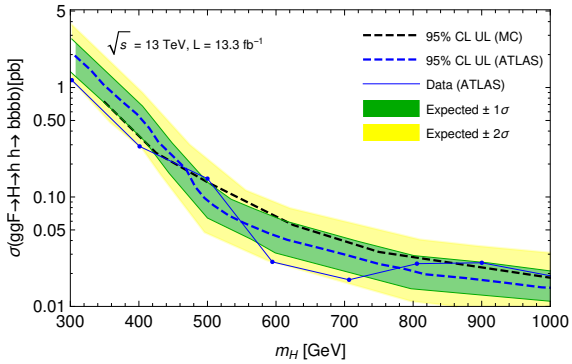

Figure 5.9: Expected 95% CL upper limits from ATLAS [94] in blue, their $\pm 2\,\sigma$ incertainty bands, the expected 95% CL upper limits from our Monte Carlo in black and, for completeness, the 95% CL upper limits obtained from the data.

decaying to SM Higgs pairs, but the differences to spin-0 resonances are expected to be small.) In Fig. 5.9 we show the expected 95% CL upper limits from ATLAS, their $\pm 2\,\sigma$ incertainty bands, the expected 95% CL upper limits from our Monte Carlo and, for completeness, the 95% CL upper limits obtained from the data. We see that our expected 95% CL upper limits coincide well with the ones expected by ATLAS.

Since the background was fitted to data at 13 TeV c.m. energy we will show our results also for 13 TeV, for 300 and 3000 fb^{-1} integrated luminosity. We choose four representative values for $m_H = 425$, 500, 750 and 1000 GeV, and show the 95% CL exclusion limits and $5\,\sigma$ discovery cross sections as function of m_{h_s} in each case. For 300 fb^{-1} integrated luminosity these are shown in Figs. 5.10, for 3000 fb^{-1} integrated luminosity in Figs. 5.11.

The sensitivities become weaker for $m_{h_s} \lesssim 50$ GeV (for $m_X = 425 - 500$ GeV) and $m_{h_s} \lesssim 100$ GeV (for $m_H = 1000$ GeV). The underlying reason is that for these masses the $b\bar{b}$ pair from h_s becomes too boosted and is no longer resolved by the standard jet clustering algorithm. These boosted regimes would require the use of jet substructure methods for the correct identification of the decay products of h and h_s.

The blue regions in Figs. 5.10 and 5.11 indicate viable values for the cross sections times branching fractions in the parameter space of the NMSSM, obtained from `NMSSMTools_5.1.0` (see section 5.2).

In the region of the NMSSM parameter space corresponding to $m_H \gtrsim 500$ GeV, the width for $h_s \to h + h$ becomes relatively large ($\approx$ 10 MeV) if kinematically allowed. As a consequence the branching fractions of h_s into $b\bar{b}$ (and the other channels considered in this paper) decrease, leading to a decrease of the possible production cross sections times branching fractions for $m_H \gtrsim 500$ GeV,

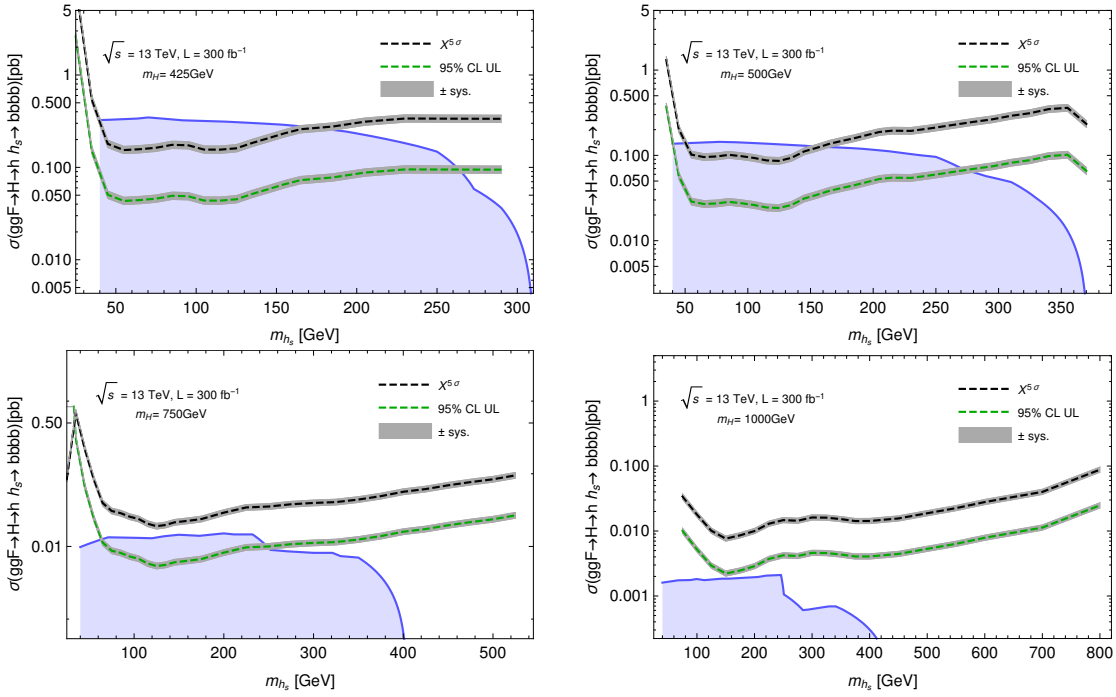

Figure 5.10: 95% CL exclusion limits and $5\,\sigma$ discovery cross sections in the $b\bar{b}b\bar{b}$ final state as function of m_{h_s} for 300 fb^{-1} integrated luminosity and $m_H = 425$ GeV (upper left), $m_H = 500$ GeV (upper right), $m_H = 750$ GeV (lower left), $m_H = 1000$ GeV (lower right). The blue regions correspond to viable cross sections for the process $ggF \to H \to hh_s \to b\bar{b}b\bar{b}$ satisfying present phenomenological constraints, obtained using `NMSSMTools` as described in sec. 5.2.

$m_{h_s} \gtrsim 250$ GeV.

The following conclusions can be drawn from Figs. 5.10 and 5.11: For $m_H \lesssim 500$ GeV wide ranges of m_{h_s} in the NMSSM parameter space can be discovered or, at least, excluded. For larger m_H testable regions in the NMSSM parameter space exist, but for $m_H \sim 1$ TeV only for 3000 fb^{-1} integrated luminosity.

We recall, however, that the sensitivities to cross sections in Figs. 5.10 and 5.11 are model independent and valid for arbitrary (e.g. non-supersymmetric) extensions of the Higgs sector.

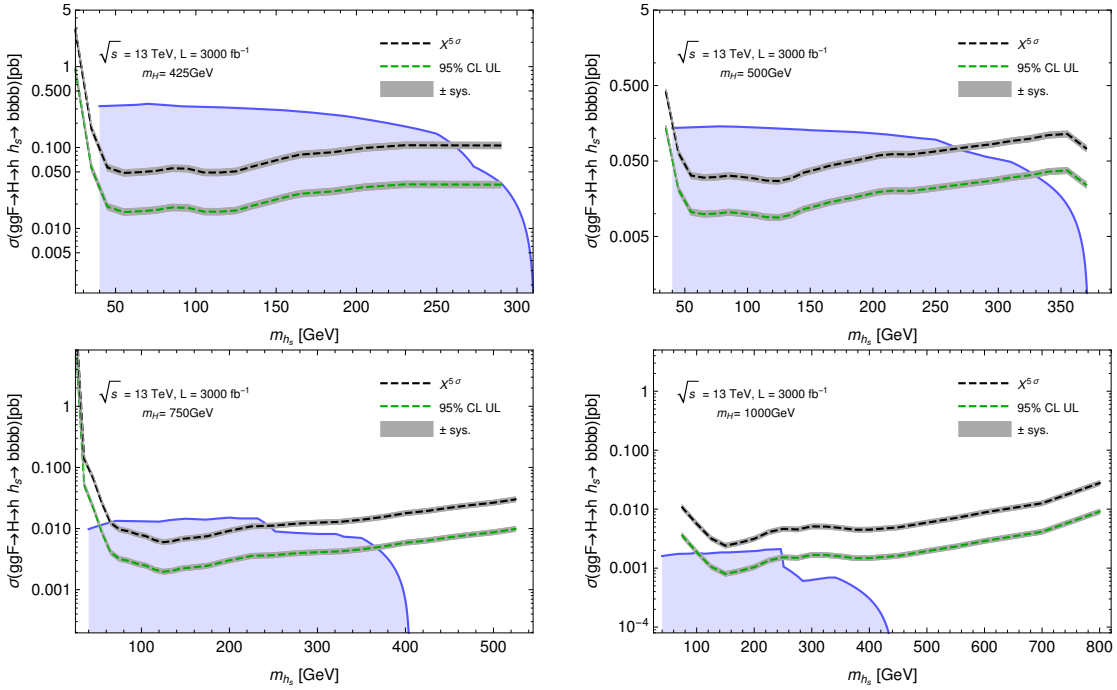

Figure 5.11: 95% CL exclusion limits and $5\,\sigma$ discovery cross sections in the $b\bar{b}b\bar{b}$ final state as function of m_{h_s} for 3000 fb^{-1} integrated luminosity and $m_H = 425$ GeV (upper left), $m_H = 500$ GeV (upper right), $m_H = 750$ GeV (lower left), $m_H = 1000$ GeV (lower right).

signal (m_H, m_{h_s})	cross sec.	bins	# bkgr	# signal	Z $(\frac{B+S}{\sqrt{B}})$
(350, 75) GeV	390 fb	[320, 360] GeV	49276	1099.8	5
(500, 125) GeV	75 fb	[460, 520] GeV	11531.2	449.41	4.8
(625,205) GeV	55 fb	[580, 640] GeV	8988.9	452.5	4.8
(1000,100) GeV	19 fb	[960, 1040] GeV	128.159	57.342	5.1

Table 5.4: Event yield for the signal and background for some benchmark scenarios and its local significance, in the analysis presented in for the $b\bar{b}b\bar{b}$ channel. All cases correspond to a c.m.e. of 13 TeV and L=300 fb^{-1} .

In table 5.4 we show the event yield for the some benchmark scenarios, with the local significance corresponding to a cut-and-count experiment on the indicated bins. Also, for the sake of illustration we show in fig. 5.12 how a discovery bump would look like in the m_X histogram for some signal benchmarks in a search following the prescriptions presented here.

5.4.4 Comparison with other heavy Higgs searches

Several searches have been carried out for a heavy state H decaying to a pair of tau leptons at the LHC [137–141]. So far this channel was the favourite one for looking for a MSSM-like state H/A for one main reason: The couplings of the MSSM Higgs bosons to down-type fermions are enhanced with respect to the SM for large $\tan\beta$ values, resulting in increased branching fractions to taus leptons and b-quarks, as well as a higher cross section for Higgs boson production in association with b-quarks. The discovery of the Higgs boson with a mass near 125 GeV strongly favours the large $\tan\beta$ scenario within the MSSM framework, making the mentioned search particularly interesting.

However, in other models with extended Higgs sectors, the situation could be radically different. In the framework of the NMSSM, the mostly SM Higgs boson receives additional contributions to its tree-level mass with respect to the MSSM (see chapter 3), namely due to singlet-mixing effects and from the λ term. The $\lambda-$term contribution could be dominant and suitably accommodate a mass of m_h =125 GeV at small/intermediate values for $\tan\beta$ and large values of λ. In this region of the NMSSM parameter space, h lies approximately in the same direction in field space as the doublet Higgs vacuum expectation value v, hence having SM-like couplings. This situation, detailed in sec 3.3.2, is clearly favoured by current data, which show a very SM behaviour for the observed 125 GeV boson. In this scenario the branching ratio of the heavy states H/A to a pair of tau leptons is not enhanced, unlike in the MSSM large $\tan\beta$ case. On the other hand, the branching

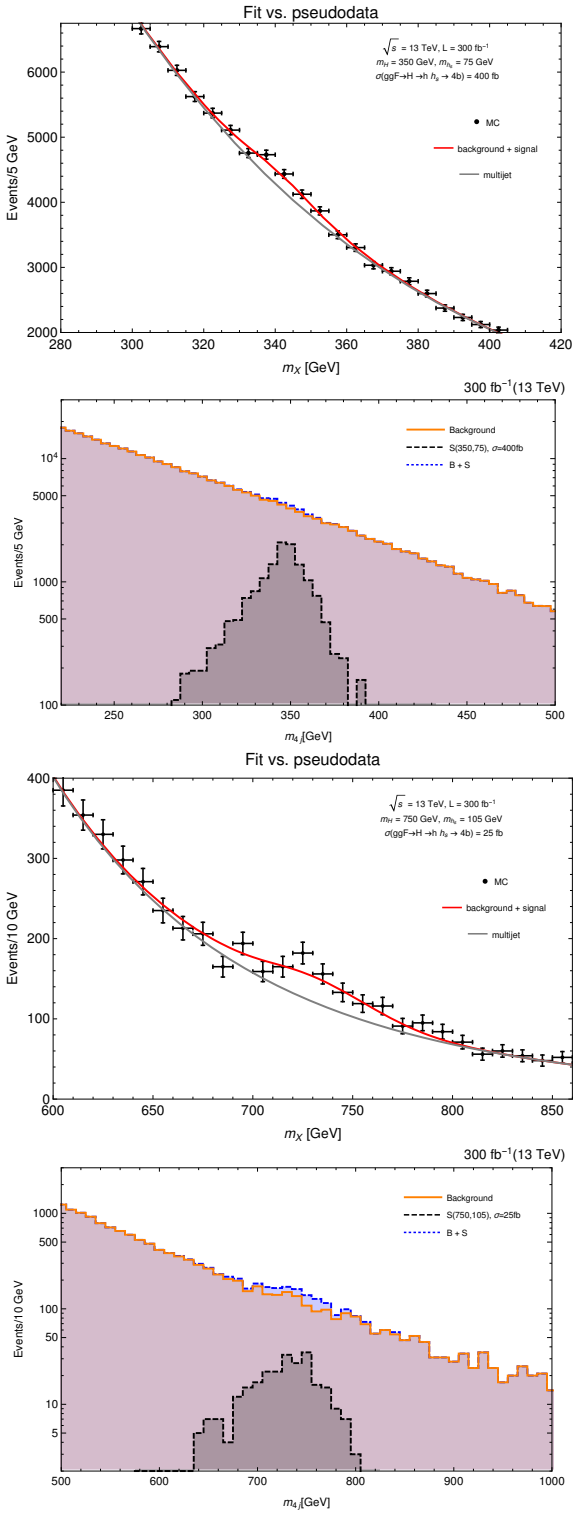

Figure 5.12: Examples of signals exceeding a 5σ sensitivity in the m_X histogram. Plots on the left- and right-hand side are equivalent, except for the bins size.

ratio $BR(H \to hh_s)$ could reach large values, and could even be dominant for a relatively light H. This is true also, to a less extent, for $BR(A \to ha_s)$. One can thus ask which search is more suitable for discovering a heavy Higgs bosons in the context of a natural realisation of the NMSSM, where the enhancement of the heavy resonances couplings to down-type fermions doesn't necessarily take place.

We address here a direct comparison of the discovery power of the traditional search for H/A in the ditau final state versus the one presented in this chapter. To this aim, we show in fig. 5.13 the latest 95% CL exclusion limits from CMS in the search $ggF \to H \to \tau\tau$ [141] [1] together with the expected 95% CL limits in the $ggF \to H \to hh_s \to b\bar{b}b\bar{b}$ process obtained from our MC study (for the $\mathcal{B}2$ strategy), computed at the same integrated luminosity. Recall that the limits in the $4b$ final state depend not only on m_H but also on the hypothesised mass m_{h_s} . Despite this extra dependence, we see that both analysis test very similar values of the cross sections. Since we are considering the same production mechanism for the heavy state H/A, namely gluon fusion, the fact that the ratios satisfy

$$\frac{BR(H \to hh_s)}{BR(H \to \tau\tau)} \sim \quad 10 - 100, \text{ and} \tag{5.15}$$

$$\frac{BR(A \to ha_s)}{BR(A \to \tau\tau)} \gtrsim \qquad 10 \tag{5.16}$$

for most part of the allowed parameter space make the proposed search much more promising than the traditional one in the ditau final state. In other words, the search in the $b\bar{b}b\bar{b}$ channel is able to test much more NMSSM allowed points than $H/A \to \tau\tau$.

[1] We present here the CMS results from [141], although an analogous search was presented by ATLAS [137] at the same integrated luminosity, obtaining very similar results.

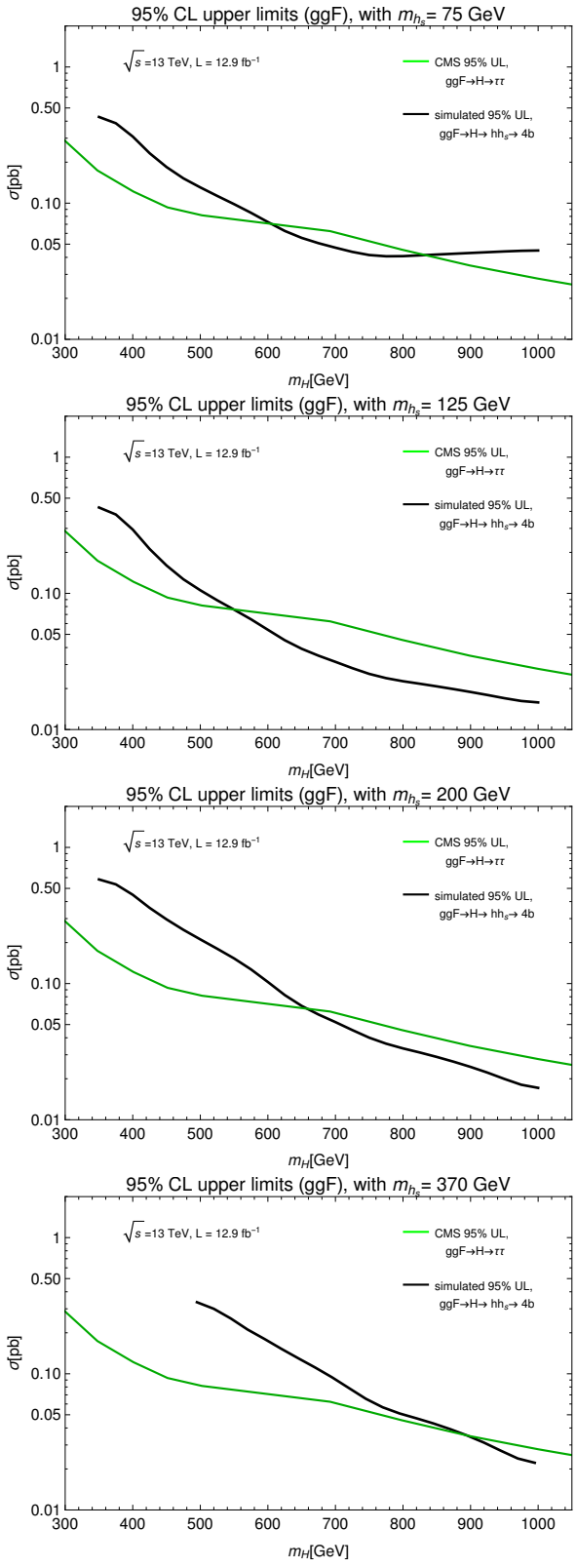

Figure 5.13: 95% CL Upper Limits reported by CMS [141] in the ditau final state, together with the expected 95% upper limits for the process $ggF \rightarrow H \rightarrow hh_s \rightarrow b\bar{b}b\bar{b}$ for different hypothesis on m_{h_s} .

5.5 The $b\bar{b}\tau\tau$ channel

Searches for resonant h pair production in the $b\bar{b}\tau\tau$ final state have been performed by ATLAS at 8 TeV [93], and by CMS at 13 TeV in [104,105,107]. Following these searches we concentrate on the $\tau_h\tau_h$, $\tau_h\tau_e$ and $\tau_h\tau_\mu$ modes. As in the case of the $b\bar{b}b\bar{b}$ final state we optimise the cuts as function of a tentative value for m_{h_s}, $m_{h_s}^{\text{test}}$.

A priori the $\tau\tau$ pair can originate from h_s or h; both cases lead in general to different kinematics (since $m_{h_s} \neq m_h$), and thus one has to define different search strategies for both topologies. We will make no assumptions on the relative branching ratios $BR(h_s \to b\bar{b})$ and $BR(h_s \to \tau\tau)$. The aim is to obtain separate 95% CL exclusion limits and $5\,\sigma$ discovery cross sections for the processes $ggF \to H \to h_s(\to b\bar{b}) + h(\to \tau\tau)$, and $ggF \to H \to h_s(\to \tau\tau) + h(\to b\bar{b})$.

5.5.1 Background simulation

The SM background in the $b\bar{b}\tau\tau$ final state at the LHC consists mainly in $t\bar{t}$ events. The top quark decays producing a W boson and a b quark in almost all cases, where the W further decays either to a pair of quarks or to a lepton-neutrino pair, the latter giving rise to an irreducible $b\bar{b}\tau\tau$ final state. Also, in the case that the W decays into quark pairs, the misidentification of light jets as hadronic taus constitutes an important source of background. 15 million $t\bar{t}$ events have been generated. The LO cross section was computed with `MadGraph5_aMC@NLO`, and the NNLO+NNLL K-factor was obtained using `top++2.0`.

Other SM processes giving rise to a $b\bar{b}\tau\tau$ final state have been considered. We generated the process $pp \to b\bar{b}\tau\tau$, obtaining its LO cross section which has been then rescaled using a NLO K-factor [124]. Some of the diagrams contributing to this process are shown in fig. 5.14. However, due to its very large cross section the $t\bar{t}$ process is the dominant source of background in practically all the phase space.

A detector simulation routine has been applied to both samples using `Delphes`, with an anti-k_T jet-clustering algorithm with $\Delta R = 0.4$. The default ATLAS card has been used with a b-tagging efficiency corresponding to the $\epsilon = 70\%$ working

Process (ME)	σ_{LO}(pb)	# events	K-factor	equiv. luminosity
$b\bar{b}\tau\tau$	2.38 pb	10^6	2.9 (NLO)	145 fb^{-1}
$t\bar{t}$	504.2 pb	$1.5 \cdot 10^7$	1.7 (NNLO+NNLL)	17.45 fb^{-1}

Table 5.5: Processes considered in the study of the contributions to the total $b\bar{b}\tau\tau$ background

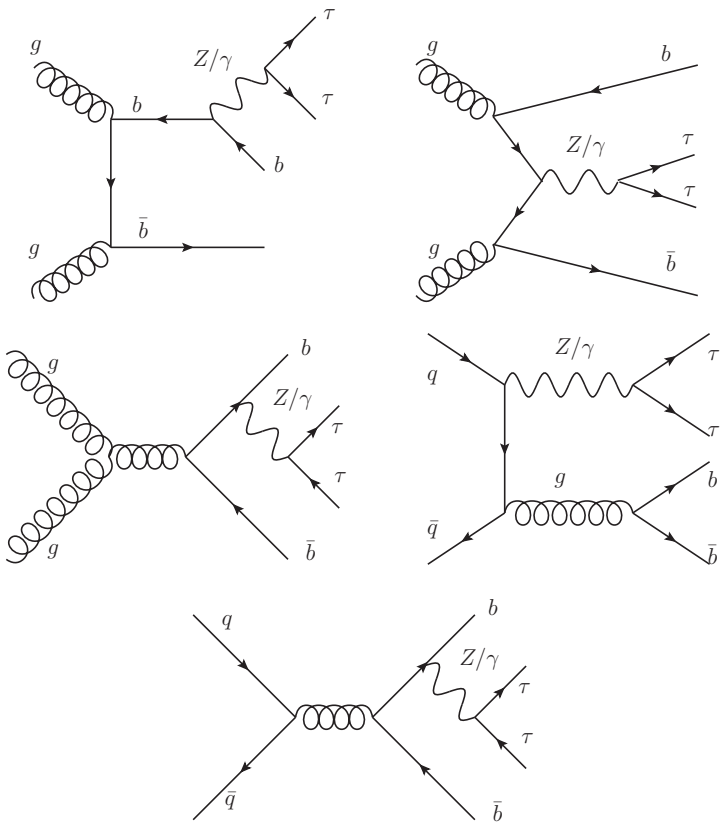

Figure 5.14: Some of the Feynman diagrams contributing to the $b\bar{b}\tau\tau$ SM background at the LHC.

point [130]. The expected tau-tagging capabilities of the ATLAS experiment at the LHC Run 2 for hadronically decaying taus has been published by ATLAS [142]. In the present simulation we use the efficiencies for τ_h identification and mistagging for the so-called medium working point reported in [142], which corresponds to a 0.7 (0.6) efficiency and 0.02 (0.01) mistag rate for 1-prong (3-prong) taus.

Validation of the background

In order to validate the background model, in this section we compare the background samples obtained with `MadGraph5_aMC@NLO` with the recent results reported by CMS in the search for resonant double SM Higgs production at $\sqrt{s} = 13$ TeV [105], which were found to be compatible with the expected SM background. The data used for the search was collected in 2016 and corresponds to an integrated luminosity of 12.9 fb^{-1} . We reproduced the event reconstruction and selection as detailed in [105]. Three different channels are considered in this search depend-

ing on the decay of one of the tau leptons: $\tau_h\tau_h$, $\tau_h e$ and $\tau_h\mu$, each one of them featuring different selection criteria.

In the leptonic channels ($\tau_h e$ and $\tau_h\mu$) the presence of a lepton (electron or muon) is required, together with an hadronic tau. The p_T requirements are $p_T >$ 23(27) GeV for muons (electrons) and $|\eta|<$ 2.1, and a τ_h with $p_T >$ 20 GeV and $|\eta|<$ 2.3. Isolation requirements are applied to the leptons present in the event. The relative isolation variable for the leptons, I_l^{rel}, is defined as

$$I_l^{\text{rel}} = \frac{\sum_i p_{T,i}}{p_{T,l}}, \tag{5.17}$$

where the sum over i corresponds to all particles within a cone of $\Delta R = 0.4$. The muon and electron candidates are required to pass the relative isolation requirement $I_l^{\text{rel}} < 0.1$. The hadronic taus are required to have a value for the isolation energy

$$I_\tau = \sum_{\text{charged, }\gamma} p_{T,i} < 3 \text{ GeV}, \tag{5.18}$$

where in this case the sum is over the charged particles and photons within a cone of $\Delta R < 0.5$.

For the fully hadronic final state, exactly two τ_h candidates should be present in the event, both with $p_T >$ 45 GeV and $|\eta|<$ 2.1. The isolation threshold for the hadronic taus is set to $I_\tau <$ 2 GeV for this channel.

In all three channels, the leptons are required to have opposite charge. Events containing more extra isolated leptons are rejected. In addition to the pair of leptons, all events are required to have exactly two b-jets of $\Delta R = 0.4$, with $p_T >$ 30 GeV and $|\eta|<$ 2.4 (the b-tagging algorithm used in the simulated samples mimic the ATLAS performance instead of those of CMS, however, we do not expect this differences to have a large impact in the final results). As in the $b\bar{b}b\bar{b}$ case, we focus exclusively on the resolved category i.e. in the region of phase space where we can resolve two separate b-jets.

The final stage of the event selection consists in applying cuts on the mass of the $\tau\tau$ and $b\bar{b}$ systems. In the actual CMS analysis, the invariant mass of the $\tau\tau$ system is reconstructed using a likelihood technique [143] that combines the information from the visible decay products of the leptons and from the missing energy in the event. Instead of this, in our approach we reconstruct $m_{\tau\tau}$ using the collinear approximation, where we assume that the neutrinos from the τ decay are collinear with the visible decay products (recall that in this approximation we work under the assumption that all the missing energy in the event is due to neutrinos). The mass cuts are:

$$80 \text{ GeV} < m_{\tau\tau} < 160 \text{ GeV} \tag{5.19}$$

$$80 \text{ GeV} < m_{b\bar{b}} < 160 \text{ GeV}. \tag{5.20}$$

	$t\bar{t}$			$b\bar{b}\tau\tau$		
	α	β	μ	μ	σ	k
$\tau_h\tau_h$	3	175.5	131.6	304.4	40.8	0.41
$\tau_h e$	10.5	521.2	-225.4	244.6	28.7	0.33
$\tau_h\mu$	10.3	519.2	-223	255.4	29.9	0.32

Table 5.6: Fit parameters for the background samples, after the cuts described in the text.

This analysis is applied on our MC samples, and the resulting distributions for the total invariant mass $m_{b\bar{b}\tau\tau}$ are fitted to analytical functions to avoid introducing large statistical uncertainties from the MC. For the $t\bar{t}$ contribution, we have found that the Frechet distribution offers a very reasonable description of the MC data in practically all the region of interest, i.e. from 300 GeV to 1 TeV. The Frechet distribution is described by three parameters, and its probability distribution function is given by:

$$f(x;\alpha,\beta,\mu) = \begin{cases} \dfrac{\alpha e^{-\left(\frac{x-\mu}{\beta}\right)^{-\alpha}} \left(\frac{x-\mu}{\beta}\right)^{-\alpha-1}}{\beta} & x > \mu \\ 0 & x \leq \mu \end{cases}. \tag{5.21}$$

In the case of the $b\bar{b}\tau\tau$ background (consisting mainly in Z+jets), we found that the 3-paremeters GaussExp function [132], used already by CMS [133] to model the total invariant mass distribution of a $b\bar{b}b\bar{b}$ background, fits well the resulting events. The GaussExp function basically consists in a gaussian with an exponential tail smoothly attached at the high side of the function. The probability density function of the GausExp is given by:

$$f(x;\mu,\sigma,k) = \begin{cases} e^{-\frac{(x-\mu)^2}{2\sigma^2}} & \dfrac{x-\mu}{\sigma} \leq k \\ e^{\frac{k^2}{2}-\frac{k(x-\mu)}{\sigma}} & \dfrac{x-\mu}{\sigma} > k \end{cases}. \tag{5.22}$$

The estimated parameters for the $t\bar{t}$ and $b\bar{b}\tau\tau$ backgrounds, obtained by means of a maximum likelihood estimation method (see appendix A for details), are shown in table 5.6 for the three subchannels.

In fig. 5.15 we show the distributions observed by CMS and the results using the background MC samples obtained as described in 5.5.1. For the three studied channels we can observe a reasonable agreement between data and MC. The ratio

between both is very close to one within the statistical errors, which are still large. Discrepancies could arise for various reasons: the different approaches to compute the $\tau\tau$ invariant mass, the difference in the b-tagging performances and/or the detector simulation. For the majority of the bins, the central values of the background simulation is less than 40% away from data, implying that the predicted expected sensitivity will be within a $\sim 29\%$ of its 'real' value.

Still we can ask which rescaling of our simulated background, independent of the total invariant mass and common to all three channels (to improve the statistics), provides a best fit to the data. We find a factor 1.01 ± 0.24, and will subsequently use ± 0.24 as an estimate of the systematic uncertainty of the background normalisation.

Event selection

Here we define the basic event selection for both searches, $H \to h(b\bar{b})h_s(\tau\tau)$ and $H \to h(b\bar{b})h_s(\tau\tau)$.

Isolation criteria and acceptance cuts common to all searches are defined. The electron and muon candidates are required to pass the relative isolation requirement $I_\ell^{\rm rel} < 0.1$ (see eq. 5.17), with $I_\ell^{\rm rel}$ defined in a cone radius $\delta R = \sqrt{(\Delta\eta)^2 + (\Delta\phi)^2} < 0.4$. The hadronic taus are required to have a value for the isolation energy

$$I_\tau = \sum_{\text{charged, } \gamma} p_{T,i} < 3 \text{ GeV}, \tag{5.23}$$

where the sum is over the charged particles and photons within a cone of $\Delta R < 0.4$.

We require all events to have exactly two b-tagged jets with $p_T^b > 30$ GeV. As in the $b\bar{b}b\bar{b}$ analysis, we will only consider here "resolved" topologies for the b-jets, which have been shown by CMS to be the most sensitive channel for invariant mass below 1 TeV in double SM Higgs searches. If the event has exactly two hadronic taus, both are required to have $p_T^{tau_h} > 45$ GeV, otherwise the event is discarded, and no isolated leptons should be present. If the event has 1 hadronic tau, then it is required to have exactly one isolated lepton, both satisfying $p_T^{tau_h} > 20$ GeV and $p_T^\ell > 20$ GeV. Any other combination is rejected to reduce the background. Finally, all objects should have a pseudorapidity $|\eta| < 2.47$.

In all three channels, the two lepton candidates are required to have opposite charges. An additional requirement is applied on the $\tau_h e$ and $\tau_h \mu$ channels: the transverse mass of the electron or muon,

$$m_T^\ell = \sqrt{2 p_T^\ell \not{E}_T \left(1 - \cos\left(\phi_{\not{E}_T} - \phi^\ell\right)\right)}, \tag{5.24}$$

is required to satisfy $m_T^\ell < 40$ GeV.

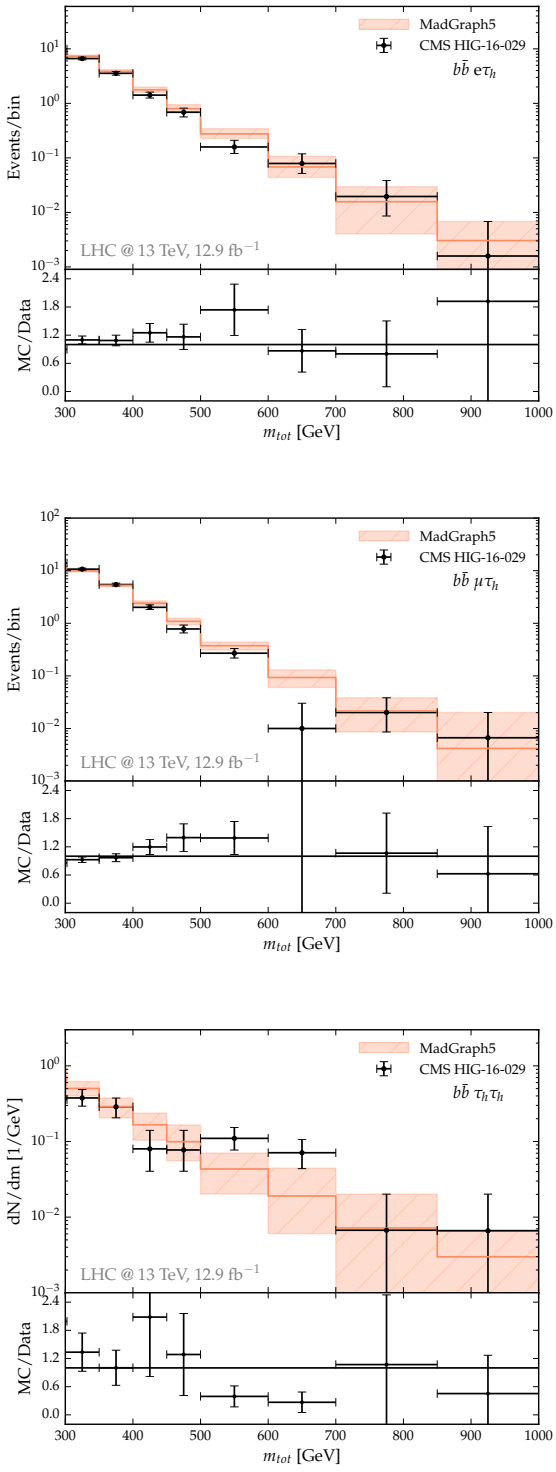

Figure 5.15: Total invariant mass distribution observed by CMS [105] contrasted with the results obtained from the MC simulations, normalized to the LO cross section computed with `MadGraph5` and an integrated luminosity of L=12.9 fb^{-1} . The results are shown for the three channels considered in the search: $b\bar{b}e\tau_h$ (top), $b\bar{b}\mu\tau_h$ (middle) and $b\bar{b}\tau_h\tau_h$ (bottom).

The stransverse mass M_{T2} [144], which has been proposed for double SM Higgs searches in the $b\bar{b}\tau\tau$ final state [145], was also studied as a potential discriminant to reduce the dominant $t\bar{t}$ background. However, we found that for the range of masses for the heavy state H considered in this work ($m_H < 1$ TeV), M_{T2} does not pose any advantage and thus it is not used for the current analysis.

5.5.2 $H \to h(b\bar{b})h_s(\tau\tau)$

After the acceptance cuts, the $b\bar{b}$ pair is used to reconstruct the SM Higgs candidate. For the case of the $\tau\tau$ system, associated to the h_s candidate, the reconstruction is more challenging due to the presence of neutrinos in the weak decays of the tau lepton. We consider three simple methods for the $h_s \to \tau\tau$ reconstruction: the visible mass, using only the visible parts of the τ decay; the transverse mass, which includes the missing transverse energy $\not{E}_T$ in the reconstruction, and the collinear mass. The latter is based on two important assumptions:

1. the neutrinos from the τ decay are nearly collinear with the corresponding visible part of the τ decay ($\theta_\nu \approx \theta_{\text{vis}}$, $\phi_\nu \approx \phi_{\text{vis}}$),

2. all the missing energy in the event is due to the neutrinos.

The τ leptons from the decay of h_s are typically produced with large momenta in the studied process, making these assumptions suitable for our case. We remark here that more sophisticated methods have been studied in the literature [143, 146, 147] to suitably reconstruct $\tau\tau$ systems, and may improve its reconstruction efficiency. Nonetheless, we have found that the collinear approximation offers a good reconstruction of the signal. For practically all values of m_{h_s}, the $\tau\tau$ invariant mass peaks at 95% of the actual mass m_{h_s} using the collinear method, as we can see in fig. 5.16.

Once the two Higgs boson candidates have been reconstructed, we define the corrected total invariant mass m_X as:

$$m_X = m_{b\bar{b}\tau\tau} - m_{b\bar{b}} + 125 \text{ GeV}, \tag{5.25}$$

where $m_{b\bar{b}\tau\tau}$ denotes the total invariant mass of the $b\bar{b}\tau\tau$ system using the collinear mass for the $\tau\tau$ pair.

We define a signal region as a cut in the invariant mass plane of the two candidates:

$$\chi_{hh_s} = \sqrt{\left(\frac{m_{b\bar{b}}(h) - 110 \text{ GeV}}{0.35 m_{b\bar{b}}(h)}\right)^2 + \left(\frac{m_{\tau\tau}(h_s) - 0.92 m_{h_s}^{\text{test}}}{\text{Max}(0.35 m_{\tau\tau}(h_s), 30 \text{ GeV})}\right)^2} < 1 \tag{5.26}$$

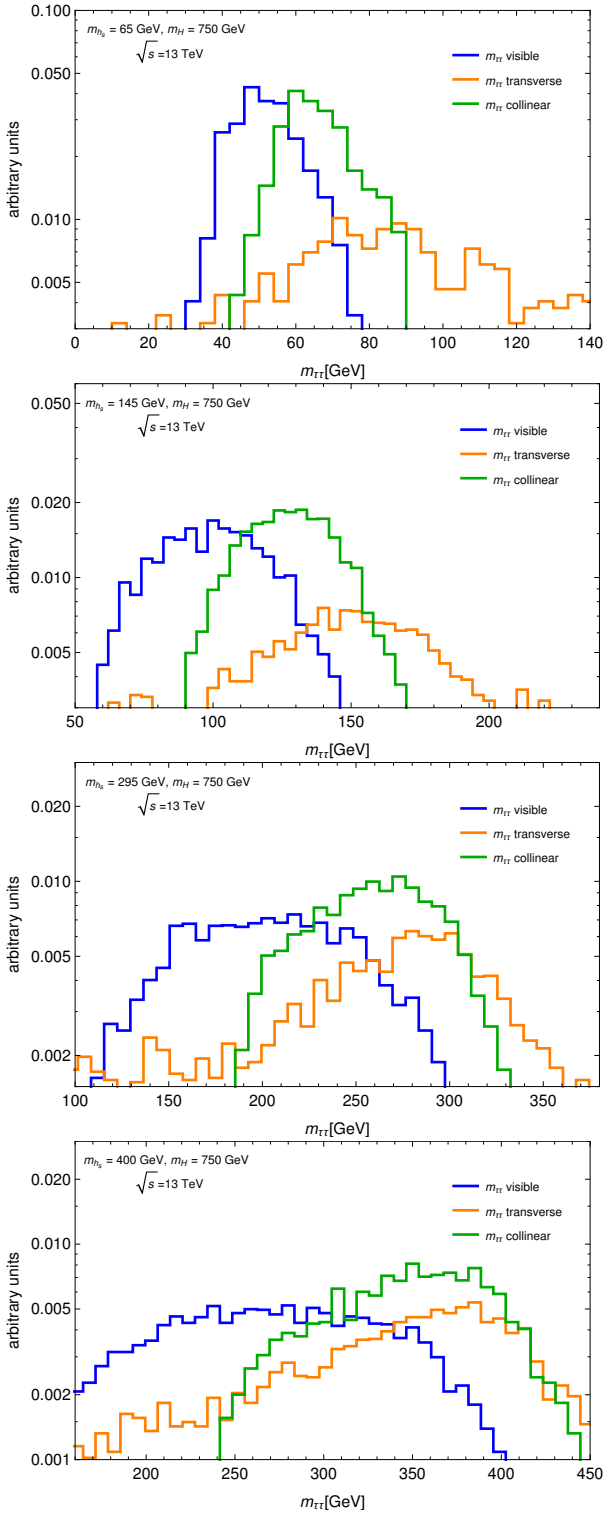

Figure 5.16: Reconstruction of the $\tau\tau$ system invariant mass, using three different methods. In all cases, the collinear mass method offers a good reconstruction of the signal mass m_{m_s}.

The size of the signal region χ_{hh_s} is designed to account for 95% of the signal events, whereas the Max$(0.35m_{\tau\tau}(h_s), 30$ GeV) is meant to avoid too small signal regions. In fig. 5.17 we show the density of signal events in the dijet invariant masses plane with the signal region denoted by the black ellipse, for the case $m_H = 500$ GeV at various values of m_{h_s}.

Kinematic cuts have been obtained for the transverse momentum of the Higgs candidates,

$$p_T^h > 52 \text{ GeV} + 0.14m_X - 0.2m_{h_s}^{\text{test}} - 202.1m_{h_s}^{\text{test}}/m_X \text{ GeV} \tag{5.27}$$

for the $b\bar{b}$ dijet and

$$p_T^{h_s} > 23.8 \text{ GeV} + 0.19m_X - 0.02m_{h_s}^{\text{test}} - 128.4m_{h_s}^{\text{test}}/m_X \text{ GeV} \tag{5.28}$$

for the $\tau\tau$ system. Recall that the cuts are computed in a per event basis, since m_X is the value of the corrected mass of the event. These cuts were obtained optimizing the signal-to-background ratio for each pair (m_H, m_{h_s}). In fig.5.18 we can see the $p_T(h)$ and $p_T(h_s)$ histograms for the background and signal before applying the kinematic cuts on the dijets p_T. No cuts are applied on angular variables.

In figs. 5.19 and 5.20 we show some examples of the signal efficiency at the different stages of the event selection as a function of m_{h_s} and m_H.

5.5.3 $H \to h(\tau\tau)h_s(b\bar{b})$

The h_s candidate is reconstructed using the two b quarks present in the event, whereas the SM Higgs candidate is reconstructed from the $\tau\tau$ system in the collinear mass approximation. The total invariant mass $m_{b\bar{b}\tau\tau}$ is corrected using the test mass $m_{h_s}^{\text{test}}$,

$$m_X = m_{b\bar{b}\tau\tau} - m_{b\bar{b}} + m_{h_s}^{\text{test}}. \tag{5.29}$$

Mass dependent cuts are applied on the p_T of the higgs candidates:

$$p_T^h > 118.23 \text{ GeV} + 0.02m_X - 0.55m_{h_s}^{\text{test}} - 379.81m_{h_s}^{\text{test}}/m_X \text{ GeV} \tag{5.30}$$

for the $\tau\tau$ dijet and

$$p_T^{h_s} > 16.1 \text{ GeV} + 0.19m_X - 0.04m_{h_s}^{\text{test}} - 137m_{h_s}^{\text{test}}/m_X \text{ GeV} \tag{5.31}$$

for the dijet system.

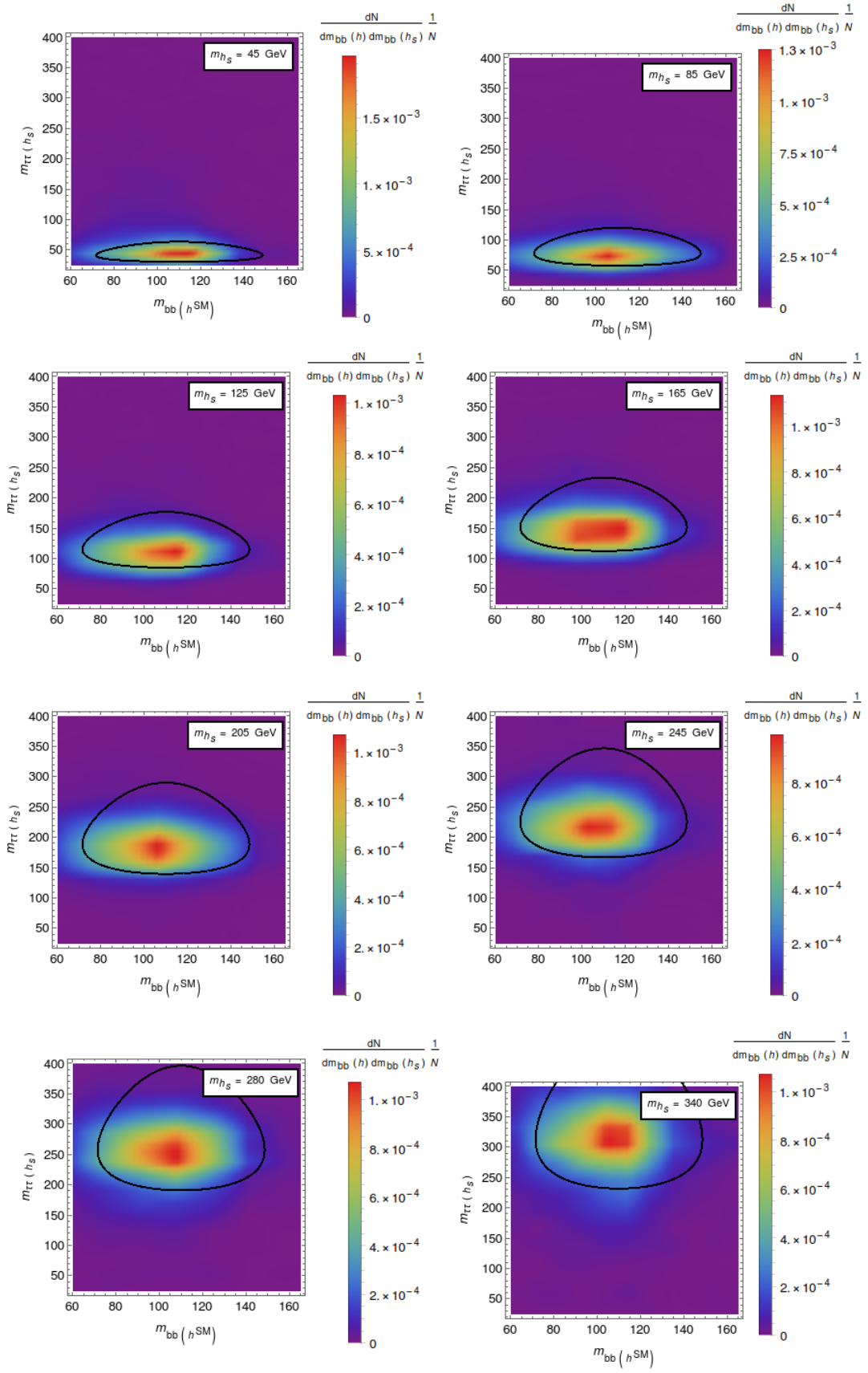

Figure 5.17: Distribution of the dijet invariant masses for m_H=500 GeV and various values for m_{h_s}. The black contour represents the signal region defined in eq. 5.26.

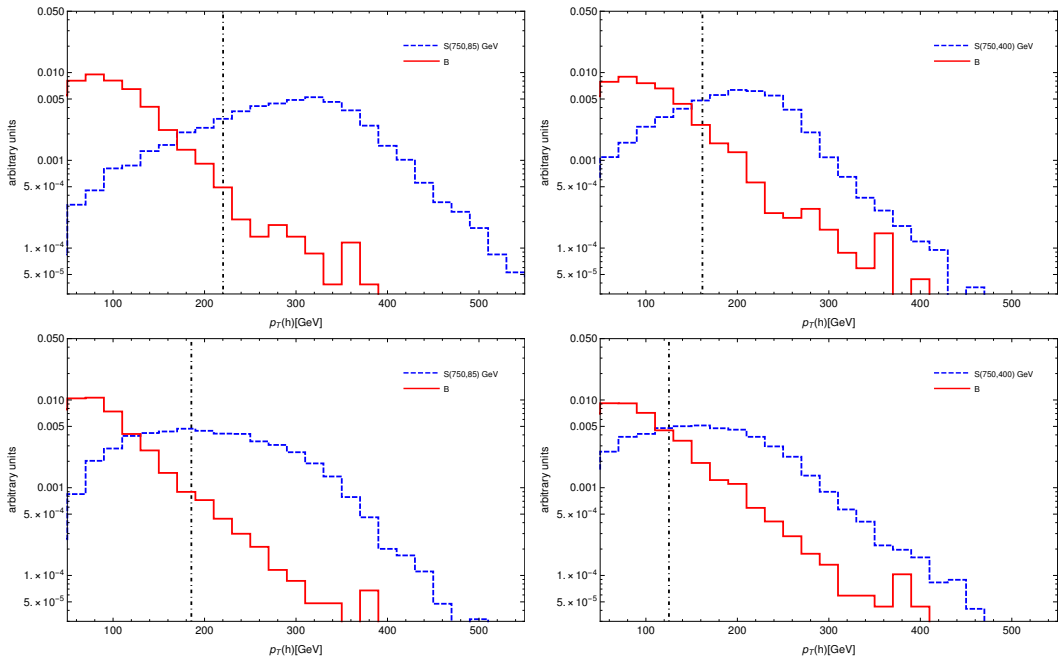

Figure 5.18: Distribution of the p_T cuts of the SM Higgs dijet (upper plots) and non-SM Higgs h_s (lower plots) for the signal and background at $\sqrt{s} = 13$ TeV, for the case $m_H = 750$ GeV and $m_{h_s} = 85$ GeV (left) and $m_{h_s} = 400$ GeV (right). The black vertical line indicates the approximated value of the cut, assuming $m_X \approx m_H$.

Modelling the background

The resulting background after the cuts described above depends of course on the mass $m_{h_s}^{\text{test}}$ that we are assuming, hence the background should be parametrized for each value of the hypothesised mass $m_{h_s}^{\text{test}}$. The two contributions that we simulated and validated in sec.5.5.1, namely $t\bar{t}$ and $b\bar{b}\tau\tau$ (the latter containing mainly Z+jets events), are fitted to analytical expressions using two different functions, the Frechet and GausExp distributions, respectively, which were already introduced in sec. 5.5.1. Both functions present a very reasonable agreement with the MC data, as we can see in fig. 5.21 with some illustrative examples.

5.5.4 Discovery cross sections $X^{5\sigma}$ and exclusion limits

Given the m_X distribution of the background for various hypothetical values of m_{h_s} and the m_X distributions of signals we can, as before, obtain values for 95% CL exclusion and $5\,\sigma$ discovery for cross sections times branching fractions into the $h \to b\bar{b}$, $h_s \to \tau\tau$ and $h \to \tau\tau$, $h_s \to b\bar{b}$ final states as function of the integrated luminosity, m_H and m_{h_s}. We choose four representative values for

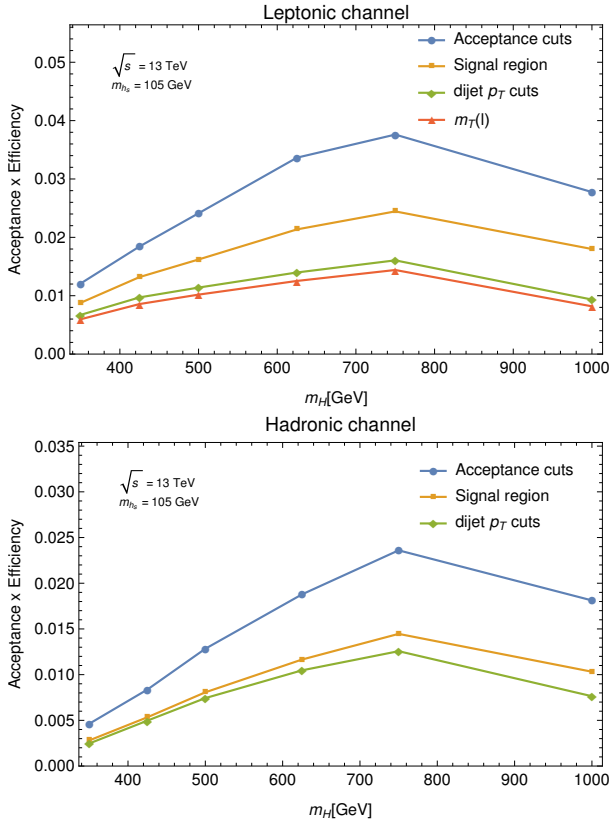

Figure 5.19: The selection efficiency for the leptonic (top) and hadronic (bottom) channels as a function of the heavy resonance mass m_H at each stage of the event selection for a mass for h_s of $m_{h_s} = 105$ GeV

$m_H = 425$, 500, 750 and 1000 GeV, and show the 95% CL exclusion limits and $5\,\sigma$ discovery cross sections as function of m_{h_s} in each case. For $h \to b\bar{b}$, $h_s \to \tau\tau$ at 300 fb^{-1} integrated luminosity these are shown in Figs. 5.22, for 3000 fb^{-1} integrated luminosity in Figs. 5.23. For $h \to \tau\tau$, $h_s \to b\bar{b}$ at 300 fb^{-1} integrated luminosity these are shown in Figs. 5.24, for 3000 fb^{-1} integrated luminosity in Figs. 5.25. The uncertainties include statistical uncertainties and, added linearly, $\pm 24\%$ considered as an estimate of the systematic uncertainty originating from the normalisation of the background.

The following observations can be made: First, the expected sensitivities on cross sections times branching ratios differ hardly among the cases $h \to b\bar{b}$ and $h_s \to \tau\tau$ versus $h \to \tau\tau$ and $h_s \to b\bar{b}$; if at all, the analyses aiming at $h \to b\bar{b}$ and $h_s \to \tau\tau$ are typically somewhat more sensitive.

Second, in Two-Higgs-doublet models of type II as well as in the NMSSM the branching fractions into $b\bar{b}$ and $\tau\tau$ of both h and h_s are always related by a factor

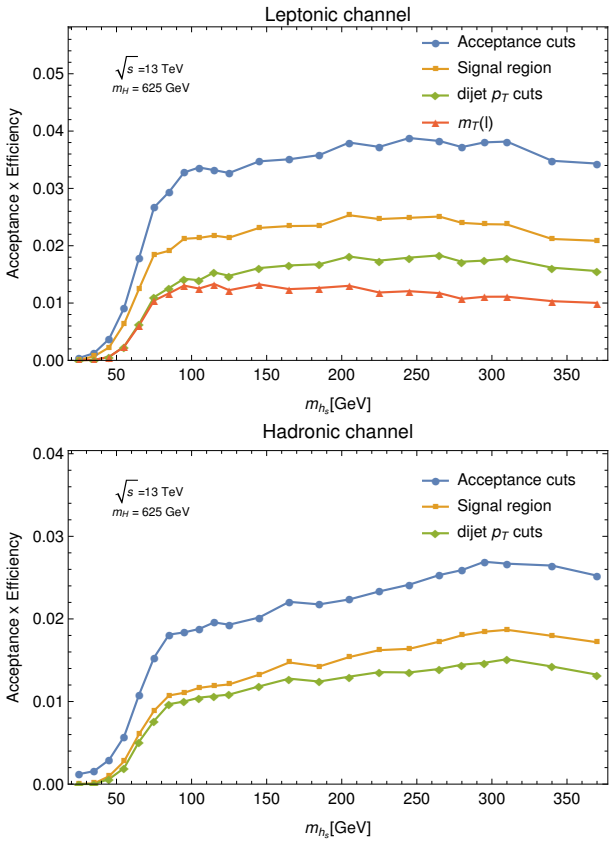

Figure 5.20: The selection efficiency for the leptonic (top) and hadronic (bottom) channels as a function of the non-SM resonance mass m_{h_s} at each stage of the event selection for a mass for H of $m_H = 625$ GeV

$\sim 9:1$. Accordingly the possible cross sections times branching fractions in the NMSSM parameter space, indicated in blue in Figs. 5.22–5.25, are $\sim 1/9$ of the ones in Figs. 5.10–5.11 for the $b\bar{b}b\bar{b}$ final state. Then one can ask, for a given point in parameter space, which of the analyses considered up to now is the most sensitive. According to our results this is the search in the $b\bar{b}b\bar{b}$ final state which allows to test somewhat larger regions in parameter space.

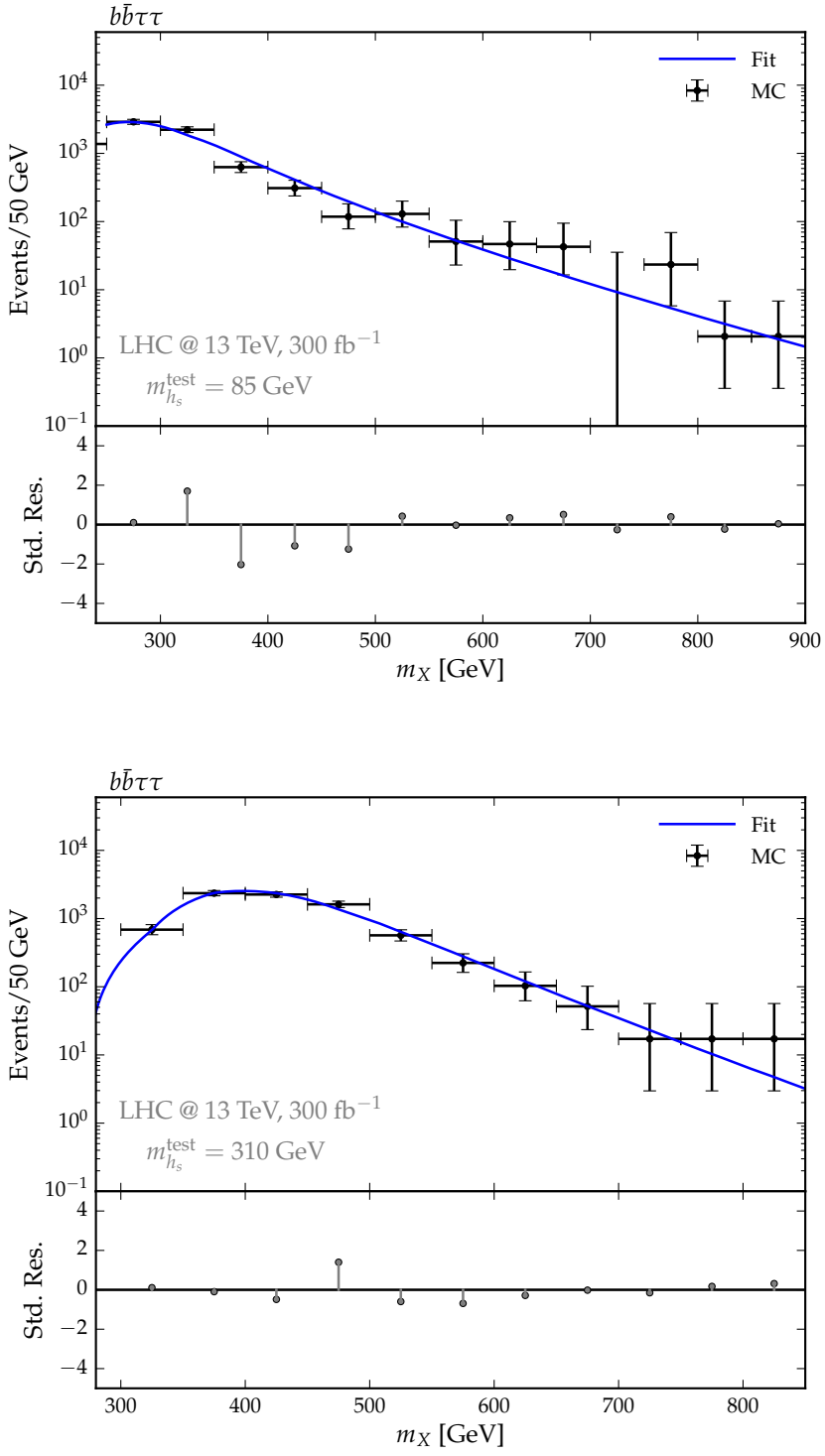

Figure 5.21: Distribution of the 4-body invariant mass m_X for the total $b\bar{b}\tau\tau$ background obtained with the Monte Carlo (error bars), and the corresponding analytical fit using the Frechet and GausExp distributions, for $m_{h_s}^{\text{test}}$= 85 GeV (up) and $m_{h_s}^{\text{test}}$= 310 GeV (down). The standardized residuals for each bin are shown below the distributions. The events yield has been normalized to L = 300 fb^{-1} for illustration purposes.

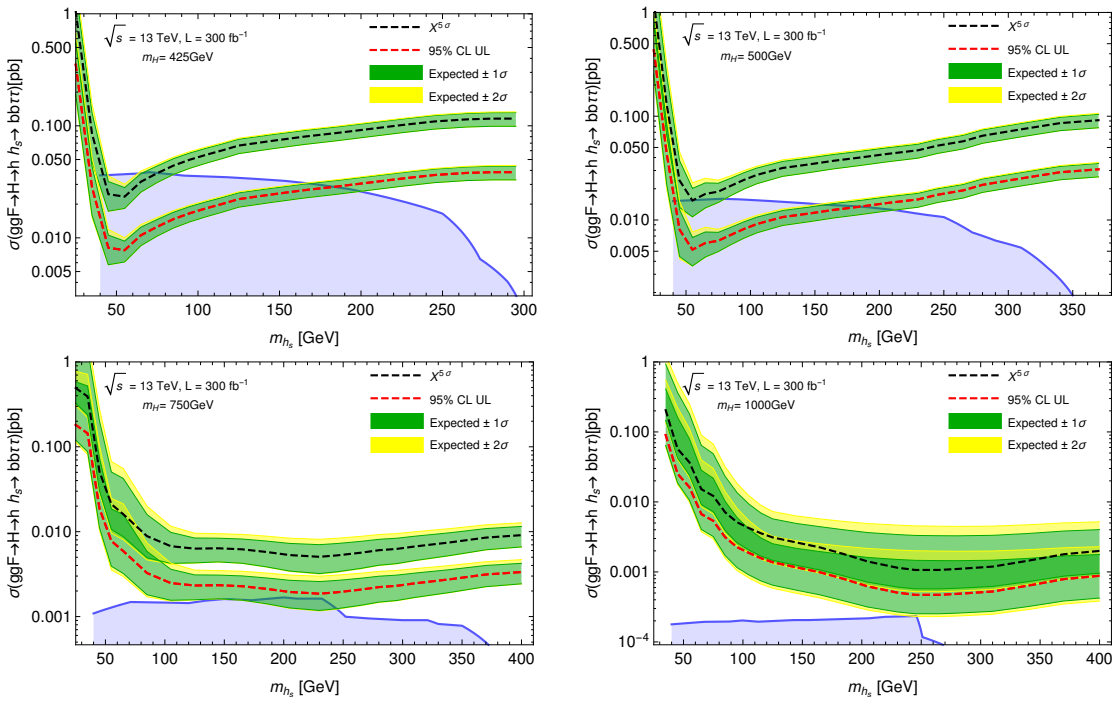

Figure 5.22: 95% CL exclusion limits and $5\,\sigma$ discovery cross sections for $h \to b\bar{b}$ and $h_s \to \tau\tau$ as function of m_{h_s} for 300 fb^{-1} integrated luminosity and $m_H = 425$ GeV (upper left), $m_H = 500$ GeV (upper right), $m_H = 750$ GeV (lower left), $m_H = 1000$ GeV (lower right).

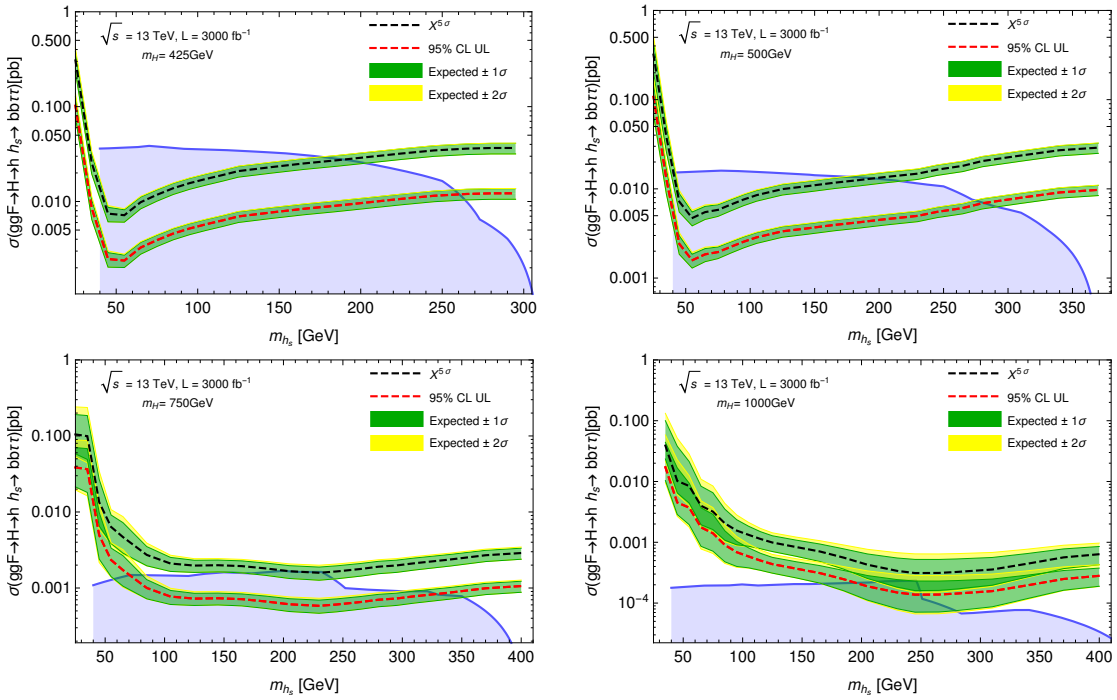

Figure 5.23: 95% CL exclusion limits and $5\,\sigma$ discovery cross sections for $h \to b\bar{b}$ and $h_s \to \tau\tau$ as function of m_{h_s} for 3000 fb^{-1} integrated luminosity and $m_H = 425$ GeV (upper left), $m_H = 500$ GeV (upper right), $m_H = 750$ GeV (lower left), $m_H = 1000$ GeV (lower right).

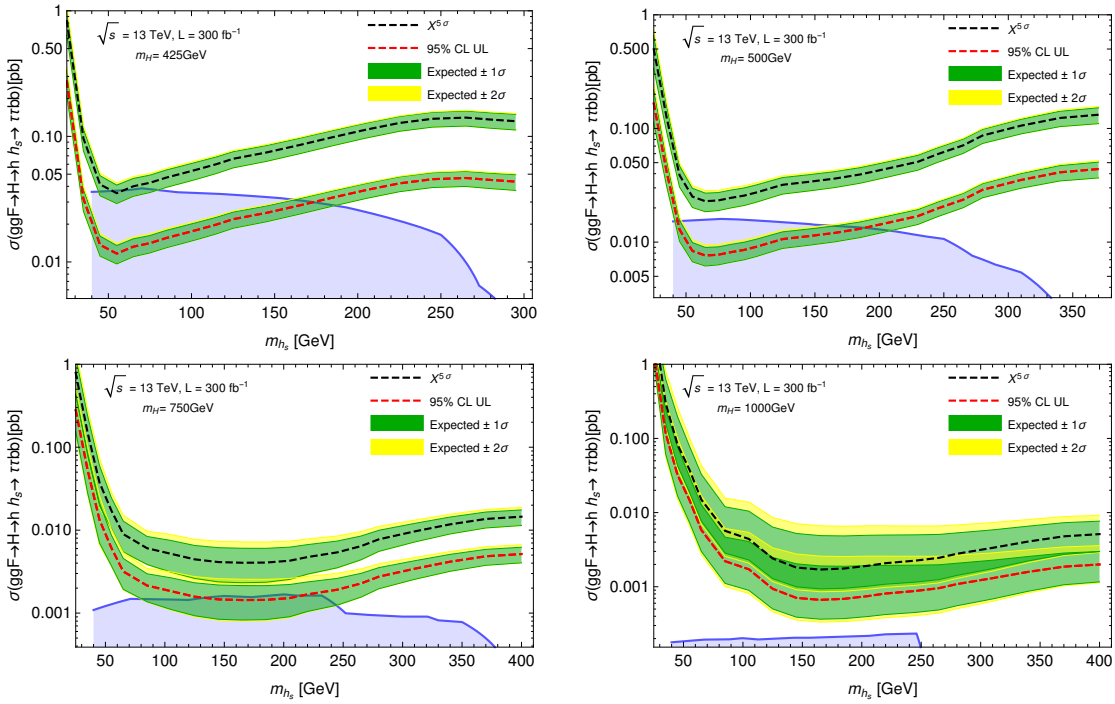

Figure 5.24: 95% CL exclusion limits and $5\,\sigma$ discovery cross sections for $h \to \tau\tau$ and $h_s \to b\bar{b}$ as function of m_{h_s} for 300 fb^{-1} integrated luminosity and $m_H = 425$ GeV (upper left), $m_H = 500$ GeV (upper right), $m_H = 750$ GeV (lower left), $m_H = 1000$ GeV (lower right).

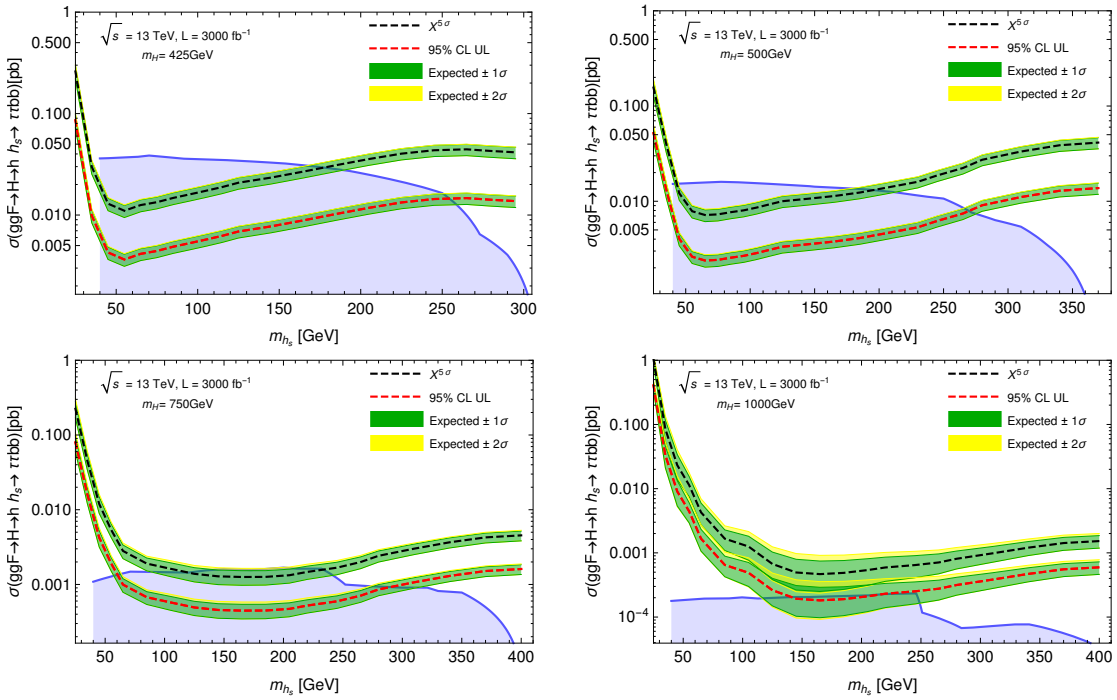

Figure 5.25: 95% CL exclusion limits and $5\,\sigma$ discovery cross sections for $h \to \tau\tau$ and $h_s \to b\bar{b}$ as function of m_{h_s} for 3000 fb^{-1} integrated luminosity and $m_H = 425$ GeV (upper left), $m_H = 500$ GeV (upper right), $m_H = 750$ GeV (lower left), $m_H = 1000$ GeV (lower right).

5.6 The $b\bar{b}\gamma\gamma$ channel

This channel offers in principle some interesting advantages for the search of Higgs bosons. In general, a Higgs-like particle has a relatively small couplings to photons due to the fact that it is a loop induced decay, mediated mainly by top quarks and vector boson loops (although of course this depends on the model under consideration). The SM branching ratio of a Higgs boson with a mass m_h =125 GeV to a pair of photons is around 0.228%, much smaller than the dominant $b\bar{b}$ channel, in which a 125 GeV Higgs decays 56.9% of the times. However, for the case of a hadron collider like the LHC, the electromagnetic background is much smaller than the QCD one, and thus a search featuring two hard photons turns out to be a very clean channel. Following this argument, the $b\bar{b}\gamma\gamma$ final state can thus be considered as a good compromise between the 'cleanness' of a diphoton final state, although having a small signal cross section; and the large branching ratio to b quarks of typical Higgs particles, at the price of having a large QCD background.

Recall also that, unlike the $b\bar{b}b\bar{b}$ or $b\bar{b}\tau\tau$ cases, the branching ratios of the two possible decays of the non-SM state, $BR(h_s \to b\bar{b})$ and $BR(h_s \to \gamma\gamma)$, are usually anticorrelated for a Higgs-like particle, as it is the case of the NMSSM singlet in a large part of parameter space (as we showed in chapter 4). Since the couplings of a Higgs-like particle to taus and bs are generically given by a coupling to down-type fermions, the final states $h(b\bar{b})h_s(\tau\tau)$ and $h(\tau\tau)h_s(b\bar{b})$ in the $b\bar{b}\tau\tau$ search usually test the same region in the parameter space of the model. On the other hand, a suppression in $BR(h_s \to b\bar{b})$ may lead to an enhancement of $BR(h_s \to \gamma\gamma)$ (see 4.4). Therefore, the searches $H \to hh_s \to h(b\bar{b})h_s(\gamma\gamma)$ and $H \to hh_s \to h(\gamma\gamma)h_s(b\bar{b})$ may be actually probing different regions of parameter space in models like the NMSSM (or 2HDM+S), offering thus an interesting complementarity.

Searches for double SM Higgs production in the $b\bar{b}\gamma\gamma$ have been carried out by both ATLAS and CMS using Run I [91, 93, 96] and Run II [106, 110, 148] data. Furthermore, the ATLAS collaboration has released an interesting study on the prospects for measuring Higgs pair production in this channel at the HL-LHC regime [149]. In our Monte Carlo approach to model the background, we take as a starting point the background studies for double SM Higgs production carried out by the experimental collaborations in this channel. However, as we deal with two different decay states, the diphotons can a priori originate from either h and h_s: Both cases are studied below. Like in the previous case, we optimize our analysis as function of the mass hypothesis $m_{h_s}^{\text{test}}$.

5.6.1 Background simulation

Apart from the irreducible $b\bar{b}\gamma\gamma$ background, one has to account for the possibility of lighter quark flavours being misidentified as b-quarks by the b-tagging algorithm. Charm quarks have a larger misidentification rate than lighter quark and gluon jets, and thus were simulated in different samples to better account for these effects. The b-tagging capabilities in our simulations are included in the detector simulation routine `Delphes`, which in this case was tuned to reproduce the b-tagging efficiencies reported by the ATLAS collaboration [130] for the $\epsilon = 0.85$ working point. Such efficiencies depend on the p_T of the jets. Analytical functions of the form of (5.7) were used to reproduce this behaviour accurately, and the fitting parameters are presented in table 5.7. The $\epsilon = 0.85$ working point, also chosen by ATLAS for the double SM Higgs search presented in [148], features rather loose criteria to identify b-jets in order to increase the b-tagging efficiency, at the price of increasing the misidentification rate. This choice was done to maximize the b quark identification efficiency to compensate the very small signal cross sections that we aim to test, specially when dealing with large mass hypothesis.

Algorithm	a	b	c	d
b-tagging	71	1.18	0.002	0.19
c-tagging	15	0.98	0.004	0.13
light-jet-tag	$\epsilon_{\text{light}} = 3.510^{-2}$			

Table 5.7: Fit parameters for the tagging algorithms as a function of p_T .

Another important source of background consists in events with jets fragmenting into pions subsequently decaying into a pair of collimated photons, which are misidentified as isolated photons (fake photons). Although the rate for jets giving rise to fake photons is small, the cross section of jets+γ is very large and thus this source gives an important contribution to the total background. We accounted for this simulating $2 \cdot 10^7$ $b\bar{b}j\gamma$ events. The detector simulation performed with `Delphes` allows indeed to account for this effect, which also depends on the photon isolation criteria, described below.

Lastly we considered single SM Higgs production through top quark association (computed at NLO) with the Higgs subsequently decaying to a pair of gammas, although it has little impact and it is only expected to play a role in the $h(\gamma\gamma)h_s(b\bar{b})$ search. Other backgrounds, like SM double Higgs production or Drell-Yann events with their decay electrons misidentified as photons were neglected, as they have been shown to have a minor impact [106, 149]. Effects from underlying event and pile-up collisions have been neglected.

The $b\bar{b}\gamma\gamma$, $c\bar{c}\gamma\gamma$ and $jj\gamma\gamma$ were generated at leading order inclusively, i.e. with an additional jet in the tree-level matrix element, suitably matched to the parton shower to avoid double-counting effects. These samples were normalized to their LO cross sections also computed with `MadGraph5`. The ttH background was generated at NLO in QCD assuming SM couplings. The $b\bar{b}j\gamma$ sample was generated at leading order exclusively, and the obtained cross section was rescaled using a QCD NLO K-factor from [124]. All the Monte Carlo samples used in this study are presented in table 5.8.

Photons were required to pass isolation criteria through the relative isolation variable for photons,

$$I_{\gamma}^{\text{rel}} = \frac{\sum_i p_{T,i}}{p_{T,\gamma}} < 0.1, \tag{5.32}$$

where the sum over i corresponds to all particles within a cone of $\Delta R = 0.4$.

Validation of the background

In this section we aim to validate our MC background model using current available data from double SM Higgs searches in the $b\bar{b}\gamma\gamma$ final state. Although this validation will only confirm our results for the case when $m_{h_s} \approx m_h \approx 125$ GeV, it serves as a good indicator for estimating the reliability of our Monte Carlo samples.

As for today, searches for double SM Higgs production in this channel at $\sqrt{s} =$ 13 TeV use low luminosities (3.2 fb^{-1} for the case of ATLAS [148] and CMS uses 2.7 fb^{-1} [106]), thus making our comparison rather loose in statistics. Both collaborations rely on data-driven methods to model the expected background.

In the following, we reproduce the ATLAS analysis [148] in order to obtain the expected number of events due to the SM background using our MC samples, to then compare it with the ATLAS result. Although the collaboration measured 0 events in the signal region, their background model, constructed entirely from

Process (ME)	σ_{LO}(pb)	# events	K-factor	equiv. luminosity
$b\bar{b}\gamma\gamma(+j)$	0.36 pb	$2 \cdot 10^6$	-	5536 fb^{-1}
$c\bar{c}\gamma\gamma(+j)$	1.17 pb	$2.4 \cdot 10^6$	-	2038 fb^{-1}
$kk\gamma\gamma(+j)$	11.23 pb	$2.1 \cdot 10^6$	-	183 fb^{-1}
$b\bar{b}j\gamma$	332.8 pb	$2 \cdot 10^7$	1.58	38 fb^{-1}
$t\bar{t}H$ (NLO)	1.13 fb	$5 \cdot 10^4$	-	$4.4 \cdot 10^4$ fb^{-1}

Table 5.8: Monte Carlo samples used in the study of the $b\bar{b}\gamma\gamma$ final state. Recall that k indicates u,d and s quarks and gluons.

data, predicted 1.63±0.3 background events after all cuts and selection criteria. We will use this value as a reference to compare our MC model.

In [148], after isolation requirements, the two leading p_T photons are required to satisfy

$$E_T^{lead}/m_{\gamma\gamma} > 0.35, \quad E_T^{subl.}/m_{\gamma\gamma} > 0.25, \quad |\eta| < 2.37 \text{ and } 1.37 < |\eta| < 1.52 \tag{5.33}$$

where $m_{\gamma\gamma}$ is the invariant mass of the diphoton system. Jets are required to have $|\eta| < 2.5$ and $p_T > 25$ GeV, and are b-tagged using a $\epsilon = 0.85$ working point. After b-jets identification, The highest p_T and the next-to-highest p_T b-jets are required to have $p_T > 55$ GeV and $p_T > 35$ GeV respectively.

Events are selected if there are at least two photons and exactly two b jets. The invariant mass of the $b\bar{b}$ system should lie within

$$95 \text{ GeV} < m_{b\bar{b}} < 135 \text{ GeV}. \tag{5.34}$$

For the diphoton system, a first mass cut is applied, requiring $m_{\gamma\gamma}$ to fall within

$$105 \text{ GeV} < m_{\gamma\gamma} < 160 \text{ GeV}. \tag{5.35}$$

Then, the actual signal region is defined by further requiring $m_{\gamma\gamma}$ to be inside

$$m_h - 3.1 \text{ GeV} < m_{\gamma\gamma} < m_h + 3.1 \text{ GeV}, \tag{5.36}$$

whereas the complementary region with (5.35) is defined as the sideband. The efficiency for events satisfying (5.35) to pass the tighter $m_{\gamma\gamma}$ cut is estimated by ATLAS using data (from a 0-b-tagged region) to be $\epsilon_{\gamma\gamma} = 0.126 \pm 0.001$. In our MC model we obtain for this efficiency $\epsilon_{\gamma\gamma} = 0.1246 \pm 10^{-4}$, in very good agreement with the ATLAS result. After passing (5.36), the ATLAS collaboration reports that the total invariant mass distribution $m_{b\bar{b}\gamma\gamma}$ is fitted using a Landau Distribution (which we present below). Although no fit parameters are presented in [148], we have also found that this function presents an excellent agreement with our MC events, and will be used later on for modelling the background even when $m_{h_s} \neq m_h$.

Finally, the total number of background events expected by ATLAS after all cuts within the mass window given by eq. (5.36) is 1.63 ± 0.3, whereas our MC model yields 1.06 ± 0.14, i.e. near 53% below the ATLAS result. Reasons for this underestimation are numerous. NLO QCD corrections are known to give rise to a substantial increase of the production cross section [150]. Other sources not accounted for, differences in the photon isolation and the modelling of the b tagging and photon identification can also alter the final result.

In order to adjust our background model to the data, we perform a rescaling to fit the ATLAS results. The best fit is obtained with a rescaling factor of 1.54 ± 0.35. As for the $b\bar{b}b\bar{b}$ case, this rescaling factor will be used when modelling the background even at $m_h \neq m_{h_s}$. In the following the uncertainty ±0.35 will be used as a systematic uncertainty.

5.6.2 Event selection

We present here the selection criteria common to both searches. The isolation criteria for the photons present in the events is the same that we adopted in sec. 5.6.1, i.e. the relative isolation variable for photons should satisfy $I_\ell^{\rm rel} < 0.1$.

Events are required to have at least 2 b tagged jets with $p_T > 40$ GeV and $|\eta| < 2.5$. The b-tagging efficiency corresponds to those reported by ATLAS [130] for the working point $\epsilon = 0.85$, as indicated above. The two p_T leading b jets are used to reconstruct the Higgs candidate (either h or h_s), and thus we stick to the resolved region as in the previous cases. This choice is rather natural for the $b\bar{b}\gamma\gamma$ channel: Since the typical signal cross sections in $b\bar{b}\gamma\gamma$ become way too small for large masses of m_H, the region of interest for this search will be approximately $m_H \lesssim 750$ GeV, where the resolved topology for the $b\bar{b}$ system accounts for practically the totality of the events.

Two or more photons are required in each event. The leading and subleading p_T photons are used to reconstruct the kinematics of the Higgs candidate. They should satisfy the asymmetric selection criteria:

$$E_T^{lead}/m_{\gamma\gamma} > 1/3, \quad E_T^{subl.}/m_{\gamma\gamma} > 1/4, \quad |\eta| < 2.47 \tag{5.37}$$

Further cuts on the kinematical variables of the reconstructed Higgs candidates are detailed in the following subsections.

5.6.3 $H \to h(b\bar{b})h_s(\gamma\gamma)$

After passing the cuts described above, the $b\bar{b}$ and $\gamma\gamma$ systems are used to reconstruct the SM Higgs and h_s candidates respectively. Instead of using the total invariant mass $m_{b\bar{b}\gamma\gamma}$, the mass of the heavy state H is reconstructed using the corrected total invariant mass m_X, defined as

$$m_X = m_{b\bar{b}\gamma\gamma} - m_{b\bar{b}} + 125 \text{ GeV}, \tag{5.38}$$

already used by CMS [106] in the double SM Higgs search in the $b\bar{b}\gamma\gamma$ channel. As in the $b\bar{b}b\bar{b}$ and $b\bar{b}\tau\tau$ channels, the variable m_X produces a much better 4-body invariant mass resolution, as we can see in fig. 5.26.

Since we focus our search on the m_X histogram, we use a test mass $m_{h_s}^{\rm test}$ as in the previous cases, which serves as a mass hypothesis for m_{h_s}. A signal region is defined as a function of $m_{h_s}^{\rm test}$ applying cuts on the invariant masses $m_{b\bar{b}}$ and $m_{\gamma\gamma}$. For the case of the dijet system, we require

$$100 \text{ GeV} < m_{b\bar{b}} < 150 \text{ GeV}, \tag{5.39}$$

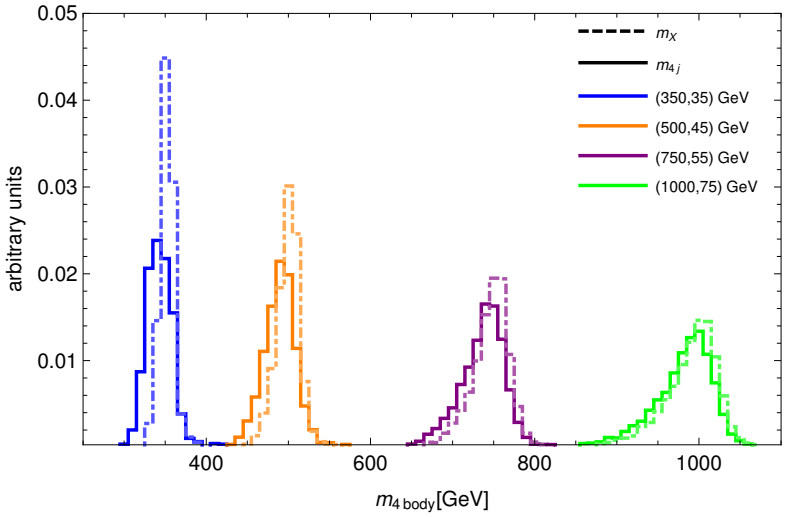

Figure 5.26: 4-body invariant mass reconstruction using $m_{b\bar{b}\gamma\gamma}$ and m_X as defined in eq. 5.38, for various signal points. All signal samples were simulated assuming a width of 1 GeV.

consistent with the mass of the SM Higgs. On the other hand, the distribution of signal events in the diphoton invariant mass histogram $m_{\gamma\gamma}$, associated to the mass of the non SM state h_s, depends on the masses m_H and m_{h_s} present in the signal. Photon measurements have a much better resolution with respect to jets, allowing us to define narrower regions to identify a signal. As we see in fig 5.27, for a fixed value of m_{h_s}, the width of the signal tends to increase as m_X increases. On the other hand, when fixing m_H, varying the mass m_{h_s} within the range of masses considered in this work barely changes the shape of $m_{\gamma\gamma}$, so we can fairly approximate the width of the distribution to be independent of the actual mass of h_s. In order to optimize the signal efficiency, we fit the $m_{\gamma\gamma}$ distribution to a Gaussian to obtain the value of the variance $\sigma^2_{\gamma\gamma}$ for each signal sample (m_H, m_{h_s}). Then, a simple analytical expression for $\sigma_{\gamma\gamma}$ is obtained as a function of m_H;

$$\sigma_{\gamma\gamma}(m_H) = 2.310 \text{ GeV} + 0.008 \cdot m_H. \tag{5.40}$$

Using this expression, we define a window for the invariant mass $m_{\gamma\gamma}$ such that approximately 95% of the signal events pass this cut, i.e. $m_{\gamma\gamma}$ should satisfy

$$\left| m_{\gamma\gamma} - m_{h_s}^{\text{test}} \right| < 2\sigma_{\gamma\gamma}(m_X) \tag{5.41}$$

where m_X is the corrected total invariant mass of the event, identified with the mass of the heavy state H. As in the previous cases, this is a mass dependent cut applied in a per-event basis, optimizing the signal-to-background discrimination.

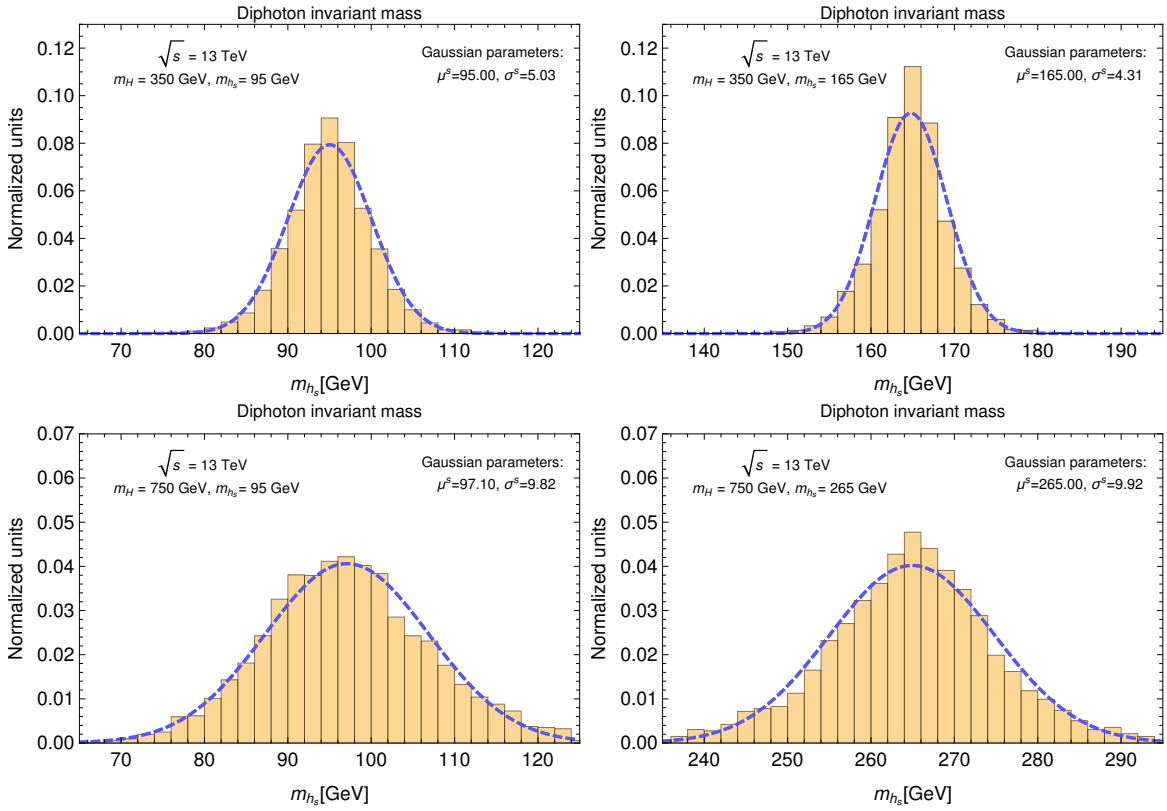

Figure 5.27: Distribution of the reconstructed $m_{\gamma\gamma}$ for some signal samples, with the fitted Gaussian distribution used to approximate the width $\sigma_{\gamma\gamma}$.

Subsequently, mass dependent cuts are applied on the kinematics of the h and h_s candidates,

$$p_T(b\bar{b}) > 16.94 \text{ GeV} + 0.18 m_X \tag{5.42}$$

and

$$E_T(\gamma\gamma) > 68.32 \text{ GeV} + 0.25 m_X. \tag{5.43}$$

For the case of the diphoton system, we applied a cut on E_T instead of p_T since in this way we can define a cut fairly independent of the mass m_{h_s}. In fig. 5.28 we present a diagram showing the different stages of the event selection for various illustrative examples. As we can see from the figures, the signal efficiency after selection lies between 5% and 10% for most masses.

After cuts, almost all the samples in table 5.8 make important contributions to the background. The samples consisting in $\gamma\gamma$+jets suppose approximately 60% of the total background, whereas the rest is due to the $\gamma + b\bar{b}j$ samples where a

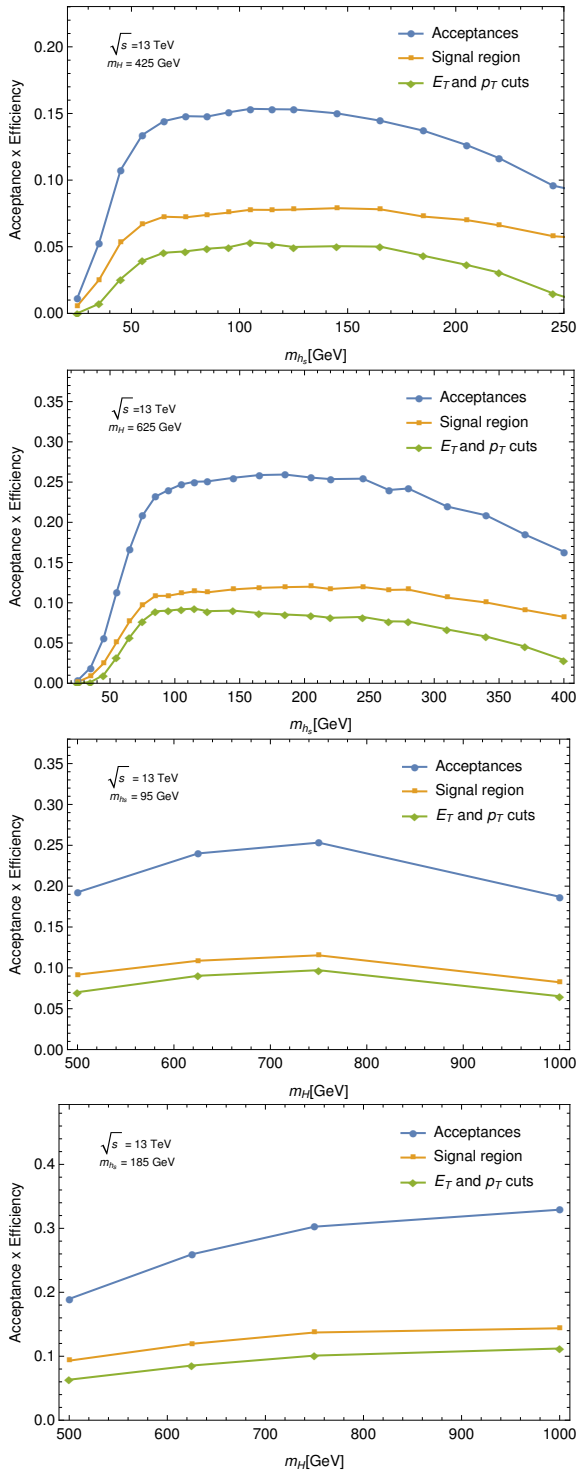

Figure 5.28: Up: Signal efficiencies for fixed values of m_H, as a function of the mass of h_s. Down: Signal efficiencies fixing the value of m_{h_s}.

gamma is faked from jet fragmentation. The $t\bar{t}H$ background only has a noticeable contribution in the region 105 GeV $< m_{h_s}^{\text{test}} <$ 145 GeV, although its contribution is always below 5%.

The m_X distributions of the events passing all the cuts in each background sample are fitted to a Landau distribution. The Landau distribution, also used by ATLAS [148] to parametrize the background in the $b\bar{b}\gamma\gamma$ channel, is a two parameters distribution, which probability distribution function is proportional to:

$$\int_0^\infty \sin(2t) e^{-t\frac{(x-\mu)}{\sigma} - \frac{2}{\pi} t \log(t)} dt. \tag{5.44}$$

All the fits show a very good agreement with the pseudodata, as we see for the cases of $m_{h_s}^{\text{test}} = 95$ GeV and $m_{h_s}^{\text{test}} = 165$ GeV in figs. 5.29.

5.6.4 $H \to h(\gamma\gamma)h_s(b\bar{b})$

We now consider a search where the 125 GeV scalar decays to a pair of photons and the extra state h_s produces a $b\bar{b}$ pair, with an invariant mass ranging from 25 GeV to 400 GeV. The strategy is similar to the one presented in the previous section. Firstly, we define the corrected invariant mass m_X as

$$m_X = m_{\gamma\gamma b\bar{b}} - m_{b\bar{b}} + m_{h_s}^{\text{test}}. \tag{5.45}$$

Subsequently a signal region is defined in the (m_h, m_{h_s}) plane. As a result of a signal-to-background study using the MC events, we obtain an optimum mass window given by the expressions:

$$|m_{\gamma\gamma} - 125 \text{ GeV}| < 2 \text{ GeV} + 0.02 \cdot m_X \tag{5.46}$$

$$0.9 \cdot m_{h_s}^{\text{test}} - 30 \text{ GeV} < m_{b\bar{b}} < 0.9 \cdot m_{h_s}^{\text{test}} + 20 \text{ GeV}, \tag{5.47}$$

where the mass window (5.46) has been optimized in the same way as we did for the diphoton window in expression (5.40). Indeed, both expression account for the fact that the signals tend to be wider as the masses m_H and m_{h_s} increase.

Kinematic cuts are applied to the Higgs boson candidates:

$$E_T(\gamma\gamma) > 7.45 \text{ GeV} + 0.33 m_X \tag{5.48}$$

for the 125 GeV state, and

$$p_T(b\bar{b}) > -5.71 \text{ GeV} + 0.29 m_X \tag{5.49}$$

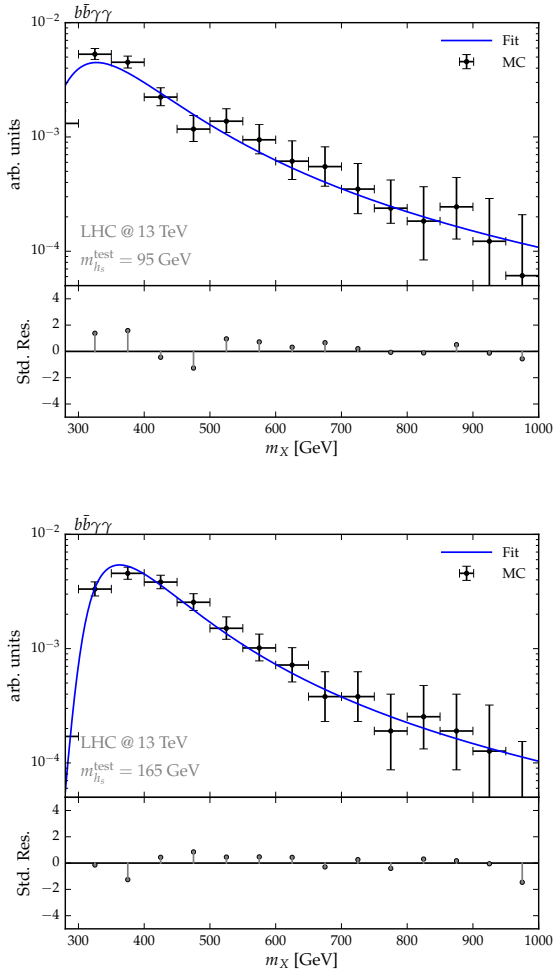

Figure 5.29: MC events for the background, using samples described in table 5.8, and the fits using a Landau distribution for $m_{h_s}^{\text{test}}$ =95 GeV (left) and $m_{h_s}^{\text{test}}$ =165 GeV (right).

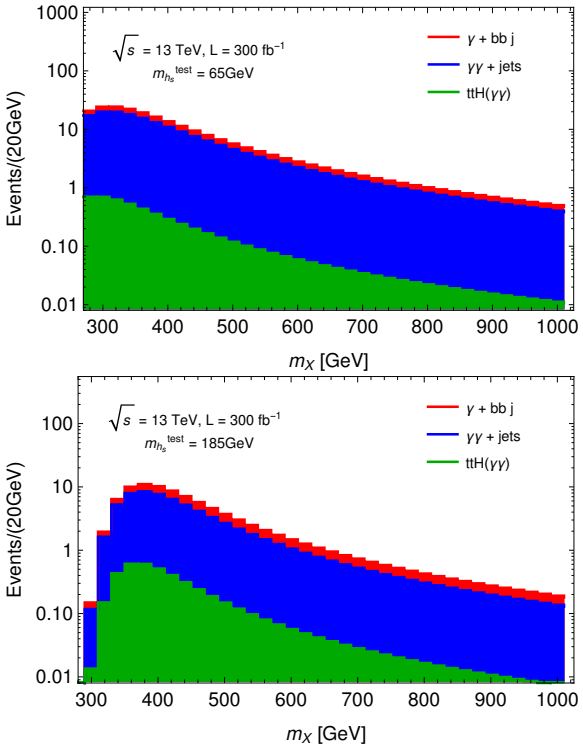

Figure 5.30: m_X background decomposition for $m_{h_s}^{\text{test}}$ =65 GeV (left) and $m_{h_s}^{\text{test}}$ = 185 GeV (right), for the search presented in sec 5.6.4. The distribution was obtained using the parametrized background model, normalized to an integrated luminosity of L=300 fb^{-1}

for h_s. The signal efficiencies are similar to the previous case, ranging from very small values for small m_{h_s} or $m_H \approx m_{h_s} + 125$ GeV, to a maximum of ∼15% for $m_{h_S} \approx 100$ GeV.

Once the cuts have been applied, we are left with sizeable contributions from all the background samples. In this case, the single SM Higgs production supposes an irreducible background for all masses of h_s, and it comprises between 2% and 4% of the total background. The remaining background consists in approximately 80% of $\gamma\gamma + jets$ whereas the rest is due to the $b\bar{b}j\gamma$ (i.e. one hard photon plus one fake photon). However, this background decomposition depends strongly on the region of m_X that we are looking at: at relatively low $m_X \lesssim 550$ GeV, the contribution arising from fake photons (modelled through the $b\bar{b}j\gamma$ sample) is below 10% for almost all $m_{h_s}^{\text{test}}$, whereas for large values it could comprise up to 45% of the total background. In fig. 5.30 we show the background decomposition as function of m_X, for $m_{h_s}^{\text{test}}$ =65 GeV and $m_{h_s}^{\text{test}}$ =185 GeV.

The same parametrization of the background holds for this search, i.e. the

Landau distribution is used to fit the background samples. Each MC sample is parametrized separately for each value of $m_{h_s}^{\text{test}}$.

signal (m_H, m_{h_s})	cross sec.	bin	# bkgr	# signal	Z
(350, 75) GeV	2.8 fb	[340, 360] GeV	39.20	39.16	4.84
(500, 145) GeV	1.35 fb	[480, 520] GeV	14.45	28.20	4.94
(625,105) GeV	0.75 fb	[580, 640] GeV	7.99	23.73	5
(750,95) GeV	0.6 fb	[700, 780] GeV	6.11	22.23	5

Table 5.9: Event yield for the signal and background for some benchmark scenarios and its local significance, computed assuming a Poissonian distribution of the events for the bin specified in the table. The results correspond to the analysis in $h(\gamma\gamma)h_s(b\bar{b})$. All cases correspond to a c.m.e. of 13 TeV and L=300 fb^{-1} .

5.6.5 Discovery cross sections $X^{5\sigma}$ and exclusion limits

Given the m_X distribution of the background for various hypothetical values of m_{h_s} and the m_X distributions of signals we can, as before, obtain values for 95% CL exclusion and $5\,\sigma$ discovery for cross sections times branching fractions into the $h \to b\bar{b}$, $h_s \to \gamma\gamma$ and $h \to \gamma\gamma$, $h_s \to b\bar{b}$ final states as function of the integrated luminosity, m_H and m_{h_s}.

After completing our analysis the CMS search [110] for $h + h \to b\bar{b}\gamma\gamma$ based on 35.9 fb^{-1} appeared. The expected 95% CL exclusion limits given in [110] can be compared to ours for $m_{h_s} = 125$ GeV for the same integrated luminosity; this comparison as function of m_H is shown in Fig. 5.31. The expected limits coincide within $1\,\sigma$ for $m_H \gtrsim 500$ GeV, and within $2\,\sigma$ everywhere. Our expected limits are systematically more conservative; we note that the CMS analysis employs Boosted Decision Tree (BDT) algorithms for the signal to background discrimination, which are more sophisticated than the traditional cuts, and give rise to a better optimization of the signal discrimination.

Our expected 95% CL exclusion limits and $5\,\sigma$ discovery cross sections for $h \to b\bar{b}$, $h_s \to \gamma\gamma$ as function of m_{h_s} at 300 fb^{-1} integrated luminosity are shown in Figs. 5.32 for four representative values for $m_H = 425$, 500, 625 and 750 GeV, and for 3000 fb^{-1} integrated luminosity in Figs. 5.23. For $h \to \gamma\gamma$, $h_s \to b\bar{b}$ at 300 fb^{-1} integrated luminosity these are shown in Figs. 5.34, for 3000 fb^{-1} integrated luminosity in Figs. 5.35. The uncertainties include statistical uncertainties and, added linearly, ±35% considered as systematic uncertainty originating from the normalisation of the background. Again we show in blue the possible cross sections times branching fractions in the NMSSM.

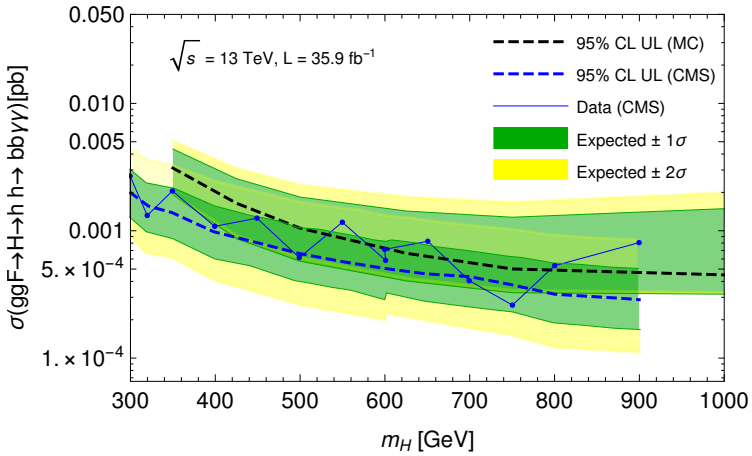

Figure 5.31: Expected 95% CL exclusion limits for $ggF \to hh \to b\bar{b}\gamma\gamma$ for 35.9 fb^{-1} from CMS [110] and from our MC simulation as function of m_H. For completeness the observed limits are shown.

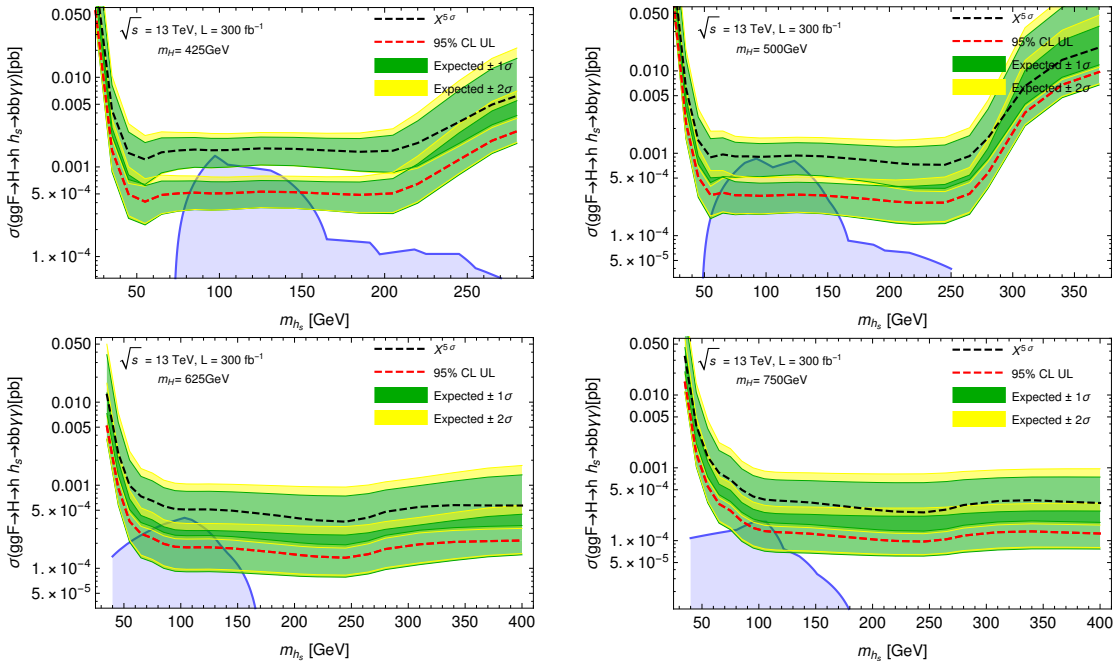

Figure 5.32: 95% CL exclusion limits and $5\,\sigma$ discovery cross sections for $h \to b\bar{b}$ and $h_s \to \gamma\gamma$ as function of m_{h_s} for 300 fb^{-1} integrated luminosity and $m_H = 425$ GeV (upper left), $m_H = 500$ GeV (upper right), $m_H = 625$ GeV (lower left), $m_H = 750$ GeV (lower right).

Two comments are in order: First, again a sizeable region in the NMSSM

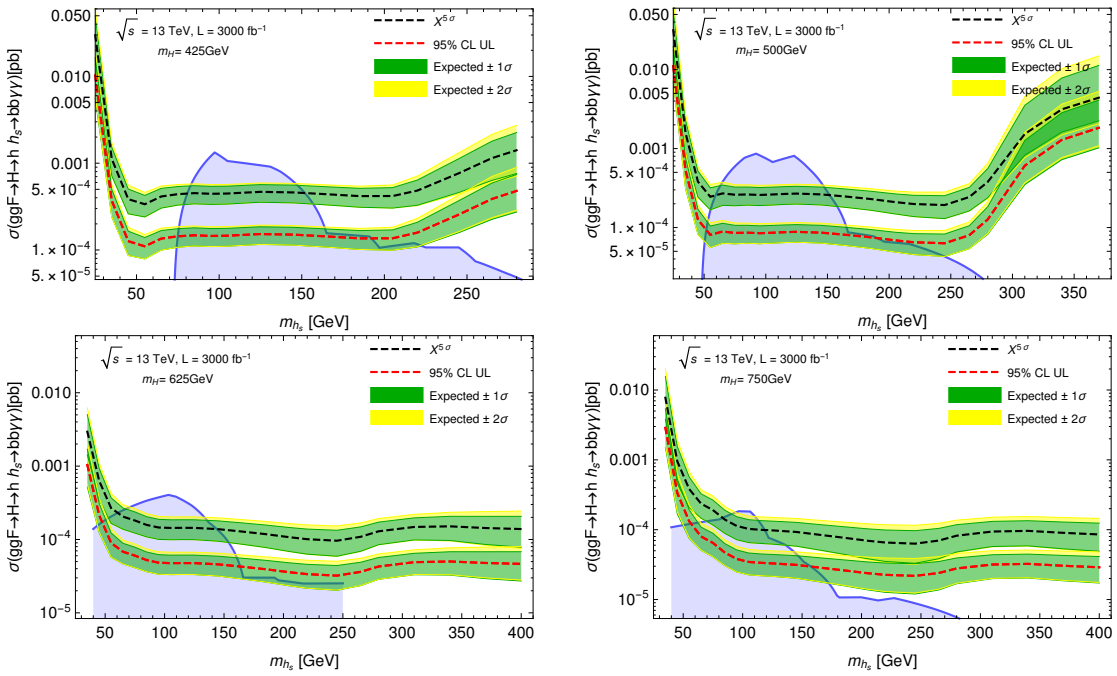

Figure 5.33: 95% CL exclusion limits and $5\,\sigma$ discovery cross sections for $h \to b\bar{b}$ and $h_s \to \gamma\gamma$ as function of m_{h_s} for 3000 fb^{-1} integrated luminosity and $m_H = 425$ GeV (upper left), $m_H = 500$ GeV (upper right), $m_H = 625$ GeV (lower left), $m_H = 750$ GeV (lower right).

parameter space can be tested in this final state provided m_H is not too large and the trilinear coupling $H - h_s - h$ is not too small. It is, however, *not* the same region potentially visible in the $b\bar{b}b\bar{b}$ final state: The branching fraction of h_s into $\gamma\gamma$ can vary in the $0.2\% \pm 0.1\%$ range, and is anticorrelated with its branching fraction into $b\bar{b}$.

Second, the comparison of the upper limits on $h \to b\bar{b}$ and $h_s \to \gamma\gamma$ versus $h \to \gamma\gamma$ and $h_s \to b\bar{b}$ has a simple answer depending on m_{h_s}: For $m_{h_s} < 125$ GeV the search for $h_s \to \gamma\gamma$ is more promising, whereas for $m_{h_s} > 125$ GeV the search for $h \to \gamma\gamma$, $h_s \to b\bar{b}$ is typically more promising (unless the branching fraction $h_s \to b\bar{b}$ is extremely enhanced).

Lastly, we show in fig. 5.36 two benchmark scenarios of how a 5σ excess would look like in an actual m_X histogram, following the strategy presented for $H \to h(b\bar{b})h_s(\gamma\gamma)$. Unlike the excesses in the $b\bar{b}b\bar{b}$ final state, the photons offer a much better resolution giving rise to sharper peaks which are easier to identify. The 'discovery peaks' are much more pronounced with respect to the $b\bar{b}b\bar{b}$ or $b\bar{b}\tau\tau$ cases, although the statistics are lower and thus the error bars larger. Also, due to the decreasing signal cross section with the mass of the heavy state H, the

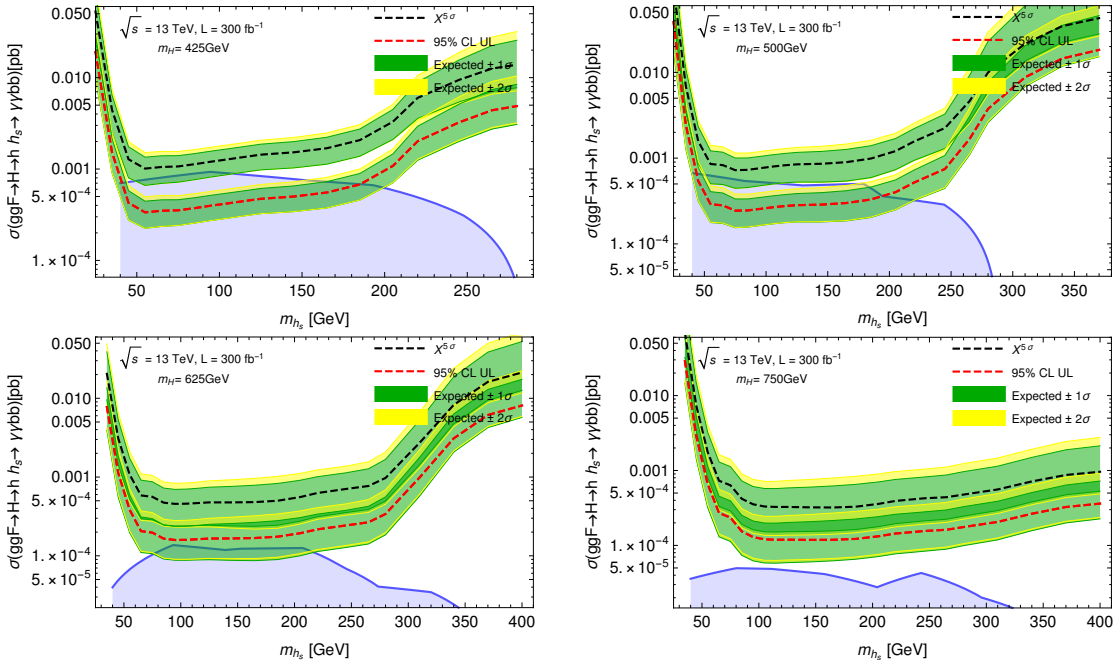

Figure 5.34: 95% CL exclusion limits and $5\,\sigma$ discovery cross sections for $h \to \gamma\gamma$ and $h_s \to b\bar{b}$ as function of m_{h_s} for 300 fb^{-1} integrated luminosity and $m_H = 425$ GeV (upper left), $m_H = 500$ GeV (upper right), $m_H = 625$ GeV (lower left), $m_H = 750$ GeV (lower right).

region of interest for this search lies typically for relatively low m_H. For very small $m_H \approx 350$ GeV, the signal excess could sit on top of the global maximum of the SM background, as is the case presented in the upper plot in fig. 5.36. This could in principle complicate the identification of the excess, since one is particularly sensitive to the modelling of the background. However, the good resolution of the corrected mass m_X (particularly good for low m_H) circumvent this issue, since the signal events concentrate in a few bins with a relatively small width.

In table 5.10 we present the number of expected events for several benchmark scenarios. Recall that, because of the reduced number of events, the approximate formula for computing the Gaussian significance, $Z = S/\sqrt{B}$, does not hold any more, and Poissonian expressions should be used instead.

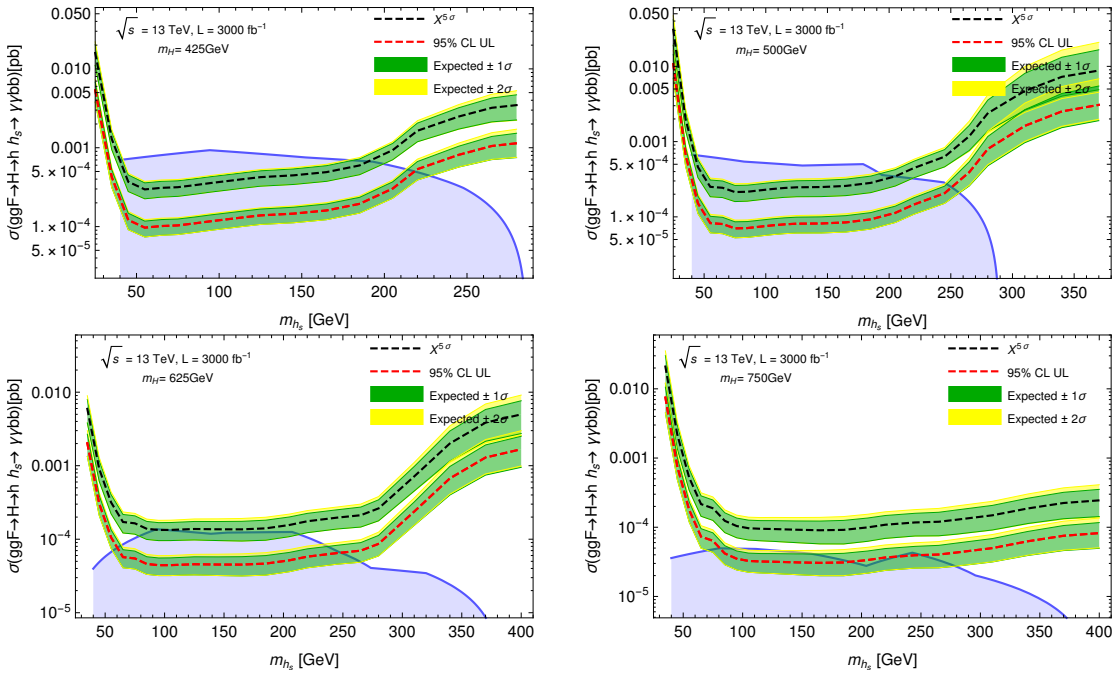

Figure 5.35: 95% CL exclusion limits and $5\,\sigma$ discovery cross sections for $h \to \gamma\gamma$ and $h_s \to b\bar{b}$ as function of m_{h_s} for 3000 fb^{-1} integrated luminosity and $m_H = 425$ GeV (upper left), $m_H = 500$ GeV (upper right), $m_H = 625$ GeV (lower left), $m_H = 750$ GeV (lower right).

signal (m_H, m_{h_s})	cross sec.	bin	# bkgr	# signal	Z
(350, 75) GeV	5 fb	[340, 360] GeV	10.11	22.98	4.6
(500, 145) GeV	1.45 fb	[480, 520] GeV	8.27	24.01	5
(625,105) GeV	0.9 fb	[580, 640] GeV	5.41	22.30	5
(750,95) GeV	0.7 fb	[700, 780] GeV	2.57	18.27	5

Table 5.10: Event yield for the signal and background for some benchmark scenarios and its local significance, computed assuming a poissonian distribution of the events for the bin specified in the table. The results correspond to the analysis presented in sec. 5.6.3. All cases correspond to a c.m.e. of 13 TeV and L=300 fb^{-1} .

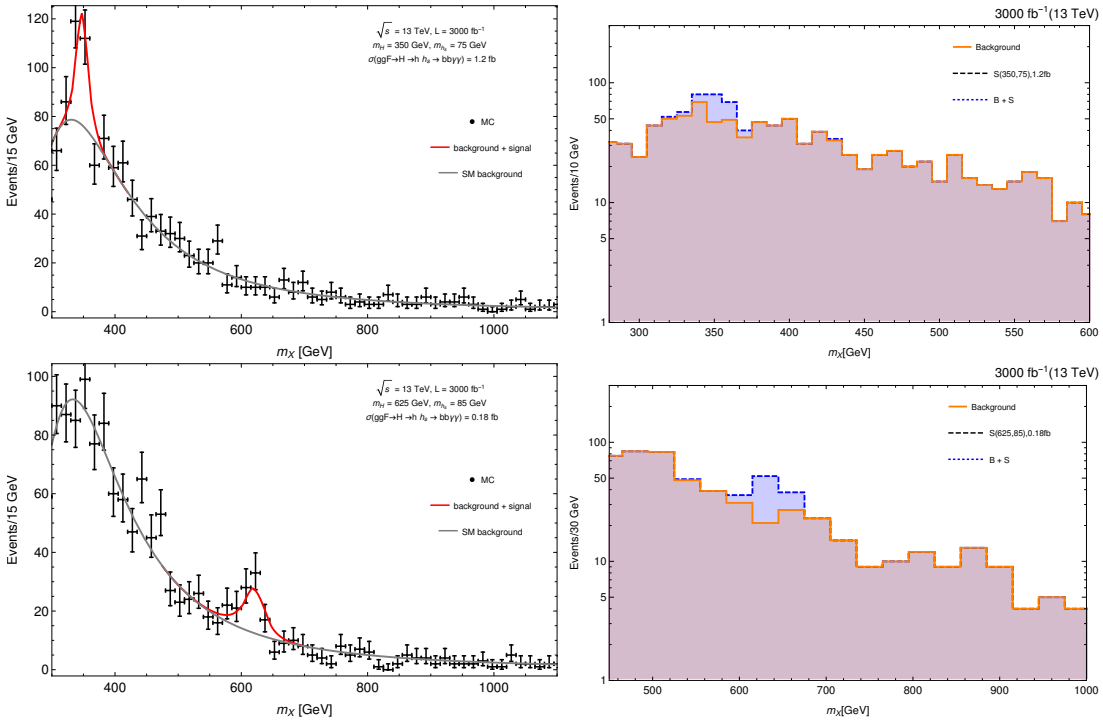

Figure 5.36: Examples of signals exceeding a 5σ sensitivity in the m_X histogram, for the $h(b\bar{b})h_s(\gamma\gamma)$ final state. Plots on the left- and right-hand side are equivalent, except for the bins size. Top: relatively light H of $m_H = 350$ GeV, decaying into a SM state h and h_s with $m_{h_s} = 75$ GeV. We see that the signal could sit on top of the maximum for sufficiently small m_H. Bottom: The signal features $m_H = 625$ GeV and $m_{h_s} = 85$ GeV. For $m_H > 400$ GeV, the resonance H shows up as an excess on top of an exponentially decaying background.

5.7 Conclusion and outlook

Searches for resonant SM Higgs pair production are performed with considerable effort by ATLAS and CMS. As explained in the introduction searches for $ggF \to \Phi \to H_1 + H_2$ can be more promising where either H_1 or H_2 can be SM-like, and the other state being possibly CP-odd (which does not affect the search methods).

This scenario is manifest in the NMSSM where the rôle of Φ is played by the MSSM-like heavy doublet, but the argument is more general. In the present chapter we have studied the prospects for corresponding searches in the $b\bar{b}b\bar{b}$, $b\bar{b}\tau\tau$ and $b\bar{b}\gamma\gamma$ final states, including SM backgrounds. The results are that significant regions in the NMSSM parameter space can be tested by these searches.

We are convinced that the here proposed search methods can still be refined, and that the estimated sensitivities to cross sections times branching fractions presented here are conservative. This becomes clear from a comparison to the recent CMS search for resonant SM-Higgs pair production [110] in the $b\bar{b}\gamma\gamma$ final state (and actually also from a comparison to the recent CMS search [107] in the $b\bar{b}\tau\tau$ final state). Thus we hope that such promising searches will be performed in the future at the LHC.

Chapter 6

Summary

Supersymmetry has been for long time one of the most popular theoretical frameworks to overcome difficulties of the Standard Model. Most SUSY models invoke new physics at the TeV scale in order to circumvent fine-tuning problems, and in all cases extended Higgs sectors are needed. These offer an opportunity for us, in the LHC era, to test SUSY extensions of the SM, to probe naturalness as a guiding principle, and to understand the EWSB mechanism realised in nature. Moreover, even without SUSY the possible existence of extra Higgs bosons beyond the SM remains a key question, and answering it will be one of the principal goals of the LHC.

In this thesis we have studied the discovery prospects for the supplementary neutral Higgs bosons predicted in the Next-to-Minimal Supersymmetric Standard Model, with particular emphasis on processes including a mostly singlet scalar/pseudoscalar. Search methods studied in this work include:

- Direct production of a new (pseudo)scalar in the diphoton final state $ggF \to h_s \to \gamma\gamma$ has been considered in chapter 4. Motivated by naturalness, we explored regions in parameter space featuring a light singlet-like state with a mass below 125 GeV. We showed that current analysis in this channel by both ATLAS and CMS at $\sqrt{s} = 8$ TeV are already sensitive to a part of the phenomenologically viable parameter space of the NMSSM. However, these searches using run 1 data are far from excluding this theoretically well-motivated scenario: new data are necessary to further constrain or to discover it. Natural points can have a very small cross section$\sigma(ggF \to h_s \to \gamma\gamma)$ and thus direct searches are not enough to test this scenario completely.

- We showed that a sizeable $h_s - h$ mixing can substantially affect the coupling to gauge bosons of the 125 GeV Higgs h. Accurate measurements of the reduced coupling $\kappa_V(h)$ can largely test scenarios where the singlet- doublet

mixing is responsible for the value of the Higgs mass beyond its MSSM-like tree-level bound. This indirect search therefore complements the direct search discussed above, since the enhance- ment of $\sigma(ggF \to h_s \to \gamma\gamma)$ and $h_s - h$ mixing effects occur in different regions of parameter space.

- Decays via Higgs cascades including a singlet-like Higgs were found to have large cross sections ($\mathcal{O}$(pb)) in natural regions explored in chapter 4, and have been studied in detail in chapter 5. We showed that the LHC will be able to cover a part of the allowed parameter space of the NMSSM through 3 different final states: $b\bar{b}b\bar{b}$, $b\bar{b}\tau\tau$ and $b\bar{b}\gamma\gamma$. The $b\bar{b}b\bar{b}$ and $b\bar{b}\gamma\gamma$ channels are particularly promising, covering different regions of the NMSSM parameter space due to the complementarity of the $BR(h_i \to b\bar{b})$ and $BR(h_i \to \gamma\gamma)$ branching ratios. Also, the topology $ggF \to H/A \to h_s/a_s + Z$ has been shown in chapter 4 to reach important values for its cross section, and recent searches using Run 1 data [153] are close to NMSSM predicted values.

Other channels not considered in this thesis have been studied in the literature, which we briefly mention here. Searches for light pseudoscalars in exotic decays of the 125 GeV Higgs have been studied in [154] and have been shown to have a good potential to constrain allowed regions of the NMSSM parameter space, and several searches have been carried out, as we see in fig. 6.1, and more recently in [156, 157]. Mostly singlet-like pseudoscalars below 1 GeV are also possible in the NMSSM, for studies on it see [155].

All these searches suppose very promising methods for discovering/excluding the extra NMSSM Higgs bosons at the LHC. As we have already pointed out, there exists a complementarity between them, allowing to test different regions of the model's parameter space. Large singlet-doublet mixing will be tested by indirect searches (measuring $\kappa_V(h)$), whereas already moderate mixing can make the singlet-like state visible in the diphoton channel through direct production. On the other hand, in the case of a very pure singlet, Higgs-to-Higgs decays can indirectly produce hs /as, making them visible in various final states depending on the branching ratios of h_s/a_s.

However, even at the high luminosity regime of the LHC there will remain unexplored corners of the NMSSM parameter space. Such invisible regions include the case of a pure singlet with suppressed trilinear couplings. This situation would make the singlet-like state very difficult to produce directly and indirectly, and more powerful machines would be necessary to reach such small cross sections. Also, if the singlet state(s) and the extra doublet(s) are heavy (hence decoupled), the same problem arises, and the NMSSM Higgs sector would practically reproduce the one of the SM.

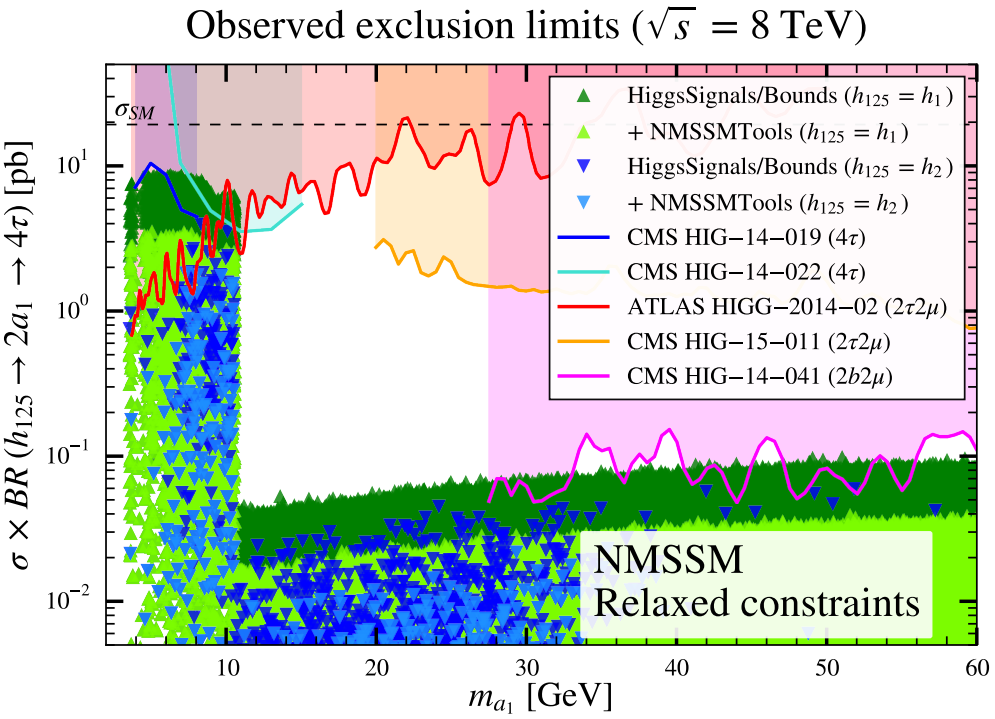

Figure 6.1: Observed exclusion limits from run 1 searches in exotic decays of the 125 GeV Higgs boson, versus scans in parameters space (from [154])

During the development of this thesis, both theoretical and experimental results have been released, and the field of particle physics has witnessed a period of high activity. Accurate results from high order calculations were obtained, sophisticated computational tools were developed, and many new results have been obtained by the experimental collaborations, to mention some.

Up to date, all experimental results seem to support the Standard Model, although many more results should arrive in the next years. The non-observation of long-awaited BSM effects questions our current understanding of particle physics; still, much work remain to be done, and accurate predictions and measurements will be needed in order to corner the hiding place of New Physics. To cite an example, the shape of the scalar potential remains unmeasured, and thus the actual mechanism that breaks the EW symmetry could be more involved than assumed within the Standard Model. This an other issues will be extremely challenging, demanding collaborations between the theoretical and experimental community to push the field towards the goal of extracting the maximum possible information from the data obtained at the LHC. Effective field Theories and precise calculations, from the theoretical side, and modern computational techniques, like ma-

chine learning and related methods, from the experimental side, will be necessary to fully exploit the opportunities that the collider offers.

Appendix A

Background fits

For fitting all the samples, we used a Maximum Likelihood Estimation (MLE) method. The method consists in maximizing a likelihood function, which could be intuitively understood as the probability of obtaining a particular set of data given the chosen statistical model. Given a certain statistical distribution parametrized by a probability density function $f(x;\theta)$ (where θ is the vector of parameters of the distribution), the likelihood function is defined as:

$$\mathcal{L}(\theta; x_1, \ldots, x_n) = \prod_{i=1}^{n} f(x_i; \theta) \tag{A.1}$$

where $x_1 \ldots x_n$ are the observed values. It is in general more convenient for performing calculations to take the logarithm of the likelihood function (known as the log-likelihood function):

$$\ln \mathcal{L}(\theta; x_1 \ldots, x_n) = \sum_{i=1}^{n} \ln f(x_i, \theta). \tag{A.2}$$

Given a set of data, the log-likelihood can be regarded as a function of the parameters of the distribution θ. Thus, given an statistical distribution f and a set of data $\{x_1, \ldots, x_n\}$, we can maximize the log-likelihood to obtain the set of parameters θ that better adjust the distribution f to the data.

When performing the background fits, we used the following distributions:

Four Parameter Gamma distribution:

$$\begin{aligned} f(M_X; \alpha, \beta, \gamma, \mu) = &\quad \frac{\gamma}{\beta\Gamma(\alpha)} e^{-\left(\frac{(M_X-\mu)}{\beta}\right)^{\gamma}} \left(\frac{M_X-\mu}{\beta}\right)^{\alpha\gamma-1} && \text{for } M_X \geq \mu\ , \\ f(M_X; \alpha, \beta, \gamma, \mu) = &\quad 0 && \text{for } M_X \leq \mu\ , \end{aligned} \tag{A.3}$$

Frechet distribution:

$$\begin{aligned} f(M_X;\alpha,\beta,\mu) = &\quad \frac{\alpha}{\beta} e^{-\left(\frac{(M_X-\mu)}{\beta}\right)^{-\alpha}} \left(\frac{M_X-\mu}{\beta}\right)^{-\alpha-1} && \text{for } M_X \geq \mu\ , \\ f(M_X;\alpha,\beta,\mu) = &\quad 0 && \text{for } M_X \leq \mu\ , \end{aligned} \tag{A.4}$$

GaussExp function:

A Gaussian with an exponential tail:

$$\begin{aligned} f(M_X;\mu,\sigma,k) = &\quad e^{-\frac{(M_X-\mu)^2}{2\sigma^2}} && \text{for } \frac{M_X-\mu}{\sigma} \leq k\ , \\ f(M_X;\mu,\sigma,k) = &\quad e^{\frac{k^2}{2}-\frac{k(M_X-\mu)}{\sigma}} && \text{for } \frac{M_X-\mu}{\sigma} > k\ . \end{aligned} \tag{A.5}$$

Landau Distribution

$$f(M_X;\mu,\sigma) = \int_0^\infty \sin(2t) e^{-t\frac{(M_X-\mu)}{\sigma} - \frac{2t}{\pi}\log(t)} dt \tag{A.6}$$

Appendix B

Statistical treatment

For the statistical treatment of the data, we follow the prescriptions presented in [136] for likelihood-base statistical tests. In this appendix we describe of the main methods and formulas described in [136], which we have used to compute the likelihoods, significances and upper limits throughout this thesis.

Given an experimental observation or a Monte Carlo experiment, we can assign a statistical significance to the observed data set with respect to a given hypothesis by means of its p-value, which is usually expressed as its equivalent Gaussian significance Z (the famous 'sigmas'). This p-value, in a test-statistics framework, measures the level of agreement of the data set with a given hypothesis $\mathcal{H}$. For instance, for discovering a new signal, we define the 'background-only hypothesis' $\mathcal{H}_0$ as the hypothesis "data is distributed according to the SM predictions". If for a given data set $\mathcal{D}$ we obtain a very small p-value, the interpretation is that the hypothesis $\mathcal{H}_0$ is incompatible with the data, hence effectively leading to a discovery of a new signal. The standard $Z = 5\sigma$ convention for discovery corresponds to $p = 2.87 \times 10^{-7}$, for which the background hypothesis $\mathcal{H}_0$ is rejected.

How do we compute such p-value for a given sample? It is a common practice in particle physics to establish discovery or to set upper limits from a given data set using a *likelihood ratio* as a test statistics to then compute the p-value.

The idea is the following: suppose that we have a data set $\mathcal{D}$, which we can represent in a histogram $\mathbf{n} = (n_1, \ldots, n_N)$ of a certain variable x. Then, according to the statistical model that we want to test (the null hypothesis), the expected number of events in the i-th bin is given by:

$$E[\text{bin}_i] = s_i(\sigma_s) + b_i, \tag{B.1}$$

where s_i and b_i denote the mean number of events in the i-th bin from the signal

and background respectively, and are given by:

$$s_i(\sigma_s) = L \cdot (\epsilon \cdot A)_s \cdot \sigma_s \int_{\text{bin } i} f_s(x; \boldsymbol{\theta}_s) dx, \tag{B.2}$$

$$b_i = L \cdot (\epsilon \cdot A)_b \cdot \sigma_b \int_{\text{bin } i} f_b(x; \boldsymbol{\theta}_b) dx. \tag{B.3}$$

Here, L is the luminosity, $(\epsilon \cdot A)_{s,b}$ the efficiency times acceptance, $\sigma_{s,b}$ the cross sections of the signal and the SM expected background, $f_s(x; \boldsymbol{\theta}_s)$ and $f_b(x; \boldsymbol{\theta}_b)$ are the probability density functions (pdfs) of the variable x for the signal and the background events, and $\boldsymbol{\theta}_s$ and $\boldsymbol{\theta}_b$ are the vector of parameters that characterize the shape of the pdfs. The background-only hypothesis corresponds to the case where the signal cross section is equal to zero, $\sigma_s = 0$. Neglecting the nuisance parameters, the probability of finding n_i events in the i-th bin, for which we expect k events according to B.1, is given by the poissonian distribution:

$$P(k \text{ events in bin}_i) = \frac{k^{n_i}}{n_i!} e^{-k}. \tag{B.4}$$

The likelihood function for the sample $\mathcal{D}$ is thus defined as the product of the Poisson probabilities for all bins:

$$L(\sigma_s) = \prod_{j=1}^{N} \frac{(s_j(\sigma_s) + b_j)^{n_j}}{n_j!} e^{-(s_j(\sigma_s)+b_j)}. \tag{B.5}$$

To test a hypothesised value of σ_s we consider the *profile likelihood ratio*:

$$\lambda(\sigma_s) = \frac{L(\sigma_s)}{L(\hat{\sigma}_s)} \tag{B.6}$$

where $\hat{\sigma}_s$ is the value of σ_s that maximizes the likelihood function, i.e. $\hat{\sigma}_s$ is the maximum likelihood estimator. Following the definition B.6, we see that $0 \leq \lambda \leq 1$. Thus, when λ is close to one there is a good agreement between the data and the hypothesised value σ_s. It is convenient though to define

$$t_{\sigma_s} = -2 \ln \lambda(\sigma_s) \tag{B.7}$$

which has a domain $[0, \infty)$. From this definition it follows that higher values of t_μ correspond to increasing incompatibility between the data and the value σ_s. We can adapt the previous definition to the assumption that any signal present in the sample can only increase the mean event rate beyond what is expected from the background alone;

$$q_{\sigma_s} = \begin{cases} -2 \ln \dfrac{L(\sigma_s)}{L(\hat{\sigma}_s)} & \hat{\sigma}_s \geq 0 \\ 0 & \hat{\sigma}_s < 0 \end{cases}. \tag{B.8}$$

Indeed, here we are considering that an observed value for $\hat{\sigma}_s$ below zero corresponds to a fluctuation of the background, and one has $t_0 = 0$. This is the statistic commonly used for discovery and upper limits.

We now use the statistic t_{σ_s} to define a test of a hypothesised value σ_s versus the data $\mathcal{D}$. The level of disagreement between the hypothesised σ_s and $\mathcal{D}$ is quantified by the p-value given by:

$$p_{\sigma_s} = \int_{t_{\sigma_s,\text{obs}}}^{\infty} f\left(t_{\sigma_s}|\sigma_s\right) dt_{\sigma_s}, \tag{B.9}$$

where $t_{\sigma_s,\text{obs}}$ is the observed value of the statistic t_{σ_s} from the sample $\mathcal{D}$ (the observed value of σ_s being $\hat{\sigma}_s$), and $f\left(t_{\sigma_s}|\sigma_s\right)$ is the probability density function of t_{σ_s} under the assumption of a signal cross section σ_s. The p-value is thus telling us the probability of finding a level of disagreement (between the hypothesised value σ_s and the data $\mathcal{D}$) as or more extreme than the actual observed value $t_{\sigma_s,\text{obs}}$. A very small value for p_{σ_s} indicates that it is very unlikely that given $\mathcal{D}$, the hypothesis of a signal σ_s is true, whereas a value close to one should be interpreted as a good agreement between the data and the hypothesis. Since the statistic t_{σ_s} is used to define the test, we call it a *test statistics*.

We need now a way to estimate the distribution of the statistic t_{σ_s}, $f\left(t_{\sigma_s}|\sigma_s\right)$. In the following we aim at giving an intuitive derivation of the final formulas instead of a full mathematical analysis, for which we refer to [136].

Suppose that we have a data sample $\mathcal{D}$ of size N distributed following a 'true' value σ'_s (that could be zero for instance in case of the complete absence of signal), for which we observe a value $\hat{\sigma}_s$. Then, if we were to make a large number of identical independent experiments obtaining $\mathcal{D}_1, \mathcal{D}_2, \ldots$, it is expected that the observed values $\hat{\sigma}_s^i$ follow a Gaussian distribution with mean at the true value σ'_s and a certain standard deviation σ. It was shown by Wald [151] that, under the assumption that $\hat{\sigma}_s$ is normally distributed and that the data sample N is large enough, the statistic t_{σ_s} follows a *noncentral chi-square* distribution for one degree of freedom:

$$f(t_{\sigma_s}|\sigma'_s) = \frac{1}{2\sqrt{t_{\sigma_s}}} \frac{1}{\sqrt{2\pi}} \left[\exp\left(-\frac{1}{2} \left(\sqrt{t_{\sigma_s}} + \frac{\sigma_s - \sigma'_s}{\sigma} \right)^2 \right) + \exp\left(-\frac{1}{2} \left(\sqrt{t_{\sigma_s}} - \frac{\sigma_s - \sigma'_s}{\sigma} \right)^2 \right) \right] \tag{B.10}$$

This expression can be further simplified for the particular cases where we want either to test a discovery or to set upper limits. For the special case of testing the background-only hypothesis ($\sigma_s = 0$), it can be shown that the expression B.10 for the pdf of q_{σ_s} reduces to:

$$f(q_0|0) = \frac{1}{2}\delta(q_0) + \frac{1}{2}\frac{1}{\sqrt{2\pi}}\frac{1}{\sqrt{q_0}}e^{-q_0/2}, \tag{B.11}$$

and its correspondent cumulative distribution function (cdf) is found to be

$$F(q_0|0) = \Phi(\sqrt{q_0}). \tag{B.12}$$

where Φ is the cdf of a standard Gaussian distribution (with zero mean and unit variance). Therefore, according to expression B.9, the p-value for the hypothesis $\sigma_s = 0$ is simply

$$p_0 = 1 - F(q_0|0). \tag{B.13}$$

Finally, we can translate this p-value to a gaussian significance by using Φ^{-1}, the inverse cumulative distribution function (inverse CDF) of the normal distribution with mean 0 and variance equal to one. We obtain

$$Z_0 = \Phi^{-1}(1 - p_0) = \sqrt{q_0}. \tag{B.14}$$

The case of setting upper limits will be reviewed in the next section.

Cut-and-count versus shape-based analysis

Consider an experiment where we measure n events, which are assumed to follow a Poisson distribution. The model at test predicts $E[n] = \mu s + b$ events, where s is the mean number of signal events from the model, b is the expected number of background events (assumed to be known with negligible uncertainty) and μ is a signal strength parameter. The likelihood function for μ is given by:

$$L(\mu) = \frac{(\mu s + b)^n}{n!} e^{-(\mu s + b)}, \tag{B.15}$$

and the maximum likelihood estimator $\hat{\mu}$ is simply

$$\hat{\mu} = (n - b)/s. \tag{B.16}$$

With the expressions B.15 and B.16 we can compute the test statistic t_μ for any value of the signal strength μ, and then the significance $Z = \sqrt{t_\mu}$. For the particular case of the test statistic for discovery ($\mu = 0$), we have

$$q_0 = \begin{cases} -2 \ln \dfrac{L(0)}{L(\hat{\mu})} & \hat{\mu} \geq 0 \\ 0 & \hat{\mu} < 0 \end{cases}. \tag{B.17}$$

Finally, we can use expression B.14 to compute the significance of the observation.

Recall that the expression for the likelihood consists in one single Poissonian distribution, since the analysis could be regarded as a single-binned histogram study. This is the case for instance when we want to test a signal at a particular

mass in an invariant mass histogram. One takes the histogram and literally cut on the interested mass region and count the number of events falling within the range of interest, to then compute the significance of the statistical test.

On the other hand, we can also consider the case where we search for a peak somewhere in an invariant mass histogram. The position of the peak is not known a priori, and then all masses in a given range are tested, i.e. we consider all bins in the range. Neglecting the nuisance parameters and assuming that the background is known with negligible uncertainty, the likelihood function is then given by expression B.5, and from it one can compute the test statistic either for discovery or for setting upper limits. Such analysis is known as *shape-based* analysis, as opposed to the previous *cut-and-count* approach. We finish this section by pointing out that, unlike the case where we know the mass of the signal that we are looking for, in a shape-based analysis one has to take into account the fact that a background fluctuation can occur at any mass within the search range. This effect is known as the "*look-elsewhere effect*", which we do not discuss here, but instead refer the reader to [152] for a detailed presentation.

B.1 Expected discovery sensitivities, $X^{5\sigma}$

In our case we are not interested in computing the significance of an experimental sample, but rather estimate which cross section for a given process would be able to reject the background-only hypothesis, i.e. to have a 5σ significance against the hypothesis $\sigma_s = 0$. We will approach this aim by means of MC methods to simulate background and signal samples.

However, recall that if we want to characterize the sensitivity of an experiment it is not enough to use directly events from a single MC experiment to compute a significance. Indeed, one single sample features statistical fluctuations in such a way that the results for a sensitivity may fluctuate depending on the size of the samples that we use. Instead, we are interested in computing the median discovery significance (also called expected significance), that is, the median significance that we would obtain if we run a very large number of Monte Carlo experiments.

For obtaining the median significance we use analytical fits of the MC samples. After having obtained a large sample of MC events, we fit the distributions for the variable x that we are interested in (usually an invariant mass) to an analytical smooth function $f(x, \boldsymbol{\theta})$. Then, it is assumed that the true expected number of

events for both the signal and the background are given by these functions[1];

$$E[s_i(\sigma_s)] = s_{\rm tot}(\sigma_s)\int_{{\rm bin}_i} f_s^{\rm fit}(x;\boldsymbol{\theta}_s)dx, \tag{B.18}$$

$$E[b_i(\sigma_s)] = b_{\rm tot}\int_{{\rm bin}_i} f_b^{\rm fit}(x;\boldsymbol{\theta_b})dx \tag{B.19}$$

where $b_{\rm tot}$ and $s_{\rm tot}$ are the total number of expected background and signal events, $f_{b,s}^{\rm fit}$ denote the fitted probability density functions and $\boldsymbol{\theta}_b$ and $\boldsymbol{\theta}_s$ are the vector of parameters characterizing such distributions. The total number of expected events of both background and signal depend of course on the luminosity, their cross sections, and also on their acceptance times efficiency for the analysis,

$$s_{\rm tot} = L\cdot\sigma_s\cdot E[(A\cdot\epsilon)_s] \tag{B.20}$$

$$b_{\rm tot} = L\cdot\sigma_b\cdot E[(A\cdot\epsilon)_b]. \tag{B.21}$$

For computing the median value for the acceptance times efficiency, ideally we would run many MC and compute them for each such experiment,

$$(A\cdot\epsilon)_{s,b} = \frac{N_{s,b}^{\rm an}}{N_{s,b}^{\rm gen}}, \tag{B.22}$$

with $N^{\rm gen}$ and $N^{\rm an}$ the number of generated events and the number of remaining events after the analysis, respectively. Then, we could obtain the gaussian mean for the resulting $(A\cdot\epsilon)_{s,b}$ distribution. However, we found sufficient to take the value obtained using the total number of simulated events, since the statistical errors for the computation of $(A\cdot\epsilon)_{s,b}$ are in practically all cases $\sim 1\%$. The background cross section is fixed to its computed value (using the best available theoretical predictions), whereas the signal cross section σ_s is precisely the value that we want to obtain from the condition of rejecting the background-only hypothesis at 5σ.

The MC experiment then consists in an 'observation' where we have a background plus an injected signal with a cross section σ_s' (which is not fixed), to be tested versus the background-only hypothesis $\sigma_s = 0$. The likelihood function is computed using the expected values B.18 and B.19,

$$L(\sigma_s = 0;\sigma_s') = \prod_{j=1}^{N}\frac{b_j^{s_j(\sigma_s')+b_j}}{(s_j(\sigma_s')+b_j)\,!}e^{-b_j}, \tag{B.23}$$

where in $L(\sigma_s;\sigma_s')$ the variable σ_s is the hypothesised signal at test and σ_s' indicates the numerical dependence on the injected signal. Clearly, the maximum likelihood

[1]More generally, we define the statistical model by the fitted functions, and we assume that the estimators for all parameters from the fitted functions give us the true parameter values.

estimator for L is precisely the value of injected signal, $\hat{\sigma}_s = \sigma'_s$. The test statistic for discovery is thus:

$$t_{0,\text{fit}} = -2 \ln \frac{L(0; \sigma'_s)}{L(\sigma'_s; \sigma'_s)} \tag{B.24}$$

where the subscript "fit" remarks the fact that we are using the fits for the evaluation of B.24. Given the expression for the likelihood and the test statistic, we can then compute the median sensitivity for a certain value of the signal cross section σ'_s from expression B.14:

$$\text{med}[Z_0|\sigma'_s] = \sqrt{t_{0,\text{fit}}}. \tag{B.25}$$

Finally, we can use this expression to numerically solve σ'_s for $\text{med}[Z_0|\sigma'_s] = 5$. The solution hence should be interpreted as the expected discovery signal cross section, $X^{5\sigma}$.

B.2 Upper limits

Given a measurement compatible with the background-only hypothesis, it is of common use to compute the the so-called exclusion limits for a signal model. The exclusion limits (or upper limits) correspond to the maximum value of the signal cross section that can not be rejected by the observation. For purposes of setting these upper limits, we consider that a signal hypothesis σ_s featuring a p-value (from eq. B.9) below a certain threshold $p_{\sigma_s} = \alpha$ is rejected given the observation compatible with $\sigma'_s = 0$. The value for σ_s such that $p_{\sigma_s} = \alpha$ is said to be excluded at a Confidence Level (CL) of $(1 - \alpha)$. In the particle physics community, the threshold for exclusion is set to $\alpha = 0.05$, implying that signal cross sections leading to a p-value smaller than 0.05 are excluded at 95% CL.

The distribution of test statistics t_{σ_s} under the hypothesis of a signal σ'_s, given in eq. (B.10), also reduces to a simpler expression for computing upper limits. Indeed, assuming that the observed data is distributed according to a 'true' value $\sigma'_s = \sigma_s$, the distribution for the test statistic q_{σ_s} is given by:

$$f(q_{\sigma_s}|\sigma_s) = \frac{1}{2}\delta(q_{\sigma_s}) + \frac{1}{2}\frac{1}{\sqrt{2\pi}}\frac{1}{\sqrt{q_{\sigma_s}}}e^{-q_{\sigma_s}/2}. \tag{B.26}$$

The corresponding cdf is thus the same as we found for q_0, namely

$$F(q_{\sigma_s}|\sigma_s) = \Phi(\sqrt{q_{\sigma_s}}), \tag{B.27}$$

the p-value for the hypothesis $\sigma_s = 0$ is simply

$$p_{\sigma_s} = 1 - F(q_{\sigma_s}|\sigma_s), \tag{B.28}$$

and finally, the equivalent gaussian significance is

$$Z_{\sigma_s} = \Phi^{-1}(1 - p_{\sigma_s}) = \sqrt{q_{\sigma_s}}. \tag{B.29}$$

The standard p-value threshold of 0.05 for the 95% CL thus corresponds to a significance $Z = \Phi^{-1}(1 - 0.05) = 1.64$.

For the case of our MC experiments, using the fitted functions from the MC samples for the signal and the background we can find the median, assuming some signal cross section σ_s', of the significance for rejecting a hypothesized value σ_s. We can then ask the question: What are the expected upper limits for our signal model assuming that, at a given luminosity L, we measure a sample compatible with the background-only hypothesis $\sigma_s' = 0$? Thus, the expected upper limit for σ_s in our MC set is obtained as the value of the signal cross section such that is rejected at 95% CL by a sample obtained taking $\sigma_s' = 0$. Recall that in a real experiment, the 'real' value for σ_s' (the actual signal cross section present in nature) might not be strictly zero but any sufficiently small value which is compatible with the background-only hypothesis in the framework of such experiment. The fact that we take $\sigma_s' = 0$ can thus be regarded as an approximation in case of the existence of a signal .

More explicitly, in the case of a shape-based analysis of a histogram with N bins of a certain variable of interest x, we construct the likelihood function as:

$$L(\sigma_s; \sigma_s' = 0) = \prod_{j=1}^{N} \frac{(s_j(\sigma_s) + b_j)^{b_j}}{b_j!} e^{-(s_j(\sigma_s)+b_j)}. \tag{B.30}$$

where s_i and b_i are given by B.18 and B.19. From this we obtain the test statistic

$$q_{\sigma_s,\text{fit}} = -2 \ln \frac{L(\sigma_s; 0)}{L(0; 0)}. \tag{B.31}$$

Using the approximations given above, we obtain the significance for the signal hypothesis σ_s by simply taking the square root of B.31. Finally, the expected (median) 95% CL upper limit could be obtained by solving numerically σ_s^{up} for

$$\text{med}[Z_{(q_{\sigma_{s,\text{fit}}^{\text{up}}}, 0]} = \sqrt{q_{\sigma_{s,\text{fit}}^{\text{up}}}} = 1.64 \tag{B.32}$$

B.2.1 Error bands

We have explained how to obtain expected upper limits for a given process by means of MC experiments: First, we used the fits to obtain the median significance, for any signal σ_s', for rejecting the hypothesis $\sigma_s = 0$. Then we computed the value σ_s^{up} such that the median significance is $Z(0|\sigma_s^{\text{up}}) = 1.64$, corresponding

to a exclusion at 95% CL. The actual data in a real experiment, however, will contain statistical fluctuations and thus the observed value of the significance will not be in general equal to the median value. These variations can be predicted, allowing us to define *error bands* for the median significance, corresponding to the $\pm N\sigma$ variations around the expected upper limit $\sigma_s^{\rm up}$. Intuitively, this could be thought of in the following way: Imagine that we compute the upper limits $\sigma_{s,1}^{\rm up}$ as we explained above using a MC sample $\mathcal{D}_1$. If we repeat the experiment using different samples $\mathcal{D}_{i=2,\cdots}$ we may obtain different results for $\sigma_{s,i}^{\rm up}$. At the end of the day, it is expected that $\sigma_{s,i}^{\rm up}$ follows some distribution with median value at $\sigma_s^{\rm up}$.

For our case, $\sigma_s^{\rm up}$ is the upper limit computed using the fitted functions. The 1 and 2 sigma values departing from the median value are obtained by varying ± 1 and ± 2 standard deviations the number of expected background events in each bin, b_i, assuming that the events are distributed following a Poisson distribution. To these statistical uncertainties, we add linearly (to be conservative) the estimated systematic uncertainties described in chapter 5.

Bibliography

[1] Georges Aad et al. Observation of a new particle in the search for the Standard Model Higgs boson with the ATLAS detector at the LHC. *Phys. Lett.*, B716:1–29, 2012, 1207.7214.

[2] Serguei Chatrchyan et al. Observation of a new boson at a mass of 125 GeV with the CMS experiment at the LHC. *Phys. Lett.*, B716:30–61, 2012, 1207.7235.

[3] G. Hinshaw *et al.* [WMAP Collaboration], "Nine-Year Wilkinson Microwave Anisotropy Probe (WMAP) Observations: Cosmological Parameter Results," Astrophys. J. Suppl. **208** (2013) 19 [arXiv:1212.5226 [astro-ph.CO]].

[4] P. A. R. Ade *et al.* [Planck Collaboration], "Planck 2013 results. XVI. Cosmological parameters," arXiv:1303.5076 [astro-ph.CO].

[5] Benoit Famaey and Stacy McGaugh. Modified Newtonian Dynamics (MOND): Observational Phenomenology and Relativistic Extensions. *Living Rev. Rel.*, 15:10, 2012, 1112.3960.

[6] M. C. Gonzalez-Garcia and M. Maltoni. Phenomenology with massive neutrinos. *physrep*, 460:1–129, April 2008, 0704.1800.

[7] B. Pontecorvo. Neutrino Experiments and the Problem of Conservation of Leptonic Charge. *Soviet Journal of Experimental and Theoretical Physics*, 26:984, May 1968.

[8] Savas Dimopoulos and David W. Sutter. The Supersymmetric flavor problem. *Nucl. Phys.*, B452:496–512, 1995, hep-ph/9504415.

[9] Stephen P. Martin. A Supersymmetry primer. 1997, hep-ph/9709356. [Adv. Ser. Direct. High Energy Phys.18,1(1998)].

[10] S. Schael et al. Search for neutral MSSM Higgs bosons at LEP. *Eur. Phys. J.*, C47:547–587, 2006, hep-ex/0602042.

[11] Abdelhak Djouadi. The Anatomy of electro-weak symmetry breaking. II. The Higgs bosons in the minimal supersymmetric model. *Phys. Rept.*, 459:1–241, 2008, hep-ph/0503173.

[12] Emanuele Bagnaschi, Gian F. Giudice, Pietro Slavich, and Alessandro Strumia. Higgs Mass and Unnatural Supersymmetry. *JHEP*, 09:092, 2014, 1407.4081.

[13] Graham G. Ross, Kai Schmidt-Hoberg, and Florian Staub. Revisiting fine-tuning in the MSSM. *JHEP*, 03:021, 2017, 1701.03480.

[14] Jihn E. Kim and H.P. Nilles. The μ-problem and the strong cp-problem. *Physics Letters B*, 138(1):150 – 154, 1984.

[15] G. F. Giudice and A. Masiero. A natural solution to the μ-problem in supergravity theories. *Physics Letters B*, 206:480–484, May 1988.

[16] U. Ellwanger, C. Hugonie and A. M. Teixeira, "The Next-to-Minimal Supersymmetric Standard Model," Phys. Rept. **496** (2010) 1 [arXiv:0910.1785 [hep-ph]].

[17] Lepsusywg, aleph, delphi, l3 and opal experiments, note lepsusywg/01-03.1.

[18] Marcela Carena, Howard E. Haber, Ian Low, Nausheen R. Shah, and Carlos E. M. Wagner. Alignment limit of the NMSSM Higgs sector. *Phys. Rev.*, D93(3):035013, 2016, 1510.09137.

[19] L. J. Hall, D. Pinner and J. T. Ruderman, "A Natural SUSY Higgs Near 126 GeV," JHEP **1204** (2012) 131 [arXiv:1112.2703 [hep-ph]].

[20] H. Baer, V. Barger and A. Mustafayev, "Implications of a 125 GeV Higgs scalar for LHC SUSY and neutralino dark matter searches," Phys. Rev. D **85** (2012) 075010 [arXiv:1112.3017 [hep-ph]].

[21] S. Heinemeyer, O. Stal and G. Weiglein, "Interpreting the LHC Higgs Search Results in the MSSM," Phys. Lett. B **710** (2014) 201 [arXiv:1112.3026 [hep-ph]].

[22] A. Arbey, M. Battaglia, A. Djouadi, F. Mahmoudi and J. Quevillon, "Implications of a 125 GeV Higgs for supersymmetric models," Phys. Lett. B **708** (2012) 162 [arXiv:1112.3028 [hep-ph]].

[23] P. Draper, P. Meade, M. Reece and D. Shih, "Implications of a 125 GeV Higgs for the MSSM and Low-Scale SUSY Breaking," Phys. Rev. D **85** (2012) 095007 [arXiv:1112.3068 [hep-ph]].

[24] M. Carena, S. Gori, N. R. Shah and C. E. M. Wagner, "A 125 GeV SM-like Higgs in the MSSM and the $\gamma\gamma$ rate," JHEP **1203** (2012) 014 [arXiv:1112.3336 [hep-ph]].

[25] O. Buchmueller *et al.*, "Higgs and Supersymmetry," Eur. Phys. J. C **72** (2012) 2020 [arXiv:1112.3564 [hep-ph]].

[26] A. Arvanitaki and G. Villadoro, "A Non Standard Model Higgs at the LHC as a Sign of Naturalness," JHEP **1202** (2012) 144 [arXiv:1112.4835 [hep-ph]].

[27] M. Papucci, J. T. Ruderman and A. Weiler, "Natural SUSY Endures," JHEP **1209** (2012) 035 [arXiv:1110.6926 [hep-ph]].

[28] P. H. Chankowski, J. R. Ellis and S. Pokorski, "The fine-tuning price of LEP," Phys. Lett. B **423** (1998) 327 [arXiv:hep-ph/9712234].

[29] R. Barbieri and A. Strumia, "About the fine tuning price of LEP," Phys. Lett. B **433** (1998) 63 [arXiv:hep-ph/9801353].

[30] G. L. Kane and S. F. King, "Naturalness implications of LEP results," Phys. Lett. B **451** (1999) 113 [arXiv:hep-ph/9810374].

[31] L. Giusti, A. Romanino and A. Strumia, "Natural ranges of supersymmetric signals," Nucl. Phys. B **550** (1999) 3 [arXiv:hep-ph/9811386].

[32] R. Barbieri, L. J. Hall, Y. Nomura and V. S. Rychkov, "Supersymmetry without a Light Higgs Boson," Phys. Rev. D **75** (2007) 035007 [hep-ph/0607332].

[33] R. Barbieri, D. Buttazzo, K. Kannike, F. Sala and A. Tesi, "Exploring the Higgs sector of a most natural NMSSM," Phys. Rev. D **87** (2013) 11, 115018 [arXiv:1304.3670 [hep-ph]].

[34] A. Delgado, C. Kolda, J. P. Olson and A. de la Puente, "Solving the Little Hierarchy Problem with a Singlet and Explicit μ Terms," Phys. Rev. Lett. **105** (2010) 091802 [arXiv:1005.1282 [hep-ph]].

[35] U. Ellwanger, G. Espitalier-Noel and C. Hugonie, "Naturalness and Fine Tuning in the NMSSM: Implications of Early LHC Results," JHEP **1109** (2011) 105
[arXiv:1107.2472 [hep-ph]].

[36] V. Barger, P. Langacker, H. S. Lee and G. Shaughnessy, "Higgs Sector in Extensions of the MSSM," Phys. Rev. D **73** (2006) 115010 [hep-ph/0603247].

[37] U. Ellwanger and C. Hugonie, "The Upper bound on the lightest Higgs mass in the NMSSM revisited," Mod. Phys. Lett. A **22** (2007) 1581 [hep-ph/0612133].

[38] R. Dermisek and J. F. Gunion, "A Comparison of Mixed-Higgs Scenarios In the NMSSM and the MSSM," Phys. Rev. D **77** (2008) 015013 [arXiv:0709.2269 [hep-ph]].

[39] R. Barbieri, L. J. Hall, A. Y. Papaioannou, D. Pappadopulo and V. S. Rychkov, "An Alternative NMSSM phenomenology with manifest perturbative unification," JHEP **0803** (2008) 005 [arXiv:0712.2903 [hep-ph]].

[40] Z. Kang, J. Li and T. Li, "On Naturalness of the MSSM and NMSSM," JHEP **1211** (2012) 024 [arXiv:1201.5305 [hep-ph]].

[41] J. J. Cao, Z. X. Heng, J. M. Yang, Y. M. Zhang and J. Y. Zhu, "A SM-like Higgs near 125 GeV in low energy SUSY: a comparative study for MSSM and NMSSM," JHEP **1203** (2012) 086 [arXiv:1202.5821 [hep-ph]].

[42] K. S. Jeong, Y. Shoji and M. Yamaguchi, "Singlet-Doublet Higgs Mixing and Its Implications on the Higgs mass in the PQ-NMSSM," JHEP **1209** (2012) 007 [arXiv:1205.2486 [hep-ph]].

[43] K. Agashe, Y. Cui and R. Franceschini, "Natural Islands for a 125 GeV Higgs in the scale-invariant NMSSM," JHEP **1302** (2013) 031 [arXiv:1209.2115 [hep-ph]].

[44] K. Choi, S. H. Im, K. S. Jeong and M. Yamaguchi, "Higgs mixing and diphoton rate enhancement in NMSSM models," JHEP **1302** (2013) 090 [arXiv:1211.0875 [hep-ph]].

[45] K. Kowalska, S. Munir, L. Roszkowski, E. M. Sessolo, S. Trojanowski and Y. L. S. Tsai, "Constrained next-to-minimal supersymmetric standard model with a 126 GeV Higgs boson: A global analysis," Phys. Rev. D **87** (2013) 115010 [arXiv:1211.1693 [hep-ph]].

[46] S. F. King, M. Mühlleitner, R. Nevzorov and K. Walz, "Natural NMSSM Higgs Bosons," Nucl. Phys. B **870** (2013) 323 [arXiv:1211.5074 [hep-ph]].

[47] N. D. Christensen, T. Han, Z. Liu and S. Su, "Low-Mass Higgs Bosons in the NMSSM and Their LHC Implications," JHEP **1308** (2013) 019 [arXiv:1303.2113 [hep-ph]].

[48] T. Cheng, J. Li, T. Li and Q. S. Yan, "Natural NMSSM confronting with the LHC7-8," Phys. Rev. D **89** (2014) 1, 015015 [arXiv:1304.3182 [hep-ph]].

[49] M. Badziak, M. Olechowski and S. Pokorski, "New Regions in the NMSSM with a 125 GeV Higgs," JHEP **1306** (2013) 043 [arXiv:1304.5437 [hep-ph]].

[50] C. Beskidt, W. de Boer and D. I. Kazakov, "A comparison of the Higgs sectors of the CMSSM and NMSSM for a 126 GeV Higgs boson," Phys. Lett. B **726** (2013) 758
[arXiv:1308.1333 [hep-ph]].

[51] K. Choi, S. H. Im, K. S. Jeong and M. S. Seo, "Higgs phenomenology in the Peccei-Quinn invariant NMSSM," JHEP **1401** (2014) 072 [arXiv:1308.4447 [hep-ph]].

[52] J. Cao, F. Ding, C. Han, J. M. Yang and J. Zhu, "A light Higgs scalar in the NMSSM confronted with the latest LHC Higgs data," JHEP **1311** (2013) 018 [arXiv:1309.4939 [hep-ph]].

[53] G. Cacciapaglia, A. Deandrea, G. D. La Rochelle and J. B. Flament, "Searching for a lighter Higgs boson: Parametrization and sample tests," Phys. Rev. D **91** (2015) 1, 015012 [arXiv:1311.5132 [hep-ph]].

[54] C. Englert, A. Freitas, M. M. Mühlleitner, T. Plehn, M. Rauch, M. Spira and K. Walz, "Precision Measurements of Higgs Couplings: Implications for New Physics Scales," J. Phys. G **41** (2014) 113001 [arXiv:1403.7191 [hep-ph]].

[55] U. Ellwanger and C. Hugonie, "The semi-constrained NMSSM satisfying bounds from the LHC, LUX and Planck," JHEP **1408** (2014) 046 [arXiv:1405.6647 [hep-ph]].

[56] M. Badziak, M. Olechowski and S. Pokorski, "Experimental signatures of a light singlet-like scalar in NMSSM," arXiv:1406.1492 [hep-ph].

[57] K. S. Jeong, Y. Shoji and M. Yamaguchi, "Higgs Mixing in the NMSSM and Light Higgsinos," JHEP **1411** (2014) 148 [arXiv:1407.0955 [hep-ph]].

[58] S. F. King, M. Mühlleitner, R. Nevzorov and K. Walz, "Discovery Prospects for NMSSM Higgs Bosons at the High-Energy Large Hadron Collider," Phys. Rev. D **90** (2014) no.9, 095014 doi:10.1103/PhysRevD.90.095014 [arXiv:1408.1120 [hep-ph]].

[59] B. Allanach, M. Badziak, C. Hugonie and R. Ziegler, "Light Sparticles from a Light Singlet in Gauge Mediation," Phys. Rev. D **92** (2015) 1, 015006 [arXiv:1502.05836 [hep-ph]].

[60] D. Buttazzo, F. Sala and A. Tesi, "Singlet-like Higgs bosons at present and future colliders," arXiv:1505.05488 [hep-ph].

[61] M. Guchait and J. Kumar, "Light Higgs Bosons in NMSSM at the LHC," arXiv:1509.02452 [hep-ph].

[62] F. Domingo and G. Weiglein, "NMSSM interpretations of the observed Higgs signal," arXiv:1509.07283 [hep-ph].

[63] The ATLAS and CMS Collaborations, "Measurements of the Higgs boson production and decay rates and constraints on its couplings from a combined ATLAS and CMS analysis of the LHC pp collision data at $\sqrt{s} = 7$ and 8 TeV," ATLAS-CONF-2015-044, CMS-PAS-HIG-15-002.

[64] Combined measurements of Higgs boson production and decay in the $H \to ZZ^* \to 4\ell$ and $H \to \gamma\gamma$ channels using $\sqrt{s} = 13$ TeV pp collision data collected with the ATLAS experiment. Technical Report ATLAS-CONF-2017-047, CERN, Geneva, Jul 2017.

[65] Measurements of properties of the Higgs boson in the diphoton decay channel with the full 2016 data set. Technical Report CMS-PAS-HIG-16-040, CERN, Geneva, 2017.

[66] Measurements of properties of the Higgs boson decaying into four leptons in pp collisions at sqrts = 13 TeV. Technical Report CMS-PAS-HIG-16-041, CERN, Geneva, 2017.

[67] [ATLAS Collaboration], ATL-PHYS-PUB-2013-014, "Projections for measurements of Higgs boson cross sections, branching ratios and coupling parameters with the ATLAS detector at a HL-LHC"

[68] [CMS Collaboration], "Projected Performance of an Upgraded CMS Detector at the LHC and HL-LHC: Contribution to the Snowmass Process," arXiv:1307.7135.

[69] G. Aad *et al.* [ATLAS Collaboration], "Search for Scalar Diphoton Resonances in the Mass Range $65 - 600$ GeV with the ATLAS Detector in pp Collision Data at $\sqrt{s} = 8\ TeV$," Phys. Rev. Lett. **113** (2014) 17, 171801 [arXiv:1407.6583 [hep-ex]].

[70] CMS collaboration, HIG-14-037

[71] S. Moretti and S. Munir, "Di-photon Higgs signals at the LHC in the next-to-minimal supersymmetric standard model," Eur. Phys. J. C **47** (2006) 791 [hep-ph/0603085].

[72] U. Ellwanger, "Enhanced di-photon Higgs signal in the Next-to-Minimal Supersymmetric Standard Model," Phys. Lett. B **698** (2011) 293 [arXiv:1012.1201 [hep-ph]].

[73] J. Cao, Z. Heng, T. Liu and J. M. Yang, "Di-photon Higgs signal at the LHC: A comparative study in different supersymmetric models," Phys. Lett. B **703** (2014) 462 [arXiv:1103.0631 [hep-ph]].

[74] R. Benbrik, M. Gomez Bock, S. Heinemeyer, O. Stal, G. Weiglein and L. Zeune, "Confronting the MSSM and the NMSSM with the Discovery of a Signal in the two Photon Channel at the LHC," Eur. Phys. J. C **72** (2012) 2171 [arXiv:1207.1096 [hep-ph]].

[75] Z. Heng, "A 125 GeV Higgs and its di-photon signal in different SUSY models: a mini review," Adv. High Energy Phys. **2012** (2012) 312719 [arXiv:1210.3751 [hep-ph]].

[76] J. W. Fan *et al.*, "Study of diphoton decays of the lightest scalar Higgs boson in the Next-to-Minimal Supersymmetric Standard Model," Chin. Phys. C **38** (2014) 073101 [arXiv:1309.6394 [hep-ph]].

[77] J. Bernon, B. Dumont and S. Kraml, "Status of Higgs couplings after run 1 of the LHC," Phys. Rev. D **90** (2014) 071301 [arXiv:1409.1588 [hep-ph]].

[78] O. Stal, G. Weiglein and L. Zeune, "Improved prediction for the mass of the W boson in the NMSSM," JHEP **1509** (2015) 158 [arXiv:1506.07465 [hep-ph]].

[79] T. Robens and T. Stefaniak, "Status of the Higgs Singlet Extension of the Standard Model after LHC Run 1," Eur. Phys. J. C **75** (2015) 104 [arXiv:1501.02234 [hep-ph]].

[80] A. Falkowski, C. Gross and O. Lebedev, "A second Higgs from the Higgs portal," JHEP **1505** (2015) 057 [arXiv:1502.01361 [hep-ph]].

[81] M. Gorbahn, J. M. No and V. Sanz, "Benchmarks for Higgs Effective Theory: Extended Higgs Sectors," JHEP **1510** (2015) 036 [arXiv:1502.07352 [hep-ph]].

[82] S. I. Godunov, A. N. Rozanov, M. I. Vysotsky and E. V. Zhemchugov, "Extending the Higgs sector: an extra singlet," arXiv:1503.01618 [hep-ph].

[83] U. Ellwanger, J. F. Gunion and C. Hugonie, "NMHDECAY: A Fortran code for the Higgs masses, couplings and decay widths in the NMSSM," JHEP **0502** (2005) 066 [arXiv:hep-ph/0406215].

[84] U. Ellwanger and C. Hugonie, "NMHDECAY 2.0: An Updated program for sparticle masses, Higgs masses, couplings and decay widths in the NMSSM," Comput. Phys. Commun. **175** (2006) 290 [arXiv:hep-ph/0508022].

[85] G. Degrassi and P. Slavich, "On the radiative corrections to the neutral Higgs boson masses in the NMSSM," Nucl. Phys. B **825** (2010) 119 [arXiv:0907.4682 [hep-ph]].

[86] Robert V. Harlander, Stefan Liebler, and Hendrik Mantler. SusHi: A program for the calculation of Higgs production in gluon fusion and bottom-quark annihilation in the Standard Model and the MSSM. *Comput. Phys. Commun.*, 184:1605–1617, 2013, 1212.3249.

[87] A. Djouadi and J. Quevillon, "The MSSM Higgs sector at a high M_{SUSY}: reopening the low tanβ regime and heavy Higgs searches," JHEP **1310**, 028 (2013) doi:10.1007/JHEP10(2013)028 [arXiv:1304.1787 [hep-ph]].

[88] A. Djouadi, L. Maiani, A. Polosa, J. Quevillon and V. Riquer, "Fully covering the MSSM Higgs sector at the LHC," JHEP **1506** (2015) 168 [arXiv:1502.05653 [hep-ph]].

[89] N. E. Bomark, S. Moretti, S. Munir and L. Roszkowski, "A light NMSSM pseudoscalar Higgs boson at the LHC redux," JHEP **1502** (2015) 044 doi:10.1007/JHEP02(2015)044 [arXiv:1409.8393 [hep-ph]].

[90] [ATLAS Collaboration], "A search for resonant Higgs-pair production in the $b\bar{b}b\bar{b}$ final state in pp collisions at $\sqrt{s} = 8$ TeV", ATL-CONF-2014-005

[91] Georges Aad et al. Search For Higgs Boson Pair Production in the $\gamma\gamma b\bar{b}$ Final State using pp Collision Data at $\sqrt{s} = 8$ TeV from the ATLAS Detector. *Phys. Rev. Lett.*, 114(8):081802, 2015, 1406.5053.

[92] Georges Aad et al. Search for Higgs boson pair production in the $b\bar{b}b\bar{b}$ final state from pp collisions at $\sqrt{s} = 8$ TeVwith the ATLAS detector. *Eur. Phys. J.*, C75(9):412, 2015, 1506.00285.

[93] Georges Aad et al. Searches for Higgs boson pair production in the $hh \to bb\tau\tau, \gamma\gamma WW^*, \gamma\gamma bb, bbbb$ channels with the ATLAS detector. *Phys. Rev.*, D92:092004, 2015, 1509.04670.

[94] [ATLAS Collaboration], "Search for pair production of Higgs bosons in the $b\bar{b}b\bar{b}$ final state using proton–proton collisions at $\sqrt{s} = 13$ TeV with the ATLAS detector ATL-CONF-2016-049

[95] The ATLAS collaboration, "Search for Higgs boson pair production in the $b\bar{b}\gamma\gamma$ final state using pp collision data at $\sqrt{s} = 13$ TeV with the ATLAS detector," ATLAS-CONF-2016-004.

[96] Vardan Khachatryan et al. Search for two Higgs bosons in final states containing two photons and two bottom quarks in proton-proton collisions at 8 TeV. *Phys. Rev.*, D94(5):052012, 2016, 1603.06896.

[97] CMS Collaboration [CMS Collaboration], "Search for di-Higgs resonances decaying to 4 bottom quarks," CMS-PAS-HIG-14-013.

[98] V. Khachatryan *et al.* [CMS Collaboration], "Searches for heavy Higgs bosons in two-Higgs-doublet models and for $t \to ch$ decay using multilepton and diphoton final states in pp collisions at 8 TeV," Phys. Rev. D **90** (2014) 112013 doi:10.1103/PhysRevD.90.112013 [arXiv:1410.2751 [hep-ex]].

[99] Vardan Khachatryan et al. Search for resonant pair production of Higgs bosons decaying to two bottom quark–antiquark pairs in proton–proton collisions at 8 TeV. *Phys. Lett.*, B749:560–582, 2015, 1503.04114.

[100] V. Khachatryan *et al.* [CMS Collaboration], "Searches for a heavy scalar boson H decaying to a pair of 125 GeV Higgs bosons hh or for a heavy pseudoscalar boson A decaying to Zh, in the final states with $h \to \tau\tau$," Phys. Lett. B **755** (2016) 217 doi:10.1016/j.physletb.2016.01.056 [arXiv:1510.01181 [hep-ex]].

[101] Vardan Khachatryan et al. Search for heavy resonances decaying to two Higgs bosons in final states containing four b quarks. *Eur. Phys. J.*, C76(7):371, 2016, 1602.08762.

[102] CMS Collaboration [CMS Collaboration], "Search for resonant pair production of Higgs bosons decaying to two bottom quark-antiquark pairs in proton-proton collisions at 13 TeV," CMS-PAS-HIG-16-002.

[103] CMS Collaboration [CMS Collaboration], "Search for heavy resonances decaying to a pair of Higgs bosons in four b quark final state in proton-proton collisions at $\sqrt{s} = 13$ TeV," CMS-PAS-B2G-16-008.

[104] Search for resonant Higgs boson pair production in the $\mathrm{b\bar{b}}\tau^+\tau^-$ final state. Technical Report CMS-PAS-HIG-16-013, CERN, Geneva, 2016.

[105] Search for resonant Higgs boson pair production in the $\mathrm{b\bar{b}}\tau^+\tau^-$ final state using 2016 data. Technical Report CMS-PAS-HIG-16-029, CERN, Geneva, 2016.

[106] Search for H(bb)H(gammagamma) decays at 13TeV. Technical Report CMS-PAS-HIG-16-032, CERN, Geneva, 2016.

[107] Albert M Sirunyan et al. Search for Higgs boson pair production in events with two bottom quarks and two tau leptons in proton-proton collisions at sqrt(s) = 13 TeV. 2017, 1707.02909.

[108] CMS Collaboration [CMS Collaboration], "Search for resonant and non-resonant Higgs boson pair production in the $b\bar{b}\ell\nu\ell\nu$ final state at $\sqrt{s} = 13$ TeV," CMS-PAS-HIG-17-006.

[109] A. M. Sirunyan *et al.* [CMS Collaboration], "A search for Higgs boson pair production in the $bb\tau\tau$ final state in proton-proton collisions at $\sqrt{s} = 8$ TeV," arXiv:1707.00350 [hep-ex].

[110] CMS Collaboration [CMS Collaboration], "Search for Higgs boson pair production in the final state containing two photons and two bottom quarks in proton-proton collisions at $\sqrt{s} = 13$ TeV," CMS-PAS-HIG-17-008.

[111] M. Maniatis, Int. J. Mod. Phys. A **25** (2010) 3505 [arXiv:0906.0777 [hep-ph]].

[112] Ulrich Ellwanger and Matias Rodriguez-Vazquez. Discovery Prospects of a Light Scalar in the NMSSM. *JHEP*, 02:096, 2016, 1512.04281.

[113] R. Costa, M. Mühlleitner, M. O. P. Sampaio and R. Santos, "Singlet Extensions of the Standard Model at LHC Run 2: Benchmarks and Comparison with the NMSSM," JHEP **1606** (2016) 034 doi:10.1007/JHEP06(2016)034 [arXiv:1512.05355 [hep-ph]].

[114] `twiki.cern.ch/twiki/bin/view/LHCPhysics/CERNYellowReportPageBSMAt13TeV`

[115] Hendrik Mantler and Marius Wiesemann. Hadronic Higgs production through NLO + PS in the SM, the 2HDM and the MSSM. *Eur. Phys. J.*, C75(6):257, 2015, 1504.06625.

[116] Richard D. Ball, Valerio Bertone, Stefano Carrazza, Luigi Del Debbio, Stefano Forte, Alberto Guffanti, Nathan P. Hartland, and Juan Rojo. Parton distributions with QED corrections. *Nucl. Phys.*, B877:290–320, 2013, 1308.0598.

[117] Andy Buckley, James Ferrando, Stephen Lloyd, Karl Nordström, Ben Page, Martin Rüfenacht, Marek Schönherr, and Graeme Watt. LHAPDF6: parton density access in the LHC precision era. *Eur. Phys. J.*, C75:132, 2015, 1412.7420.

[118] S. Dittmaier et al. Handbook of LHC Higgs Cross Sections: 1. Inclusive Observables. 2011, 1101.0593.

[119] Michelangelo L. Mangano, Mauro Moretti, and Roberto Pittau. Multijet matrix elements and shower evolution in hadronic collisions: $Wb\bar{b} + n$ jets as a case study. *Nucl. Phys.*, B632:343–362, 2002, hep-ph/0108069.

[120] S. Catani, F. Krauss, R. Kuhn, and B. R. Webber. QCD matrix elements + parton showers. *JHEP*, 11:063, 2001, hep-ph/0109231.

[121] Johan Alwall et al. Comparative study of various algorithms for the merging of parton showers and matrix elements in hadronic collisions. *Eur. Phys. J.*, C53:473–500, 2008, 0706.2569.

[122] Stefan Hoeche, Frank Krauss, Marek Schonherr, and Frank Siegert. QCD matrix elements + parton showers: The NLO case. *JHEP*, 04:027, 2013, 1207.5030.

[123] Rikkert Frederix and Stefano Frixione. Merging meets matching in MC@NLO. *JHEP*, 12:061, 2012, 1209.6215.

[124] J. Alwall, R. Frederix, S. Frixione, V. Hirschi, F. Maltoni, O. Mattelaer, H. S. Shao, T. Stelzer, P. Torrielli, and M. Zaro. The automated computation of tree-level and next-to-leading order differential cross sections, and their matching to parton shower simulations. *JHEP*, 07:079, 2014, 1405.0301.

[125] Michal Czakon and Alexander Mitov. Top++: A Program for the Calculation of the Top-Pair Cross-Section at Hadron Colliders. *Comput. Phys. Commun.*, 185:2930, 2014, 1112.5675.

[126] J. Katharina Behr, Daniela Bortoletto, James A. Frost, Nathan P. Hartland, Cigdem Issever, and Juan Rojo. Boosting Higgs pair production in the $b\bar{b}b\bar{b}$ final state with multivariate techniques. *Eur. Phys. J.*, C76(7):386, 2016, 1512.08928.

[127] Georges Aad et al. Performance of b-Jet Identification in the ATLAS Experiment. *JINST*, 11(04):P04008, 2016, 1512.01094.

[128] Performance of b-Tagging Algorithms in Proton Collisions at 13 TeV using the 2016 Data. Jul 2016.

[129] Expected performance for an upgraded ATLAS detector at High-Luminosity LHC. Technical Report ATL-PHYS-PUB-2016-026, CERN, Geneva, Oct 2016.

[130] Expected performance of the ATLAS b-tagging algorithms in Run-2. (ATL-PHYS-PUB-2015-022), Jul 2015.

[131] Search for pair production of Higgs bosons in the $b\bar{b}b\bar{b}$ final state using proton−proton collisions at $\sqrt{s} = 13$ TeV with the ATLAS detector. Technical Report ATLAS-CONF-2016-049, CERN, Geneva, Aug 2016.

[132] Souvik Das. A simple alternative to the Crystal Ball function. 2016, 1603.08591.

[133] Search for resonant pair production of Higgs bosons decaying to two bottom quark-antiquark pairs in proton-proton collisions at 13 TeV. Technical Report CMS-PAS-HIG-16-002, CERN, Geneva, 2016.

[134] Jonathan M. Butterworth, Adam R. Davison, Mathieu Rubin, and Gavin P. Salam. Jet substructure as a new Higgs search channel at the LHC. *Phys. Rev. Lett.*, 100:242001, 2008, 0802.2470.

[135] Gavin P. Salam. Towards Jetography. *Eur. Phys. J.*, C67:637–686, 2010, 0906.1833.

[136] Glen Cowan, Kyle Cranmer, Eilam Gross, and Ofer Vitells. Asymptotic formulae for likelihood-based tests of new physics. *Eur. Phys. J.*, C71:1554, 2011, 1007.1727. [Erratum: Eur. Phys. J.C73,2501(2013)].

[137] Search for Minimal Supersymmetric Standard Model Higgs Bosons H/A in the $\tau\tau$ final state in up to 13.3 fb^{-1} of pp collisions at $\sqrt{s}$= 13 TeV with the ATLAS Detector. Technical Report ATLAS-CONF-2016-085, CERN, Geneva, Aug 2016.

[138] Georges Aad et al. Search for neutral Higgs bosons of the minimal supersymmetric standard model in pp collisions at $\sqrt{s} = 8$ TeV with the ATLAS detector. *JHEP*, 11:056, 2014, 1409.6064.

[139] Georges Aad et al. Search for the neutral Higgs bosons of the Minimal Supersymmetric Standard Model in pp collisions at $\sqrt{s} = 7$ TeV with the ATLAS detector. *JHEP*, 02:095, 2013, 1211.6956.

[140] Search for additional neutral Higgs bosons decaying to a pair of tau leptons in pp collisions at $\sqrt{s} = 7$ and 8 TeV. Technical Report CMS-PAS-HIG-14-029, CERN, Geneva, 2015.

[141] Search for a neutral MSSM Higgs boson decaying into $\tau\tau$ with 12.9 fb^{-1} of data at $\sqrt{s} = 13$ TeV. Technical Report CMS-PAS-HIG-16-037, CERN, Geneva, 2016.

[142] Reconstruction, Energy Calibration, and Identification of Hadronically Decaying Tau Leptons in the ATLAS Experiment for Run-2 of the LHC. Technical Report ATL-PHYS-PUB-2015-045, CERN, Geneva, Nov 2015.

[143] Lorenzo Bianchini, John Conway, Evan Klose Friis, and Christian Veelken. Reconstruction of the Higgs mass in $H \to \tau\tau$ Events by Dynamical Likelihood techniques. *J. Phys. Conf. Ser.*, 513:022035, 2014.

[144] Rakhi Mahbubani, Konstantin T. Matchev, and Myeonghun Park. Reinterpreting the Oxbridge stransverse mass variable MT2 in general cases. *JHEP*, 03:134, 2013, 1212.1720.

[145] Alan J. Barr, Matthew J. Dolan, Christoph Englert, and Michael Spannowsky. Di-Higgs final states augMT2ed – selecting hh events at the high luminosity LHC. *Phys. Lett.*, B728:308–313, 2014, 1309.6318.

[146] A. Elagin, P. Murat, A. Pranko, and A. Safonov. A New Mass Reconstruction Technique for Resonances Decaying to di-tau. *Nucl. Instrum. Meth.*, A654:481–489, 2011, 1012.4686.

[147] Ben Gripaios, Keiko Nagao, Mihoko Nojiri, Kazuki Sakurai, and Bryan Webber. Reconstruction of Higgs bosons in the di-tau channel via 3-prong decay. *JHEP*, 03:106, 2013, 1210.1938.

[148] Search for Higgs boson pair production in the $b\bar{b}\gamma\gamma$ final state using pp collision data at $\sqrt{s} = 13$ TeV with the ATLAS detector. Technical Report ATLAS-CONF-2016-004, CERN, Geneva, Mar 2016.

[149] Prospects for measuring Higgs pair production in the channel $H(\to \gamma\gamma)H(\to b\bar{b})$ using the ATLAS detector at the HL-LHC. Technical Report ATL-PHYS-PUB-2014-019, CERN, Geneva, Oct 2014.

[150] Daniel Faeh and Nicolas Greiner. Diphoton production in association with two bottom jets. 2017, 1706.08309.

[151] Abraham Wald. Tests of statistical hypotheses concerning several parameters when the number of observations is large. *Transactions of the American Mathematical Society*, 54(3):426–482, 1943.

[152] Eilam Gross and Ofer Vitells. Trial factors or the look elsewhere effect in high energy physics. *Eur. Phys. J.*, C70:525–530, 2010, 1005.1891.

[153] CMS Collaboration. Search for H/A decaying into Z+A/H, with Z to ll and A/H to fermion pair. *CMS-PAS-HIG-15-001*, https://cds.cern.ch/record/2014119.

[154] R. Aggleton et al.. Review of LHC experimental results on low mass bosons in multi Higgs models. *J.HEP*, JHEP 1702 (2017).

[155] R. Aggleton et al.. Update of the flavour-physics constraints in the NMSSM. *J.HEP*, JHEP 1703 (2017) 052.

[156] CMS Collaboration. Search for beyond Standard Model light bosons decaying into muon pairs. *CMS-PAS-HIG-16-035*,

[157] ATLAS Collaboration. Search for Higgs boson decays to Beyond-the-Standard-Model light bosons in four-lepton events with the ATLAS detector at $\sqrt{s} = 13$ TeV. *ATLAS-CONF-2017-042.*

université PARIS-SACLAY

NNT : 2017SACLS317

ÉCOLE DOCTORALE
Physique en île-de-France (EDPIF)

UNIVERSITÉ PARIS SUD
Comprendre le monde, construire l'avenir

La recherche de bosons de Higgs supplémentaires au LHC

Thèse de doctorat de l'Université Paris-Saclay
préparée à l'Université Paris-Sud

École doctorale n°564 Physique en île-de-France (EDPIF)
Spécialité de doctorat : Physique

Thèse présentée et soutenue à Orsay, le 28 Septembre 2017, par

Matías Rodríguez Vázquez

Composition du Jury :

Asmaa Abada Professeur, LPT Orsay	Président
Stefano Moretti Professeur, University of Southampton	Rapporteur
Geneviève Bélenger Professeur, LAPTh Annecy	Rapporteur
Fabio Maltoni Professeur, CP3 Louvain	Examinateur
Ulrich Ellwanger Professeur, LPT d'Orsay	Directeur de thèse

Thèse de doctorat

université PARIS-SACLAY
ÉCOLE DOCTORALE
Physique en île-de-France (EDPIF)

Titre : La recherche de bosons de Higgs supplémentaires au LHC

Mots clés : physique des particules, supersymétrie, hautes énergies, LHC

Résumé : Malgré un succès expérimental incontestable, le Modèle standard (MS) de la physique des particules laisse de nombreuses questions fondamentales sans réponse, comme le problème de hiérarchie et l'origine de la matière noire, motivant l'étude de la "nouvelle physique". Le Next-to-Minimal Supersymmetric Standard Model (NMSSM) est une extensión très intéressante du MS répondant à ces deux problèmes. Il comprend une riche phénoménologie, en principe accessible au Grand Collisionneur de Hadrons (LHC). En particulier, son secteur de Higgs est étendu par rapport au MS, générant six scalaires. Le but de cette thèse est d'étudier le potentiel de découverte de ces bosons de Higgs supplémentaires au LHC. Après une introduction du NMSSM et de ses motivations, nous étudions d'abord les perspectives de découverte d'un scalaire, plus léger que la résonance à 125 GeV mise en évidence au CERN, en passant en revue ses possibles modes de production et de détection dans les phases à venir du LHC, et ses possibles impacts sur les couplages du boson de Higgs du MS. Ensuite, les perspectives de recherche via les cascades de Higgs, impliquant des bosons de Higgs supplémentaires légers et lourds, est présentée. Des études détailléees au moyen de méthodes Monte-Carlo ont été réalisées, et de nouvelles analyses dédiées sont présentées. Ces derniers résultats ne sont pas restreints au NMSSM, et peuvent être interprétés dans une large classe de modèles.

Title : Search for supplementary Higgs Bosons at the LHC

Keywords : particle physics, supersymmetry, high energy physics, LHC

Abstract : Despite its incontestable experimental success, the Standard Model of particle physics leaves unanswered many fundamental questions like the hierarchy problem and the origin of dark matter, motivating the study of physics beyond its scope. The NMSSM is a well-motivated extension of the SM addressing these two issues. It features a rich phenomenology accessible, in principle, at the LHC. In particular, the Higgs sector of the NMSSM is extended with respect to the SM giving rise to six scalars. It is the aim of this thesis to study the discovery potential of these extra Higgs bosons at the LHC. After introducing the NMSSM and its motivation, we first study the discovery prospects for a scalar lighter than the 125 GeV resonance found at CERN, reviewing its possible production and detection at the upcoming runs of the LHC and its possible impact on couplings of the Standard Model Higgs boson. Next, prospects for searches via Higgs cascades involving extra light and heavy Higgs bosons are presented. Detailed studies by means of Monte Carlo methods are performed, and new dedicated analysis are proposed. These last results are not confined to the NMSSM and can be interpreted in a wide class of models.

Université Paris-Saclay
Espace Technologique / Immeuble Discovery
Route de l'Orme aux Merisiers RD 128 / 91190 Saint-Aubin, France